Draft Final Report

Prevention of Bridge Deck Icing Using Geothermal Heat -- Test Bridge Sections

Principal Investigators

Jeffrey D. Spitler, Associate Professor
School of Mechanical and Aerospace Engineering

Timothy D. Hogue, Assistant Professor
School of Civil and Environmental Engineering

Research Assistants
Ojas Wadivkar
Chen-Jui Liao

College of Engineering, Architecture and Technology
Oklahoma State University
Stillwater, Oklahoma 74078-0533

SI (METRIC) CONVERSION FACTORS

Approximate Conversions to SI Units

Symbol	When you know	Multiply by	To Find	Symbol
	LENGTH			
in	inches	25.40	millimeters	mm
ft	feet	0.3048	meters	m
yd	yards	0.9144	meters	m
mi	miles	1.609	kilometers	km
	AREA			
in^2	square inches	645.2	square millimeters	mm
ft^2	square feet	0.0929	square meters	m^2
yd^2	square yards	0.8361	square meters	m^2
ac	acres	0.4047	hectares	ha
mi^2	square miles	2.590	square kilometers	km^2
	VOLUME			
fl oz	fluid ounces	29.57	milliliters	mL
gal	gallons	3.785	liters	L
ft^3	cubic feet	0.0283	cubic meters	m^3
yd^3	cubic yards	0.7645	cubic meters	m^3
	MASS			
oz	ounces	28.35	grams	g
lb	pounds	0.4536	kilograms	kg
T	short tons (2000 lb)	0.907	megagrams	Mg
	TEMPERATURE (exact)			
°F	degrees Fahrenheit	(°F-32)/1.8	degrees Celsius	°C
	FORCE and PRESSURE or STRESS			
lbf	poundforce	4.448	Newtons	N
lbf/in^2	poundforce per square inch	6.895	kilopascals	kPa

Approximate Conversions from SI Units

Symbol	When you know	Multiply by	To Find	Symbol
	LENGTH			
mm	millimeters	0.0394	inches	in
m	meters	3.281	feet	ft
m	meters	1.094	yards	yd
km	kilometers	0.6214	miles	mi
	AREA			
mm^2	square millimeters	0.00155	square inches	in^2
m^2	square meters	10.764	square feet	ft^2
m^2	square meters	1.196	square yards	yd^2
ha	hectares	2.471	acres	ac
km^2	square kilometers	0.3861	square miles	mi^2
	VOLUME			
mL	milliliters	0.0338	fluid ounces	fl oz
L	liters	0.2642	gallons	gal
m^3	cubic meters	35.315	cubic feet	ft^3
m^3	cubic meters	1.308	cubic yards	yd^3
	MASS			
g	grams	0.0353	ounces	oz
kg	kilograms	2.205	pounds	lb
Mg	megagrams	1.1023	short tons (2000 lb)	T
	TEMPERATURE (exact)			
°C	degrees Celsius	9/5+32	degrees Fahrenheit	°F
	FORCE and PRESSURE or STRESS			
N	Newtons	0.2248	poundforce	lbf
kPa	kilopascals	0.1450	poundforce per square inch	lbf/in^2

Executive Summary

The project covered by this final report, Prevention of Bridge Deck Icing Using Geothermal Heat -- Test Bridge Sections has two important aspects - the thermal performance of the test system and the structural effects of the test system. Two investigate both aspects, the project team is made up of both mechanical engineers and civil engineers. In particular, one graduate student from each area is working on the project and will be completing a master's thesis on the work. Accordingly, the final report is divided up into two sub-reports: "Thermal Performance of a Geothermal Bridge Deck De-icing System" and "Thermal Stress Predictions for Geothermally Heated Bridge Decks". Both of these sub-reports are attached.

It is the purpose of this executive summary to highlight a few of the main conclusions from the project. In addition to the funded research, a significant amount of additional modeling work was done on both aspects of the has provided some additional perspective to help in the interpretation of the results. The chief conclusions are as follows:

- The bridge deck deicing system, as built, appears to be a feasible system, however it was unsuccessful in melting any ice without the aid of solar radiation during the test phase. This was because for all the experiments performed, the system was switched on only after the slab temperature was below freezing. A more careful review of the literature revealed the necessity for the idling of such snow melting systems in advance of the freezing conditions to effectively melt snow / ice on the slab surface. The design heat requirements for snow melting systems presented in the ASHRAE handbook presume idling of the system prior to the freezing event. For low input fluxes, and extremely low air temperatures, the system does not raise the slab temperature above freezing, despite idling the system.

- The numerical simulation demonstrated the feasibility of using the current system to melt snow for two different freezing precipitation events. The time necessary for applying heat varied with the inlet temperature. For these events, the heating system had to be turned on anywhere from 15 minutes to 75 minutes before the bridge deck surface would have otherwise frozen.

- For a third test day, with a clear sky and cold temperatures, in which no actual precipitation occurred, the simulation predicted that only an inlet temperature of 130 F or higher would be sufficient to prevent icing. However, the statistical likelihood of precipitation actually occurring under those conditions was not established, but is thought to be remote.

- The computer model developed to predict the performance of the bridge deck calculated higher inputs then those recommended by ASHRAE guidelines, despite calculating the input heat flux requirements for ASHRAE by using the most extreme weather conditions. The computer model predicted the transient response of the system and calculated higher input requirements for the system than those developed by ASHRAE. Convection and radiation losses as calculated by ASHRAE were found to be much lower than those computed by the numerical model.

- The thermally induced strains and stresses are considered small enough that no additional bridge design features will be required to accommodate them safely. Some flow patterns may be slightly better than others from a thermal stress standpoint.

Draft Final Report

Thermal Performance of a Geothermal Bridge Deck ~~De-~~ De-icing System

Ojas Wadivkar, Research Assistant

Jeffrey D. Spitler, Associate Professor

School of Mechanical & Aerospace Engineering
Oklahoma State University

School of Mechanical and Aerospace Engineering
College of Engineering, Architecture and Technology
218 Engineering North
Oklahoma State University
Stillwater, Oklahoma 74078-0533

TABLE OF CONTENTS

1. INTRODUCTION

1.1 Overview

1.1.1 The problem of bridge icing

Snow, sleet and freezing rain can cause hazardous conditions for unsuspecting or inattentive motorists. Loss of control of the vehicle because of the slick road may lead to dangerous accidents. The formation of ice or frost on bridge decks, while the other part of the road remains ice free is a well known phenomenon and is called preferential icing. Numerous accidents result every year during the winter season due to this. This has led to many countermeasures being developed and new methods being researched at many locations. In a study done in the late 70's, it was estimated that 25,000 accidents occurred annually in the United States alone, due to ice and frost on bridge decks (Blackburn et al., 1978). It is therefore extremely important to prevent this preferential icing effect. In the past various strategies have been employed. The responses may range from using deicing agents or embedded heating elements to high intensity infra red heaters. Some of these methods are in use universally while others have only been tested at certain locations.

1.2 Background and Literature Review

This section lists some of the conventional and non conventional approaches to dealing with road icing and the heat requirements for a system to melt the ice from the surface.

1.2.1 Conventional approach

The application of deicing agents is the conventional method of preventing preferential icing. Materials like salt, sand or other such gritty material can be used to for ice removal. Practically any material which is water soluble and can lower the freezing point of water can be used as a deicer. The chemicals commonly in use today are sodium chloride (common salt), calcium chloride, potassium chloride and urea ("Deicing," 1991). These deicers all work in the same fashion. After coming in contact with some moisture, they form a liquid brine. This brine has a lower freezing temperature than water and causes the ice to melt on contact. These deicers spread out under the ice, "undercutting" it, thus breaking the bond between the ice and the road surface. After sufficient loosening, the ice can be easily removed. Deicers differ markedly in their performance. For temperatures below 25 °F, sodium chloride, urea and potassium chloride begin to lose their effectiveness. Calcium chloride on the other hand is effective to temperatures below -20 °F. Heat generated by the friction of the moving traffic is also helpful in increasing the effectiveness of the deicing agents. The shape of the deicer pellets also affects performance.

These deicers however have some undesirable side effects ("Deicing," 1991). Deicer residue that gets tracked into buildings and leaves unsightly marks upon drying. All the chloride salts have a potential for damaging plant life, if used in high concentration. However the major disadvantage of the long term use of these deicers is the corrosive effect they have on metal. Water in which salt is dissolved gets splashed on to cars and parts of the bridge. Corrosion of unpainted iron or unprotected steel can be accelerated if the saline water stays on it for long. In case of the bridge deck, saline water seeps through small cracks in the concrete to corrode the embedded reinforcing steel inside the concrete. Corrosion of the reinforcing steel can lead to premature deterioration of the bridge deck. Protection strategies (Babaei and Hawkins, 1987) to prevent this deterioration have included the use of denser concrete or latex modified concrete or epoxy coated reinforcing steel. Non-corrosive material like urea can replace the salts. The addition of anti-corrosive materials to salts has also been tested (Fleeg, 1990). These materials form a protective barrier on the metal surface. These alternatives are considerably more expensive and have to be used sparingly. In many cases however money can be wasted if the deicer is distributed early and later found unnecessary (Malloy, 1994). The decision to salt in most cases depends upon local experience and judgment. This decision can be aided by the monitoring of the road surface to predict ice formation.

1.2.2 Prediction of ice formation

Many major airports use runway surface monitoring systems for detecting ice formation. A similar system has been incorporated to combat preferential icing on bridge decks. The system includes a number of small sensors embedded at intervals of the bridge deck ("Deicer," 1994). The deck temperature, condition (wet, dry, freezing), air temperature and other important information is monitored continuously. "Just in time" winter road maintenance is possible with such sensors.

It is observed that the sensors in themselves are not sufficient. They only convey what is happening at the present moment. In some cases this may be too late or salting may take place even though the temperature does not drop below freezing as expected. Also the location of the sensor itself can lead to an error in deicing response if it is located in a cold spot. It can be dangerous if the sensor is in a warm spot and the rest of the road is freezing. A predictive dimension must be added to the sensor information. Various models have been developed to predict formation of ice (Nysten 1980, Thornes 1984, Parmenter and Thornes 1986, Rayer 1987, Stephenson 1988, Thompson 1988, Shao 1990, Kempe 1990, Isaka et al. 1990, , and Shao 1991, Sass 1992) at different parts of the world. Some of these are available on a commercial basis. These models utilize the input data from the sensors from the site and predict the future road conditions which can be used for making deicing decisions. Typical input parameters measured are the surface temperature, wetness, air temperature, humidity, wind speed, radiation, etc. A thermal mapping (Ponting, 1984) procedure was devised to deal with the geographical differences in the stretch of the road being monitored.

1.2.3 Infrared radiant heating

Infrared heating systems are used extensively for comfort heating, but can be designed specifically for snow melting or to prevent preferential icing on bridge decks (ASHRAE 1987). For the snow melting systems, the emphasis is on horizontal surfaces, while for comfort heating, it is on the vertical surfaces of the human body. For snow melting systems, a radiation spill may occur at the edges of the horizontal surface being heated as a uniform distribution of heat for the entire slab surface requires an overhead fixture. The radiant output of the infra red lamp will scatter outside the target area. That is considerably more expensive. An alternative is to place fixtures at intermediate positions, which would scatter radiation above the design average value at the center of the slab and below design value towards the edges. This however may lead to snow build up at the edges. An advantage of infra red systems is the fast heating time, as compared to embedded systems. This equipment can be turned on when the snow fall just starts.

1.2.4 Embedded electrical heating elements

Ice melting systems which use electricity as their energy source make use of mineral insulated (MI) cable or a resistance wire assembly embedded in the bridge deck (ASHRAE 1995). The concrete slabs housing these cables have to be designed with expansion-contraction joints, reinforcement and drainage to prevent the slab cracking or the crack induced shearing or tensile forces, which may break the heating wire or cable. High cost of electricity make these systems expensive to operate. The large heat capacity of the concrete structure necessitates a long lead time or a high start up power wattage ("Space age," 1975). An electric deicing system was installed in Louisville Kentucky as conventional methods would have led to traffic congestion (Havens et al., 1979). The system was found to be functional, however installation and operating costs were high.

1.2.5 Use of Nuclear waste materials

In a bid to investigate alternative methods of deicing, Dynatherm Corporation built a system making use of nuclear wastes to produce heat. This heat was transferred to the earth below the surface to be heated, by a heat exchange fluid ("Space age," 1975). The earth proved to be a good storage. Heat pipes were used to transport this heat to the surface. The system was successful, however the safety issue due to the use of nuclear waste and its limited availability made it unfeasible. Disposal of nuclear waste also posed a problem for highway authorities. This project however made apparent the potential for using geothermal heat.

1.2.6 Use of hot fluid circulated in embedded pipes

Inslab hydronic heating has been used for building heating purposes and also for deicing surfaces. Hot fluid is circulated in pipes embedded below the surface of the bridge deck to de-ice the surface. The piping may be made out of metal, rubber or thermoplastic. The circulating fluid may be heated by a conventional energy source like fossil fuels or by using an alternative low grade thermal energy source like natural hot springs, geothermal heat or some other constant temperature energy source, like a large water reservoir (The temperature may be "boosted" by one or more heat pumps). Use of geothermal heat is an economically attractive option and is also environmentally friendly.

1.2.7 Prevention of ice formation using Geothermal heat

The earth is an unlimited reservoir of heat. It can be used as a heat source or sink as need be. Temperatures a few meters below ground level are essentially constant throughout the year, even when the ambient temperature above the ground varies with the different seasons. Earth can hence be used to either absorb heat or reject it. There have been many systems which make use of this form of geothermal heat.

1.2.7.1 Passive Geothermal Deck Heating Systems

"Heat pipes" are a passive geothermal heating system. Heat pipes were first introduced in 1944, but were not used till 1961. Use of the heat pipe to de-ice bridge decks using geothermal heat was demonstrated by research conducted in Wyoming, Oklahoma, West Virginia, and Japan (Nydahl et al., 1984; Lee et al., 1986).

Heat pipes

A heat pipe is a closed container evacuated of all non-condensable gases, containing a working fluid which transfers heat from a region of higher temperature (earth) to that of lower temperature (bridge deck). The fluid used must be in a two phase equilibrium between these two operating temperatures. For temperatures in the cryogenic zone, nitrogen is used and for very high temperatures a metal is used as the working fluid ("Space age," 1975). A schematic representation of a heat pipe is shown in Fig. 1.1.

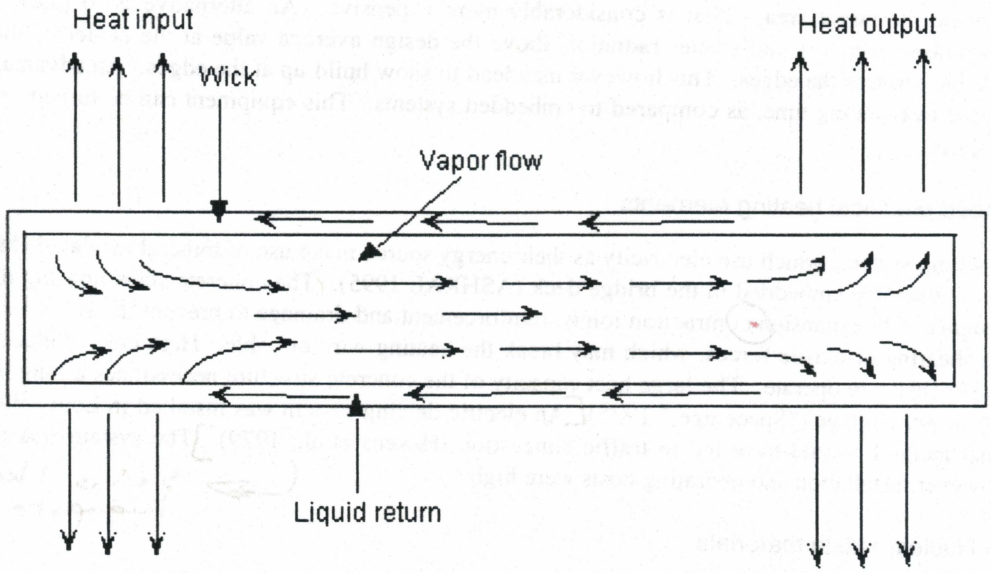

Figure 1.1:- Schematic representation of the heat pipe

Heat is absorbed at the higher temperature end or the evaporator as a heat input which converts the liquid to vapor. At the low temperature or condenser end the fluid condenses back to a liquid outputting the latent heat of condensation. In applications, such as bridge deck de-icing, the pipe is oriented so as to allow gravity return of the liquid to the high temperature end. In a gravity free operation, such as outer space applications, a wick using capillary action performs this task.

Fig. 1.2 is a schematic, depicting the use of the heat pipe in a bridge deck deicing operation. An evaporator pipe or set of pipes is embedded into the ground near a bridge and filled with liquid, usually ammonia. The liquid is evaporated by the heat of the earth and the vapor travels upward into condenser pipes installed in the bridge deck. The vapor then gives up its heat to the deck, condensing in the process. Finally, the condensed liquid flows by gravity back down into the evaporator(s) to complete the cycle.

This system is passive in that it operates without need of pumps, control systems, external power, or any human intervention. The evaporation-condensation cycle is in operation whenever the bridge deck is cooler than the earth. Heat is removed from the earth even when ice wouldn't form. This extra removal of heat is not a problem from the standpoint of operating costs as there are none. But the pipe size and/or depth must be increased to compensate for the excessive heat loss.

The inside of each heat pipe must be carefully cleaned. Plumbing in the bridge deck must have just enough slope so that condensed liquid flows back to the evaporators. Because of the complications of preparing and constructing, the installation cost of the heat pipes is prohibitive—59% of the cost of the combined bridge and heating system (Nydahl et al., 1984).

Furthermore, it is likely that one or a few condenser pipes may end up being installed without the required slope. Also, it may happen that not all plumbing is correctly cleaned (Nydahl et al., 1984). In both these circumstances, ice will form on the bridge near the problem pipe(s). The heating system cannot be repaired without tremendous cost and effort (e.g., tearing up the bridge deck or digging up the surrounding earth).

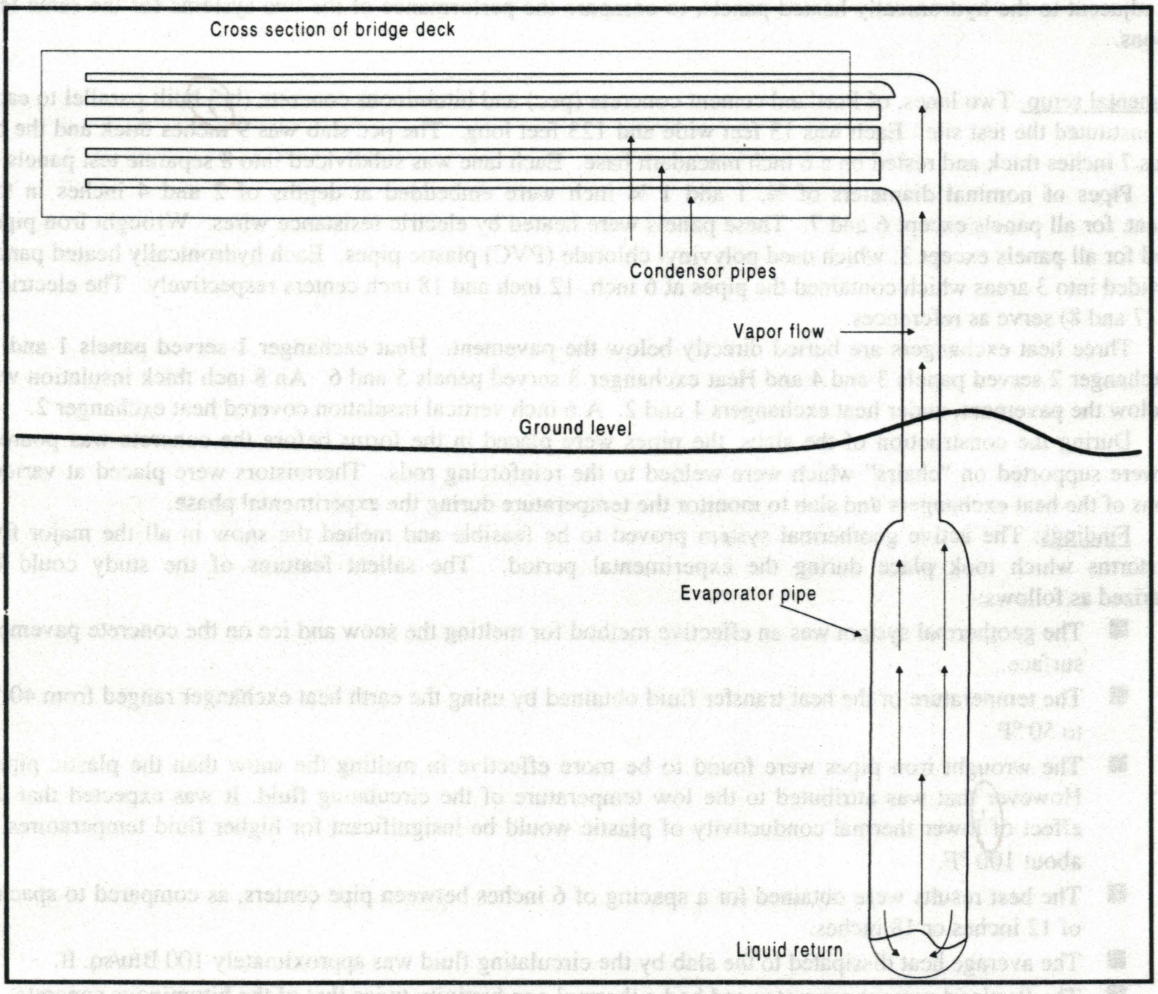

Fig. 1.2:- Schematic Arrangement of "Heat Pipe" Bridge Deck Heating System

1.2.7.2 Active Geothermal Deck Heating Systems

Sufficient geothermal heat is available to eliminate preferential bridge deck icing, even in relatively cold climates. Therefore, a cost effective heat delivery system would have broad applicability throughout the United States. Active geothermal deck heating holds the promise of being economical. The term "active" means the heat system is controlled. Heat is conserved and any operating costs of conveying heat to the deck are minimized.

An experimental test set up was constructed in 1977 at Trenton by the New Jersey Department Of Transportation to investigate an active geothermal system. The objective of the study was to provide design data for similar systems using embedded pipes and also the feasibility of utilizing the ground heat for de-icing road surfaces.

Pavement heating system at Trenton (New Jersey Department of Transportation)
(Winters., 1977)

An experimental heated pavement was constructed to develop improved methods of snow and ice control. Wrought iron pipes and plastic pipes of varying diameters were embedded in slabs of Portland cement concrete and bituminous concrete. A solution of ethylene glycol was circulated through the pipes and readings were taken during snow fall to see the feasibility of the system. Geothermal heat was used to raise the temperature of the ethylene glycol. The antifreeze solution of 50 percent ethylene glycol and 50 percent water was circulated by a pump through heat exchangers buried below the pavement which extracted the heat from the ground and transferred it to the fluid which then was circulated through the embedded pipes in the slab. A grid of electric resistance wires heated the panels adjacent to the hydronically heated panels, to compare the performance of the two systems for the same test conditions.

Experimental setup Two lanes, of Portland cement concrete (pcc) and bituminous concrete (bc) built parallel to each other constituted the test site. Each was 13 feet wide and 123 feet long. The pcc slab was 9 inches thick and the bc slab was 7 inches thick and rested on a 6 inch macadam base. Each lane was subdivided into 8 separate test panels.

Pipes of nominal diameters of ¾, 1 and 1 ¼ inch were embedded at depths of 2 and 4 inches in the pavement, for all panels except 6 and 7. These panels were heated by electric resistance wires. Wrought iron pipes are used for all panels except 3, which used polyvinyl chloride (PVC) plastic pipes. Each hydronically heated panel, was divided into 3 areas which contained the pipes at 6 inch, 12 inch and 18 inch centers respectively. The electrical panels (7 and 8) serve as references.

Three heat exchangers are buried directly below the pavement. Heat exchanger 1 served panels 1 and 2, heat exchanger 2 served panels 3 and 4 and Heat exchanger 3 served panels 5 and 6. An 8 inch thick insulation was used below the pavement, under heat exchangers 1 and 2. A 6 inch vertical insulation covered heat exchanger 2.

During the construction of the slabs, the pipes were placed in the forms before the concrete was poured. Pipes were supported on "chairs" which were welded to the reinforcing rods. Thermistors were placed at various locations of the heat exchangers and slab to monitor the temperature during the experimental phase.

Findings: The active geothermal system proved to be feasible and melted the snow in all the major five snow storms which took place during the experimental period. The salient features of the study could be summarized as follows:-

- The geothermal system was an effective method for melting the snow and ice on the concrete pavement surface.
- The temperature of the heat transfer fluid obtained by using the earth heat exchanger ranged from 40 °F to 50 °F.
- The wrought iron pipes were found to be more effective in melting the snow than the plastic pipes. However that was attributed to the low temperature of the circulating fluid. It was expected that the effect of lower thermal conductivity of plastic would be insignificant for higher fluid temperatures of about 100 °F.
- The best results were obtained for a spacing of 6 inches between pipe centers, as compared to spacing of 12 inches or 18 inches.
- The average heat dissipated to the slab by the circulating fluid was approximately 100 Btu/sq. ft.
- The Portland cement concrete used had a thermal conductivity twice that of the bituminous concrete.
- The geothermal system was much cheaper to operate than the electric system primarily because of the demand charge of electricity.

- Running the system in the summer would 'charge' the ground reservoir which would lead to higher fluid temperatures in the following winter.

Ground source heat pump

The above study demonstrates the feasibility of such an active geothermal system to melt ice on the concrete surface. Increasing the temperature of the circulating fluid would improve the effectiveness of this deicing system. A viable alternative to increase this temperature, whilst also making use of the earth heat, would be to incorporate a ground source heat pump into the system.

A ground source heat pump has been developed through pioneering research at Oklahoma State University (OSU) over the past 20 years. This thermal system has been used in many residential and commercial applications in the last decade and is even in use at the Oklahoma State Capitol. A ground-coupled heat pump can heat a home for about 35% of the cost of an electrical resistance system. Pipe liquid may be heated to temperatures above 100°F. In a bridge deck heating system, this level of heat would allow for a reduction in the amount of piping required.

Figure 1.3 shows the schematic representation of an active geothermal deicing system incorporating a ground source heat pump. Fluid could also be circulated on some hot days in the summer. The sun's radiant heat would be transported from the deck to "recharge" the ground (Katsuragi et al., 1989). Heat removed during the previous cold season would be replaced.

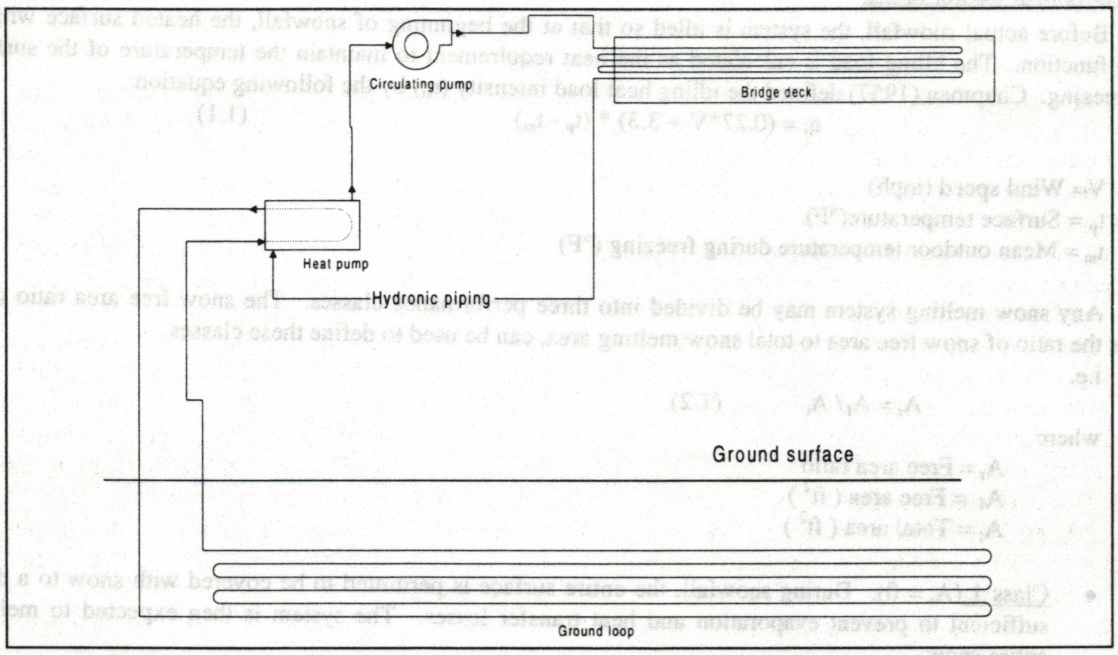

Figure 1.3:- Active heat pump

1.2.8 Heat requirements for hydronic snow-melting systems

The *ASHRAE handbook* provides guidelines to calculate the amount of heat required to melt snow from a surface. The same heat requirements can be used for freezing rain, or frost. Air temperatures during snowfall are lower than those during the occurrence of freezing rain or frost. Heat requirements calculated for melting snow for any surface will also be sufficient to melt ice due to freezing rain or frost. To determine the heat requirement for melting the snow on any surface, the snow melting phenomenon is to be considered. The first snow flakes fall on a warm and dry surface. This snow must be warmed up to 32°F before it is melted. On melting, a film of water is formed over the area, which, if the heat input is continued begins to evaporate. There is also a heat transfer from the surface to the atmosphere due to convection and radiation.

The heating requirement for snow melting depends on four atmospheric factors.

- Rate of snowfall
- Air temperature
- Relative humidity
- Wind velocity

The rate of snowfall determines the heat required to raise the temperature of the snow to 32°F and to melt it. Evaporation of the water from the surface depends on the wind speed, relative humidity, and the ambient temperature. The convection and radiation loss from the surface depends on the film coefficient and the temperature difference between the air and the slab surface.

Snow melting by using hydronic heating elements has been used before and its practicality has been proved in many installations. The source of heat for heating the circulating fluid may differ, as discussed in the previous sections. The heating requirements for such hydronic systems has been provided in the *ASHRAE Handbook.* It is the reference for most of the snow melting systems in North America and many other countries. Heating requirements are useful in designing the systems according to the class of snow-melting systems required and its location. The models for calculating heat requirements discussed in the following sections are not transient models. They assume quasi- steady state conditions. The surface is already heated and is ready to melt the snow as soon as it starts falling. The surface heating system is 'idled' for some time before actual snowfall.

Heat Requirement during Idling

Before actual snowfall, the system is idled so that at the beginning of snowfall, the heated surface will be ready to function. The idling load is calculated as the heat requirement to maintain the temperature of the surface above freezing. Chapman (1957) defined the idling heat load intensity (q_i) by the following equation:

$$q_i = (0.27*V + 3.3) * (t_p - t_m) \qquad (1.1)$$

where

V= Wind speed (mph)
t_p = Surface temperature(°F)
t_m = Mean outdoor temperature during freezing (°F)

Any snow melting system may be divided into three performance classes. The snow free area ratio (*Ar*), which is the ratio of snow free area to total snow melting area, can be used to define these classes.

i.e.

$$A_r = A_f / A_t \qquad (1.2)$$

where

A_r = Free area ratio
A_f = Free area (ft^2)
A_t = Total area (ft^2)

- Class 1 ($A_r = 0$): During snowfall, the entire surface is permitted to be covered with snow to a depth sufficient to prevent evaporation and heat transfer losses. The system is then expected to melt the entire snow.
- Class 2 ($A_r = 0.5$): During the snowfall, 50 % of the surface is permitted to be covered with snow.
- Class 3 ($A_r = 1.0$): During the snowfall, the entire surface is kept free from snow accumulation. The system must melt the snow so rapidly that the accumulation is zero. In this system the heat is lost from the surface of the melted snow to the atmosphere by radiation, convection and evaporation. Bridge decks are included in this class.

1.2.8.1 ASHRAE Handbook guidelines

The guidelines presented in the latest relevant *ASHRAE handbook* (1995) are based on work done by Chapman and Katunich (1956), who derived the general equation for the required slab output (q_o) to melt snow as:

$$q_o = q_s + q_m + A_r (q_e + q_h) \qquad (1.3)$$

where

q_s = Sensible heat transferred to the snow (Btu/hr ft^2)
q_m = Heat of fusion (Btu/hr ft^2)

A_r = Ratio of snow free area to total area
q_e = Heat of evaporation (Btu/hr ft^2)
q_h = Heat transfer by convection and radiation (Btu/hr ft^2)

The sensible heat to warm the snow to 32°F is

$$q_s = s\, c_p\, \rho\, (32 - t_a) / 12 \qquad (1.4)$$

where

s = rate of snowfall (in. of water equivalent per hour)
c_p = Specific heat of snow (0.5 Btu/lb. °F)
ρ = Density of water equivalent of snow (62.4 lb/ft^3)
t_a = Air temperature (°F)

The heat of fusion q_m to melt the snow is given by

$$q_m = s\, h_f\, \rho / 12 \qquad (1.5)$$

where

h_f = Enthalpy of fusion for water (143.5 Btu/lb.)

The heat of evaporation q_e is

$$q_e = h_{fg}\, (0.0201\, V + 0.055)\, (0.188 - p_{av}) \qquad (1.6)$$

where

h_{fg} = Heat of evaporation at the film temperature (Btu/lb.)
V = Wind speed (mph)
p_{av} = Vapor pressure of moist air (in. of mercury)

The heat transfer q_h (convection and radiation) is

$$q_h = 11.4\, (0.0201\, V + 0.055)\, (t_f - t_a) \qquad (1.7)$$

where

t_f = Water film temperature (°F), usually taken as 33°F

Heat requirements for a hydronic snow melting system can be determined by using Equations (2) through Equations (6). The solution of the equations requires weather data. Annual averages or maximums of the weather parameters cannot be used as they may not be occurring simultaneously. A frequency analysis of the solutions to Equation (2) is performed over a period of several years for determining the required design heat output for any particular location. An analysis of 33 cities in the United States was performed. This data can be obtained in the *ASHRAE Handbook*. The maximum heat outputs for the different classes of snow melting system located at Oklahoma City are:

q_o = 350 Btu/hr. ft^2 (Class 3)
q_o = 81 Btu/hr. ft^2 (Class 2)
q_o = 66 Btu/hr. ft^2 (Class 1)

Back and edge losses increase the required slab output. These losses may vary from 4 to 50 % (Adlam 1950). These losses can be minimized by insulating the edges.

1.2.8.2 Proposed modifications to the ASHRAE Handbook guidelines

The guidelines provided in the *ASHRAE Handbook* provides design information for 33 cities in the United States. Its fundamental dependence on the snowfall frequency analysis makes it unsuitable for other locations. Also comparison of the design data does not match well with installed systems. A study conducted by Kilkis (1994), suggested modifications to the existing guidelines, to develop a simple and universal technique, that was not as dependent on detailed meteorological data. This new method required

- Design air temperature
- Wind speed
- Maximum recorded daily snowfall

The ASHRAE guidelines make use of the rate of snowfall. However this data is available only for selected locations. An expression is developed to determine the design rate of snowfall (s') for other locations

$$s' = (SF/24) * C * (\Omega / 62.4) \quad (1.8)$$

where

SF = Maximum recorded snowfall in 24 hours (in. of snow). The SF values have been compiled from Adlam's (1950) studies, which reflect the U.S. Weather Bureau data.

C = Snow melting performance class (dimensionless)

Ω = Density of snow (lb/ft^3)

Ω depends on the air temperature. A correlation given by using meteorological data from Adlam:

$$\Omega = 2.6 + 0.06* t_a + 0.0027* t_a^2 \quad (1.9)$$

In Equation (6) q_h does not recognize the different contributions due to radiation and convection losses. A better approach would be to use different expressions for these different modes of heat loss. Using the equations developed by Williams (1976) we obtain:

$$q_h = q_r + q_c \quad (1.10)$$

where

q_r = Radiant heat loss ($Btu/hr.\ ft^2$),

for cloudy skies,

$$q_r = 10.3 + 8.14*10^{-10}*[(t_f + t_a) + 920]^3*(t_f - t_a) - 7.68*10^{-10}*[255.2 + t_a/1.8]^4 \quad (1.11)$$

for clear skies,

$$q_r = 30.15 + 0.74*(t_f - t_a) \quad (1.12)$$

and q_c = Convective heat loss ($Btu/hr.\ ft^2$), given by

$$q_c = (0.14*V + 0.39) *(t_f - t_a) \quad (1.13)$$

Instead of using the air temperature obtained by the snowfall frequency, as in the ASHRAE guidelines, the design air temperature is used. However, this temperature does not coincide with the air temperature during actual snowfall. A simplistic expression has been derived to determine the coincident air temperature (t_c) during the snowfall by making use of the design air temperature.

$$t_c = t_b + \frac{(33 - t_b)}{(0.1 + 1.2 * C)} \quad (1.14)$$

where

t_b = Design air temperature at 97.5% frequency level (°F)

C = Snow melting class

The evaporative heat load intensity (q_e) can be predicted in terms of the convective heat load intensity (Williams 1976):

$$q_e = q_c / R* (p_s - p_{av}) / (t_f - t_a) \quad (1.15)$$

where

$$R = 0.01* p_a / 29.9 \quad (1.16)$$

R = Bowen's ratio (in. Hg/ °F)

p_a = atmospheric pressure (in. Hg)

Heat requirement after snowfall

The previous discussions have dealt with calculating the heat load intensity to melt snow, during snowfall. However for classes 1 and 2, there remains some snow to be melted even after the snowfall. Frequently, a low air

temperature follows the snowfall, and the sky may clear (Adlam 1950; Williamson 1967). This may lead to an increase in the snow melting heat load intensity, despite the absence of fusion and sensible heat loads. In these cases, the design heat load will be the post snowfall heat load (q_{oa}).

i.e.

$$q_o = q_{oa} \text{ if } q_{oa} > q_o \qquad (1.17)$$

The same equations are used for calculating q_{oa} as were used for q_o, with the corresponding weather data after the snowfall period.

Algorithm for calculating design heat load for snow melting

Making use of all the equations derived for the different stages of snow melting, an algorithm was proposed to calculate the design heat load for such systems (Kilkis, 1994). Table 1 outlines the algorithm.

LOAD INTENSITIES			PERFORMANCE CLASS			COMMENTS
			1	2	3	
SNOW MELTING	q_s		Eqn. 1.4	Eqn. 1.4	Eqn. 1.4	$t_a = t_c$ (Eqn. 1.14)
	q_m		Eqn. 1.5	Eqn. 1.5	Eqn. 1.5	s = s'(Eqns. 1.8,1.9)
	q_e		-	Eqn. 1.15	Eqn. 1.15	Adjust the wind speed.
	q_h	q_r	-	Eqn.1.11	Eqn.1.11	$q_h = q_r + q_c$
		q_c	-	Eqn.1.13	Eqn.1.13	
PHASE	q_o		$q_s + q_m$	$q_s + q_m$ +0.5 (q_e+q_h)	$q_s + q_m$ $+q_e + q_h$	In class 1, if $q_h > qm + qs$ then qo = qh. In class 2, if qh>qm+qs +0.5(qe + qh) then qo=qh
AFTER SNOW PERIOD	q_{ea}		Eqn.1.15	Eqn.1.15	Eqn.1.15	$t_a = t_b$
	q_{ha}	q_{ra}	Eqn.1.11	Eqn.1.11	0	$q_{ha} = q_{ra} + q_{ca}$
		q_{ca}	Eqn.1.13	Eqn.1.13	0	$t_a = t_b$
	q_{oa}		$q_{ea} + q_{ha}$	$q_{ea} + q_{ha}$	0	
IDLING	q_i		Eqn.1.1	Eqn.1.1	Eqn.1.1	$t_a = t_m$
DESIGN	q_y		$q_y > q_o$ or $q_y = q_o$			if $q_i > q_o$ and q_{oa}; $q_y > q_i$ if $q_{oa} > q_i$ and q_o; $q_y > q_{oa}$

TABLE 1
Proposed Algorithm for snow melting load calculations

1.3 Objectives

The objectives of the project were the following:

1. Build a test setup of an active ground source heat pump system, to prevent the ice formation on a concrete slab representative of a section of a bridge deck.
2. To investigate the thermal performance of the test setup and establish the feasibility of using such a deicing system.
3. Determine the heat requirements of the system to melt ice on the concrete surface.
4. Develop a finite difference model of the concrete slab and validate it by using experimental data from the test set-up and weather data from the Oklahoma weather station or the 'Mesonet'.

2. Experimental Facility and Instrumentation

2.1 Overview

A prototype of an active ground source heat pump system has been built to investigate the feasibility of deicing a small scale model of a bridge deck. Fig 2.1 depicts the layout of the different components of the experimental facility. The main constituents of the test set up are :

1.A 10 foot by 3 foot by 8 inch concrete slab representing a section of a bridge deck with embedded hydronic tubing
2.A water to water heat pump
3.The ground loop heat exchanger
4.The bridge loop
5.Instrumentation

The heat pump transfers heat from the ground loop heat exchanger to the bridge deck piping embedded in the bridge deck. The data acquisition equipment is used to monitor various parameters during the course of the experiment and records data onto a personal computer in real time.

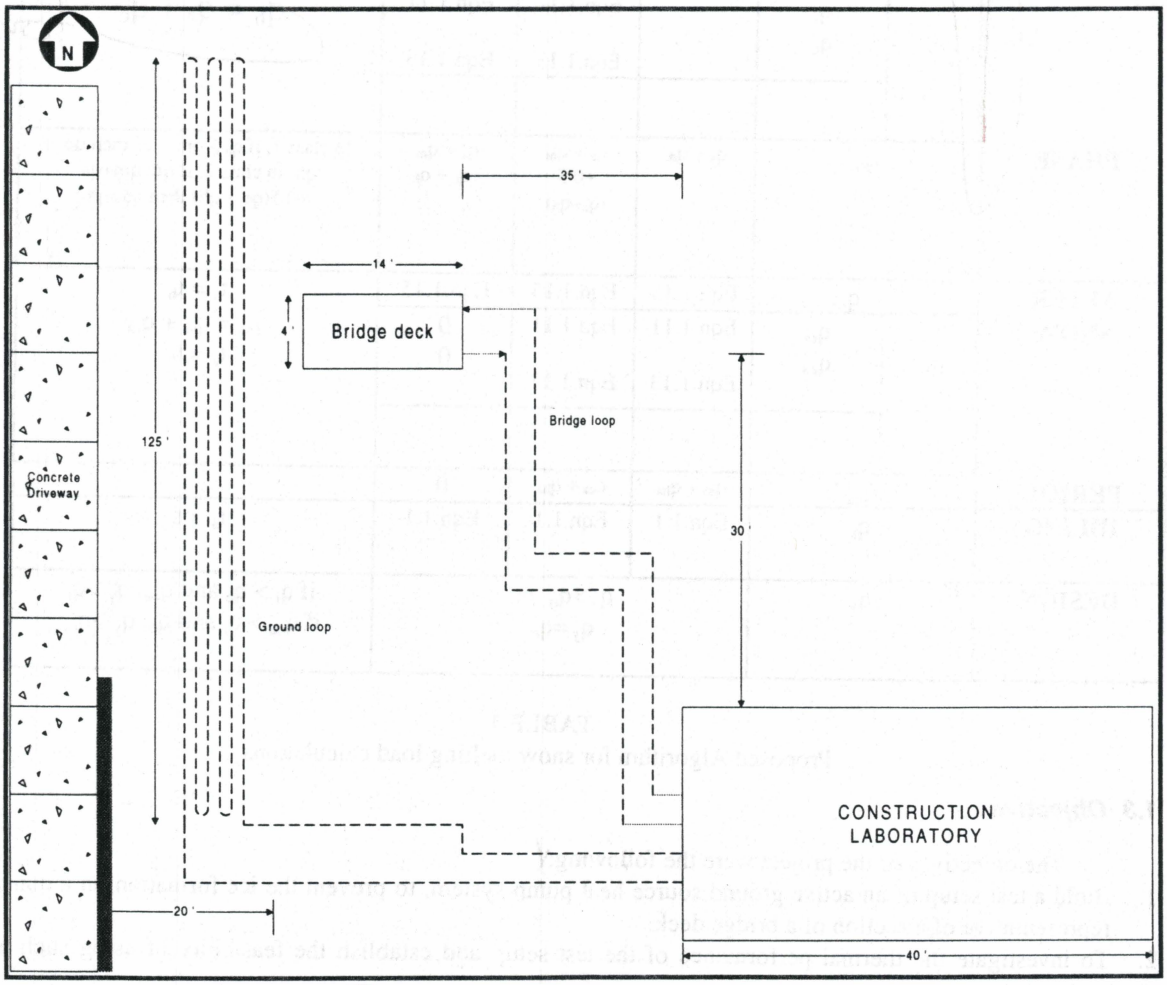

Figure 2.1: Schematic representation of the experimental layout

2.2 Experimental Facility

2.2.1 The Bridge deck section

The bridge deck test section is shown in Figure 2.2. It is placed in the open, for providing actual weather conditions, like radiation to the sky, etc. A scaffolding has been built on the side for easy access to the top surface of the slab. A steel frame has been built to support and raise the slab to a height of 7 feet above the ground.

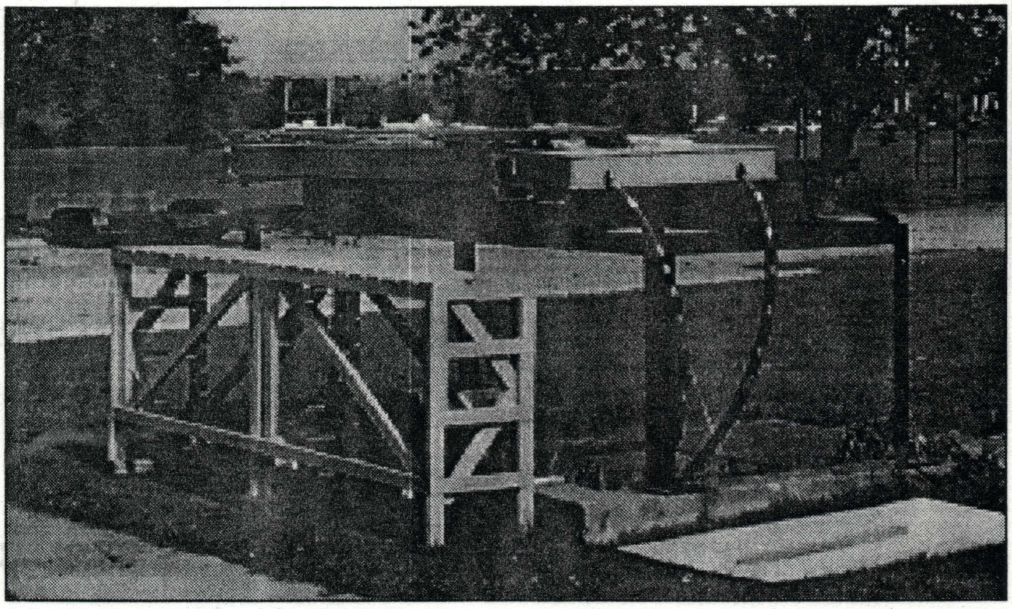

Figure 2.2 The experimental bridge deck section

2.2.1.1 The slab

Figure 2.3 shows the bridge deck section and all its construction details.

The Concrete slab:- The test section is an 8 inch thick, 3 foot by 10 foot concrete slab. The 10 foot length is one fourth of a typical roadway width of 40 feet. The 3 foot width is designed to accommodate six embedded pipes at equal spacing of 6.5 inches from each other. The 8 in. thickness is typical of an actual concrete bridge deck. The slab is made of Portland cement concrete, rock aggregates and sand. Rebar is present in the slab to reinforce the slab. A detailed description of the structural details is given by Liao (1996).

Pipes:- Six, polybutylene pipes, each 10 feet long with ¾ inch nominal diameter are embedded in the slab at a depth of 2.5 inches from the surface. The pipes centers are equally spaced from each other at 6.5 inches. The fluid inlet and outlet pipes are at a distance of 1.75 inches from the ends of the slab. The pipes have been connected to each other by 'U' shaped rubber tubing. This forms a continuous loop heat exchanger within the slab. The rubber tubing has been used instead of welded plastic joints to allow greater flexibility in changing the flow configurations for future work. Pressure/Temperature ports ('Pete's ports') have been inserted into the piping at the inlet and outlet of the slab. Fluid inlet and outlet temperatures are measured with thermocouple probes inserted into these ports.

Frame:-A wooden frame has been built around the slab to enclose the peripheral insulation and house the piping at the two ends of the slab. The pipe housing at the two ends has been provided with removable covers with handles for easy access to the insulated pipe ends. The frame has been painted to weatherproof it.

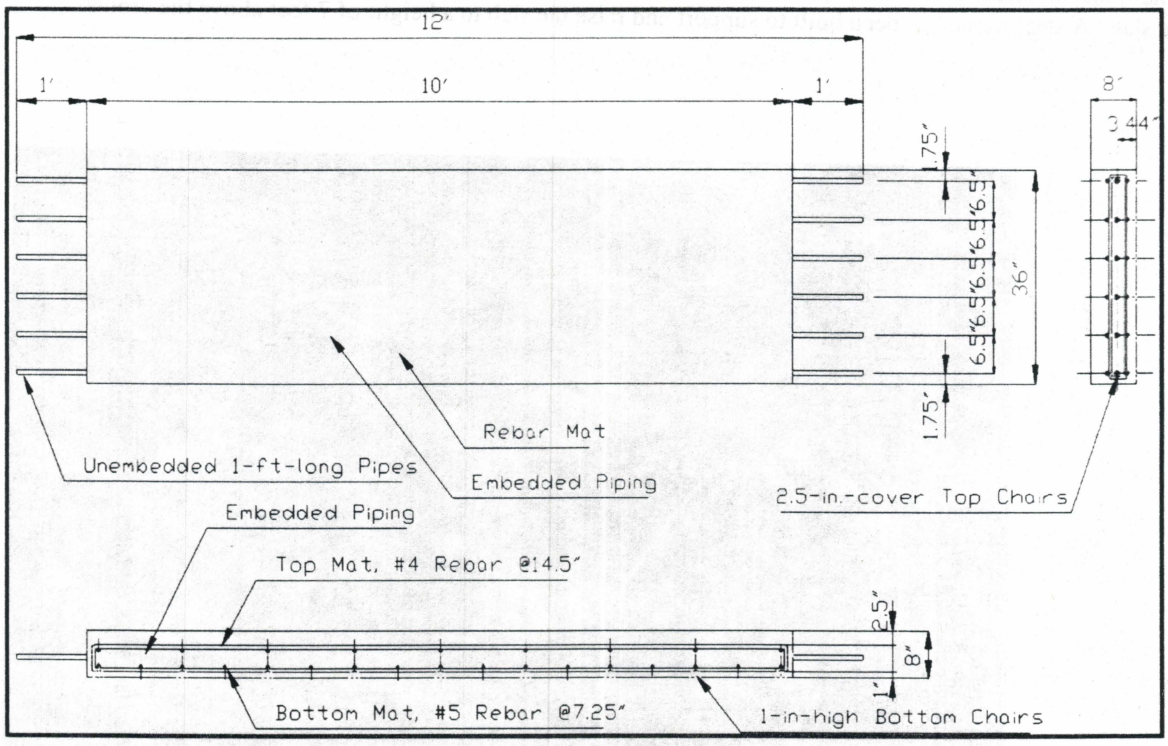

Figure 2.3: Constructional details of the slab

2.2.1.2 Insulation

The slab has been insulated on all four sides minimize edge losses thereby allowing the test bridge deck to represent the mid section of a bridge deck (Fig 2.4). This assumes that the mid-section of a bridge deck has negligible horizontal heat transfer, and the primary mode of heat conduction is longitudinal. The 10 foot long sides are insulated by 6 inches of Styrofoam. The 3 foot sides are insulated by 1 inch of Styrofoam insulation. The insulation used was Dow Styrofoam sheets with an R value of 5. A 1 inch thickness of the Dow Styrofoam was used to insulate the slab bottom for certain experimental configurations.

Each of the polybutylene and rubber pipe loops is individually insulated with wrap around insulation for pipes. The insulation was then kept in place with duct tape. The entire pipe housing at the two ends has been filled with 'bead' foam insulation.

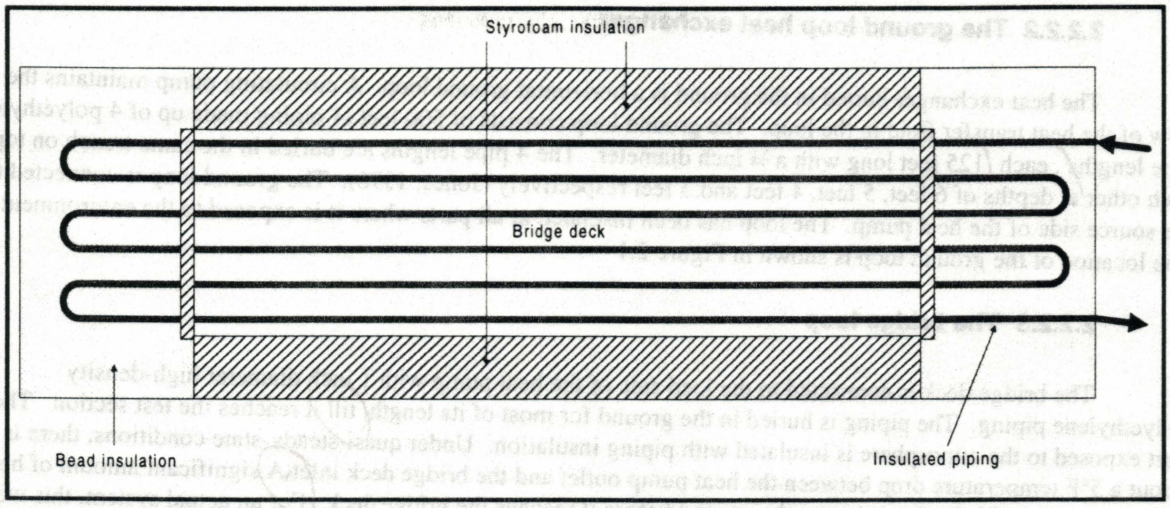

Figure 2.4: Schematic representation of slab insulation and piping

2.2.2 The Ground Source Heat pump system

2.2.2.1 The heat pump

Initially a water to water heat pump of 36,000 Btu/hr nominal capacity was connected to the system. After a few test runs, this heat pump was found to be too large. The heat pump raised the fluid temperature so high that the high temperature cut off was activated and the heat pump cut itself off during the test runs. An additional load of an air handler was connected downstream to offset the excess heat being produced by the heat pump. This, however lead to complications involving the fractions of the heat produced being diverted to the slab and the air handler. The problem was solved by installing a new lower capacity heat pump.

The present heat pump in use is a water to water heat pump with a nominal capacity of 18,000 Btu/hr. It uses the ground as its source and the test bridge deck section as its heating load Pressure and temperature controls installed in the heat pump prevent the overloading of the system. However, no other controls have been utilized. Generally, the operation of a heat pump used in this application would be controlled with a thermostat, perhaps with a temperature sensor mounted in the pavement. However for these initial experiments, a continuous heating process was desired, so as to simplify the interpretation of the experimental results.

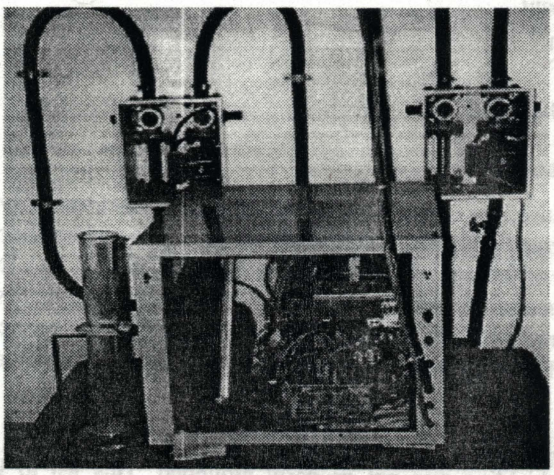

Figure 2.5 The heat pump

2.2.2.2 The ground loop heat exchanger

The heat exchanger buried in the ground is a horizontal ground loop. A circulating pump maintains the flow of the heat transfer fluid in the loop. The ground loop consists of 500 feet of piping made up of 4 polyethylene pipe lengths, each 125 feet long with a ¾ inch diameter. The 4 pipe lengths are buried in the same trench on top of each other at depths of 6 feet, 5 feet, 4 feet and 3 feet respectively (Jones, 1996). The ground loop is connected to the source side of the heat pump. The loop has been insulated at all parts where it is exposed to the environment. The location of the ground loop is shown in Figure 2.1

2.2.2.3 The bridge loop

The bridge deck is connected to the load side of the heat pump with 1 inch diameter high-density polyethylene piping. The piping is buried in the ground for most of its length, till it reaches the test section. The part exposed to the atmosphere is insulated with piping insulation. Under quasi-steady-state conditions, there is about a 5°F temperature drop between the heat pump outlet and the bridge deck inlet. A significant amount of heat, approximately 8000 Btu/hr, is lost to the ground before it reaches the bridge deck. For an actual system, this would be undesirable. For the experimental system, it may be thought of as simulating a larger bridge deck. In any case, the temperatures are measured at the inlet and outlet of the bridge deck so that heat input to the test section may be calculated.

2.2.2.4 The Heat transfer fluid (GS-4™)

The heat transfer fluid circulated in the pipes is GS-4™. It is manufactured by Vanguard Plastics Inc. and is essentially a mixture of 50% potassium acetate and 50% water. It was developed at Oklahoma State University and is a low viscosity, environmentally safe antifreeze. Potassium acetate makes the solution biodegradable and non-hazardous. The GS-4™ is mixed with water to form the heat transfer solution being used. The amount of freeze protection required decides the percentage of GS-4™ added to water. The properties of the brine solution also change with the amount of GS-4™ being used. For the purpose of this project, a 40 percent by weight (33 percent by volume) solution of GS-4™ has been used. This ensures a freeze protection of 10°F.

2.3 Instrumentation

The instrumentation equipment being used is for the purpose of :-

1. Temperature measurement
2. Flow measurement
3. Data acquisition
4.

2.3.1 Temperature measurement

2.3.1.1 Temperature Sensors

The thermocouples used are constructed out of 20 gauge, shielded[1], T type thermocouple wire[2]. The thermocouple beads were formed using a thermocouple welder. The welded thermocouple junctions have been placed flush with the surface of the slab. This was achieved by grinding 1 inch long slits, parallel to the length of the embedded pipes, on the surface of the slab to a depth of approximately 0.2 inches. The thermocouple wire was inserted in the slits and covered with cement paste till it was flush with the surface. An attempt was made to obtain cement paste color close to that of the slab, so as to have a uniform absorbtivity across the slab surface. A total of

[1] Regrettably, the shielding was not properly grounded. This led to increased fluctuation in some of the temperature measurements due to EMF interference.

[2] T20-2-510 wire -manufactured by The Pelican Wire Company, Inc.

28[3] thermocouples have been placed on the top surface. 18 of these have been placed directly over the pipes transporting the fluid and 10 between the pipes on the top surface of the slab.

4 thermocouples have been attached to the bottom surface of the slab. Two of them are directly below the inlet and outlet pipes and the other two are between two adjacent pipes. A configuration of all the thermocouples has been depicted in Figure 2.6 along with the labeling system used. A diagram with the dimensioned locations is provided in the Appendix. All thermocouple locations on the top surface directly above the pipes are denoted by numbers (1,2,...,28) and those between the pipes are labeled with letters.(a,b,....j). Thermocouples on the slab bottom are labeled with numbers preceded by "bottom" (bottom1,....bottom4).

Two T-type thermocouple probes[4] have been inserted at the inlet and outlet of the bridge deck piping. In addition to measuring the inlet and outlet temperature, the probes are used to calculate the temperature drop in the fluid during its flow through the concrete slab. Two other similar probes have been connected to the input and output of the load side of the heat pump. This temperature measurement was used in a few experiments for calculating the temperature drop in the fluid due to its flow in the ground before it reaches the bridge deck and after it leaves the bridge deck and returns to the heat pump at the input side of the load section.

Two other thermocouple junctions are used to record the ambient air temperature and the ground temperature, just below the slab. The air temperature thermocouple is suspended below the slab surface; and was wrapped with aluminum foil which acted as a radiation shield. The thermocouple measuring the ground temperature is buried approximately ½ inch below ground level. All the temperature sensors were connected to a Fluke Hydra datalogger which recorded their output.

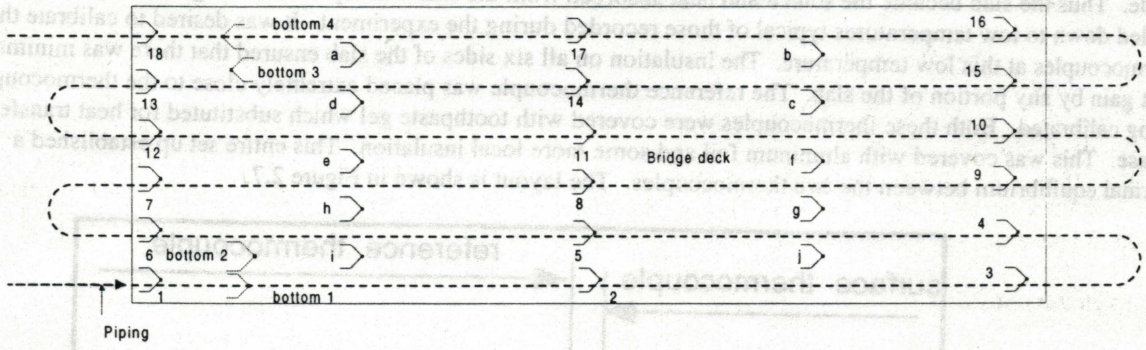

Figure 2.6:- Locations of the thermocouple junctions on the slab

2.3.1.2 Calibration

Calibration of reference thermocouple and thermocouple probes

The thermocouples have been calibrated with the aid of a reference thermocouple. The reference thermocouple and the thermocouple probes were calibrated by using the ice point and the boiling point of water as references. The reference thermocouple to be calibrated was placed along with a reference thermometer in an ice bath insulated on all sides. It is assumed that the reference thermometer is free of errors. After a while, thermal equilibrium was established between the thermocouple and the thermometer. At this point both the temperatures

[3] Not all themocouples were used at anyone time. Only 20 temperatures were measured in any one experiment.

[4] Manufactured by Omega Engineering Inc.

must be the same. The reference temperature was then adjusted with the help of the software incorporated in the data acquisition equipment. The reference thermocouple reading was offset by a factor of 'B' to coincide with the thermometer and the ice bath temperature of 0°C. This reference thermocouple and the thermometer were then elevated to the boiling point of water of 100°C in an insulated container. The reference thermocouple temperature reading was then multiplied by a factor 'M' to coincide with the temperature of the thermometer.

The same procedure was followed for the calibration of the thermocouple probes. Hence each of the temperature measurements are modified as:-

$T_{calibrated} = Mx + B$

where

x : Raw temperature reading of thermocouple or thermocouple probe.

B : Offset factor used to conform calibrated temperature to the ice point.

M : Multiplier factor used to conform calibrated temperature to the boiling point.

This concluded the initial calibration procedure.

The next stage of calibration consisted of calibrating each of the individual thermocouples on the surface of the test bridge deck. Ideally these thermocouples should also be calibrated as done for the thermocouple probes. However due to time constraints, with the cold weather front being unpredictable, these thermocouples were placed in position on the slab and the readings were obtained. Later, all the thermocouple readings were corrected for the thermocouples after their individual calibration.

Individual calibration procedure

The entire slab surface was insulated and the heat pump was reversed to operate in the cooling mode. Thus the slab became the source and heat absorbed from the slab was rejected to the ground. The slab was cooled down to low temperatures typical of those recorded during the experiment. It was desired to calibrate the thermocouples at this low temperature. The insulation on all six sides of the slab ensured that there was minimal heat gain by any portion of the slab. The reference thermocouple was placed extremely close to the thermocouple being calibrated. Both these thermocouples were covered with toothpaste gel which substituted for heat transfer grease. This was covered with aluminum foil and some more local insulation. This entire set up established a thermal equilibrium between the two thermocouples. The layout is shown in Figure 2.7.

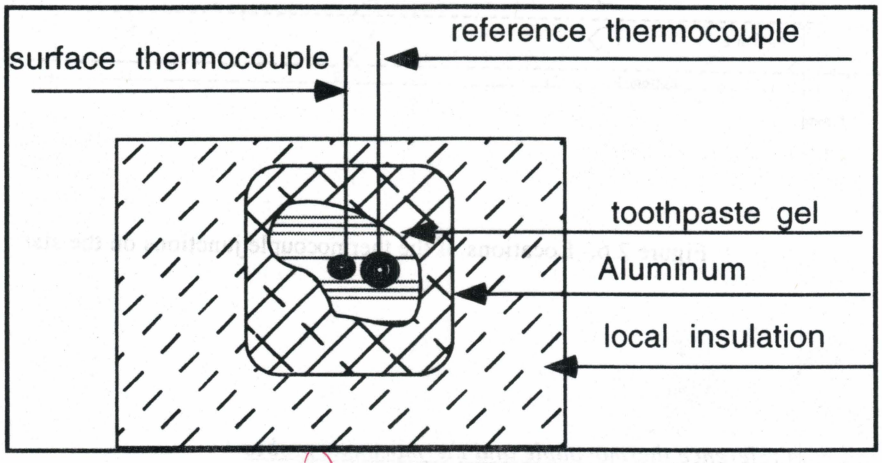

Figure 2.7:- Surface thermocouple calibration

After the thermocouples had achieved equilibrium, readings were recorded for a period of one hour. The thermocouple being calibrated was offset by the constant difference observed between the two thermocouples. This conformed it to the reference thermocouple. This completed the calibration procedure for the thermocouple. The same procedure was carried out for all the surface thermocouples. After each of the thermocouples was calibrated, the readings taken previously were corrected using the individual calibration offsets.

2.3.2 Flow measurement

The flow measurement was done by a flowmeter. The flowmeter was located upstream of the bridge loop. It measured the flowrate of GS-4 flowing through the bridge deck.

2.3.2.1 The flowmeter

The flowmeter used is a turbine flowmeter[5]. A turbine flowmeter was preferred as it is simple, durable and provides good accuracy at a comparatively low cost. It provides a convenient pulse output which can be converted into the required output by a signal conditioner. The rated accuracy of the flowmeter is ±0.5% of the reading.

The flowmeter was installed with 4 feet of piping at its inlet side and 3 feet of piping at its outlet. For the ¾ inch nominal diameter pipe, this corresponds to approximately 65 pipe diameters upstream and 50 pipe diameters downstream. These dimensions are within the requirements of the flowmeter for providing a uniform flow at the turbine wheel.

The pulse output was picked up by an integrally mounted signal conditioner. This conditioner amplified the sensor output and converted it into a high level output which could be used by the data acquisition system. This output was less likely to be affected by ambient conditions, like an electronically noisy environment. The signal conditioner used for this project provided a 0-5 V dc output.

2.3.2.2 Calibration of the flowmeter.

Bucket and stopwatch method

The principle difficulty in calibrating the flowmeter was that the fluid used was not water (The flowmeter is provided with calibration curves for water), and the fluid temperature changed during experimentation which changed the fluid properties. The calibration of the flowmeter was accomplished by the "bucket and stop watch method" (Figure 2.8). The system plumbing was reconnected to travel through a "purge tank". In this system, the fluid returns through the purge tank. The return flow can be diverted from the open purge tank into an open bucket without disturbing the flow rate. The flow was diverted into a bucket for a fixed time interval, then the fluid collected was weighed on a balance scale. Simultaneously, voltage output from the flow meter was recorded at one second intervals. A simple average of these readings obtained in terms of dc volts was calculated to minimize error. This reading corresponded to the flowrate of the fluid in gallons per minute calculated for that particular voltage output.

The maximum amount of flowrate of the fluid flowing to the bridge is limited by the capacity of the circulating pump. This was found to be approximately 4 gpm. The flowmeter can read flows from 2 gpm to 29.9 gpm. Using the 'SPAN' adjustment of the signal conditioner, the voltage output signal from the signal conditioner was set to read from 0 to 6 gpm corresponding to the range of the voltage output of 0 to 5 volts. Calibration was carried out for a range of fluid temperatures to obtain calibration curves for the fluid being used.

Typical calibration procedure

Since the viscosity of the GS-4/water mixture varied with temperature, it was necessary to calibrate the flowmeter over a range of flowrates and temperatures. The following calibration procedure was followed for each of the temperature ranges. The fluid was heated or cooled to the required temperature by running the heat pump in the heating or cooling mode. The purge tank was connected in the system. This tank was used to "bleed" the fluid to the bucket.

At the required temperature, the fluid was made to flow at full throttle. This fluid was diverted to the bucket and the stopwatch was started simultaneously. For a period of 2 minutes for low flows and 1.5 minutes for higher flows, the fluid was collected in buckets. At the end of the time duration, the fluid flow was diverted back to the purge tank. At the same time, the output of the flowmeter was recorded every second into a personal computer. The simple average of these outputs was taken as the constant output obtained at that particular flowrate. The fluid collected was carefully weighed on a balance and the amount of fluid flow was calculated in terms of gallons per

[5] model FTB-105 manufactured by Omega Engineering Inc.

minute (gpm). This flowrate corresponded to the voltage output recorded. The flow was then reduced by approximately 0.5 gpm and the procedure was repeated. As the flowmeter being used could not measure flows less than 2 gpm, the calibration was done for flows above that value. A plot of flowrate versus voltage output was made. This provided the calibration curve at the particular temperature. During the test runs, a flowrate of 3 - 4 gpm was maintained.

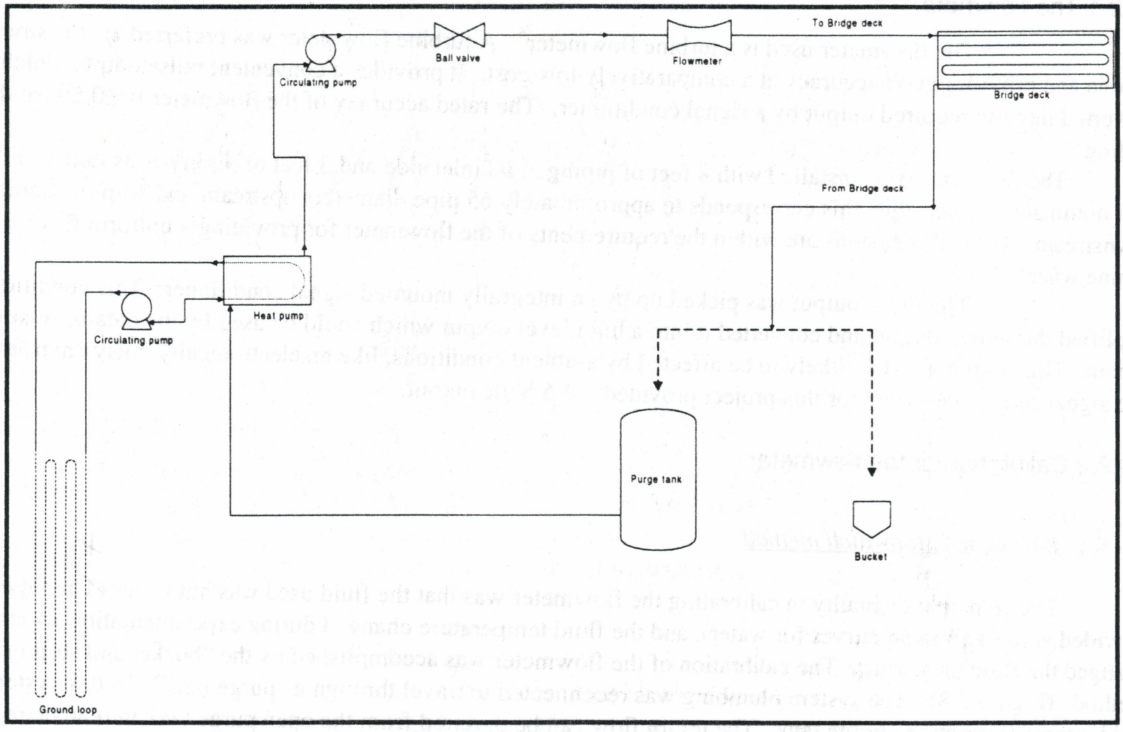

Figure 2.8:- Flow Calibration Schematic

2.3.3 Data Acquisition

The data acquisition equipment used are:-

1. A Fluke Hydra WL 2625A datalogger for the temperature measurement.
2. A DAS 800 board for the flow measurement.

2.3.3.1 Datalogger

The 2625A WL datalogger is a remote wireless data acquisition unit. It is placed at the site of the experimental bridge deck (as shown in the first Figure 2.1). The slab thermocouples and fluid thermocouple probes are connected to it. It has 21 input channels of which 20 are used. The 0^{th} channel is not being used as it does not support temperature measurement. Except for 2 channels which are connected to the inlet and outlet thermocouple probes, all the other working channels are connected to the surface thermocouples at various locations on the slab. A detailed analysis of the inputs to each of these channels is provided in section 3. The data are broadcast by a remote modem to a base modem connected to a microcomputer by a RS-232 cable. The data are received and are recorded onto a file.

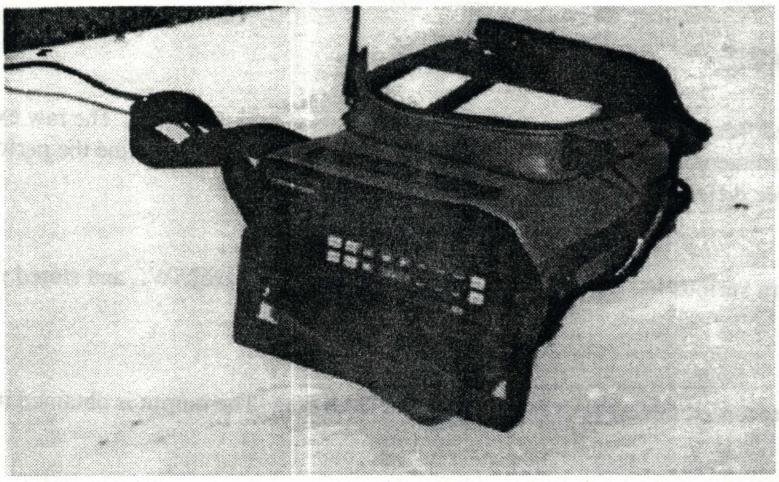

Figure 2.9:- The 2625 WL datalogger

Wireless logger for Windows™ software

The raw data received from the Hydra is handled by the wireless logger software. The software is also used to configure each of the individual channels before downloading the data. It can be used to modify the following parameters of data acquisition.

1. Channel input type (thermocouple, voltage, resistance, etc.)
2. Data scan interval
3. Enable file recording
4. Name of file to be used
5. Mx +B factor (used for thermocouple calibration)
6. Measurement rate (slow / fast)
7. Communication parameters (modem speed, address, etc.)

The software can be used to obtain real time plots. The data file can later be viewed by using any spreadsheet package.

2.3.3.2 DAS 800

The flowmeter voltage output was measured by another microcomputer with a DAS 800 board in it. This board was also used for strain measurements[6] made on the bridge deck. The output of the flowmeter is in dc volts. The output terminals of the flowmeter were connected to the DAS 800 board. The output data was not stored but was recorded manually at intervals.

[6] These measurements are made for a parallel experiment being carried out on the same test set-up, for analyzing thermal stresses in the slab due to the flow of hot fluid through it (Liao., 1996).

3. DATA ANALYSIS

Data obtained from three different sources have been used in this project. The raw experimental data obtained from the instrumentation is used to calculate derived quantities to determine the performance of the bridge deck system. The three different sources are described below.

1.Datalogger data
Temperature data from various locations on the slab are recorded by the 2625WL and stored in real time on the personal computer.

2.DAS 800 data
Flowmeter output is recorded manually at intervals by the DAS 800. The output is obtained in terms of volts.

3.'Mesonet' data
The weather data was downloaded via the campus network from the Oklahoma 'Mesonet' Internet site.

3.1 Datalogger data

The following raw data were obtained for most tests using the datalogger:

1. Thermocouple measurements of eight slab surface locations just above the embedded pipes.
2. Thermocouple measurements of four slab surface locations between the embedded pipes.
3. Thermocouple measurements of four slab surface locations on the bottom surface of the slab.
4. Two thermal probe measurements of the inlet and outlet temperature of the fluid flowing through the slab.
5. One thermocouple to measure the air temperature.
6. One thermocouple to measure the ground temperature.

This totals 20 temperature measurements (°F) from the datalogger.

3.2 DAS 800

The DAS 800 displays the flowmeter voltage output (volts). This datum was noted at irregular intervals. Note: The DAS 800 board can be programmed to receive data at regular intervals and record it into a file. Regrettably this facility was not used during experimentation, and the flowrate datum was manually noted at irregular intervals. Hence the flowrate used in the calculations is an average for large intervals during experimentation, and not the actual flowrate for smaller regular intervals, (as in the case of the datalogger data). This leads to an increased error in the calculations of the derived quantities.

3.3 'Mesonet' data

The 'Mesonet' is the weather station project in Oklahoma. A total of 108 stations across the state monitor various parameters of the weather continuously. The station in Stillwater is very close to the experimental site and its data is assumed to be the same as that at the site. The weather data is downloaded using the OSU campus network from the 'Mesonet' site for the different days. The parameters of interest are

1. Air temperature (°F)
2. Wind direction (degrees from North)
3. Wind speed (m/sec)
4. Solar radiation (W/m^2)
5. Relative humidity (%)
6. Precipitation (inches of water)

These data are available from the weather station at intervals of 15 minutes, and are used as inputs to the computer model.

3.4 Computation of the derived quantities

The data are compiled and analyzed on the basis of the days on which they were recorded. The data have been recorded at 5 minutes intervals by the datalogger. both during and before the period of operation of the heat pump. The methodology for calculating the derived quantities used in the analysis is described in the following sections.

3.4.1 Average slab top surface temperature

The average slab top surface temperature has been calculated by using the slab temperature readings at various locations on the slab top surface. As the fluid flows through the slab, it transfers its heat to the slab thereby reducing in temperature. The areas of the slab just above the pipe have a higher temperature, than those between pipes. The slab temperature profile is depicted qualitatively in Figure 3.1.

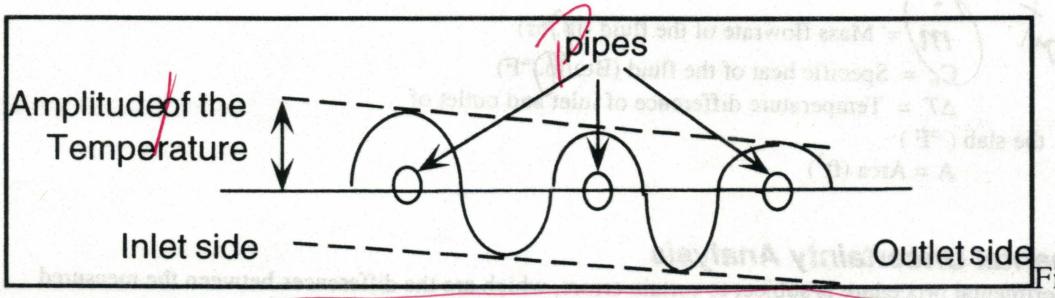

Figure 3.1:- Temperature profile at the slab cross section

The amplitude of the temperatures will vary as the fluid flows through the slab. At the inlet side the temperature is higher and reduces as the fluid flows through the system. A weighted average of the thermocouple readings has been taken for our purpose to depict the average surface temperature. The temperature has been averaged over the pipes and between the pipes separately, as an unequal number of thermocouples measurements were used to calculate the two separate averages.
Hence

$$T_{avg} = \frac{[T_{above} + T_{between}]}{2} \qquad (3.1)$$

where

T_{avg} = Average top slab temperature (°F)
T_{above} = Average top slab temperature for locations directly above pipes

$$T_{above} = \sum_{a=1}^{n} \frac{T_a}{n}$$

T_a = Thermocouple readings above pipes (°F)
n = number of readings made above pipes
$T_{between}$ = Average top slab temperature for locations between pipes

$$T_{between} = \sum_{b=1}^{m} \frac{T_b}{m}$$

T_b = Thermocouple readings between pipes(°F)
m = number of readings made between pipes

There were eight thermocouples on the pipe and four between the pipes. A plot of the average surface temperature and the ambient air has been made to see the rise in the slab temperature with time as the hot fluid

flowing through the slab transmits heat to it. The plots can be seen in the results section. The average slab surface temperature was used to determine the freezing condition of the surface along with a visual inspection.

3.4.2 Determination of the Heat flux

As the heated fluid flows through the slab, heat is conducted by the slab. This raises the temperature of the cold slab. The heat flux transmitted to the slab by the fluid can be calculated as

$$Q_{\text{input flux}} = \frac{\dot{m} * Cp * \Delta T}{A} \qquad (3.2)$$

Where

$Q_{\text{input flux}}$ = Heat flux to the slab by the fluid (Btu/hr/ft^2)

$\dot{m}$ = Mass flowrate of the fluid (lb./hr)

C_p = Specific heat of the fluid (Btu/lb./°F)

ΔT = Temperature difference of inlet and outlet of the slab (°F)

A = Area (ft^2)

3.5 Experimental Uncertainty Analysis

Any experimental procedure is subject to certain errors, which are the differences between the measured value and the actual value of a quantity. This difference may be due to a number of factors: instrument error, sensor error, sensor position error, human error, etc. For the complete study of any experimental procedure, an uncertainty analysis is necessary for a better understanding of the data. The uncertainty analysis done in this study follows the principles of Taylor [1982].

Uncertainty in experimental results can be of the following types:-

- Uncertainties in individual measurements, such as temperature measurement and flow measurement. These uncertainties are discussed in 3.5.1 through 3.5.4.
- Individual uncertainties may be further propagated by taking spatial averages, such as the average slab top surface temperature discussed in 3.5.6.
- Uncertainties are also propagated when individual measurement values are used to obtain derived quantities, such as the heat flux. This is discussed in 3.5.5.

Uncertainty can be expressed as a fraction of the measured quantity, or as an absolute value. In some cases, both may be used. A fractional uncertainty may be expressed as:-

$$e_X = \pm y\% \qquad (3.3)$$

where

X is the measured quantity

y% is the magnitude of the fractional uncertainty

Hence maximum and minimum values of X can are:

$$X_{max} = \overline{X} + y\% * \overline{X} \qquad (3.4)$$

$$X_{min} = \overline{X} - y\% * \overline{X} \qquad (3.5)$$

If expressed as an absolute term, the uncertainty is independent of the quantity being measured.

$$e_X = \pm z \qquad (3.6)$$

where z is the absolute uncertainty and has the same units as X.

Hence maximum and minimum values of X can are:

$$X_{max} = \overline{X} + z \qquad (3.7)$$

$$X_{min} = \overline{X} - z \qquad (3.8)$$

Some quantities may contain both, fractional and absolute uncertainties. These uncertainties can be represented as:

$$e_X = \pm y\% \pm z \qquad (3.9)$$

3.5.1 Uncertainties in temperature measurement for surface thermocouples

The temperatures measurements for the slab surface have been made using the 2625 A WL datalogger. This datalogger provides the reading in temperature units. The datalogger has an inherent error in measuring this temperature which is provided in its specifications as being ±0.6°C or 1.08°F. The thermocouple wire is a T type wire and may have its own inherent uncertainty. However as the thermocouples were calibrated (using the Mx+B feature), this uncertainty is accounted for. The calibration procedure of the individual surface thermocouples as described in section 2.3.1.2 itself is estimated to have an error of ±1°F. This is because many of the thermocouples made from the same wire had to be offset by different values at different temperatures with respect to the reference thermocouple. The calibration procedure was carried out at the typical low temperatures to minimize this error. For a typical temperature measurement the errors can be depicted as shown in Figure 3.2.

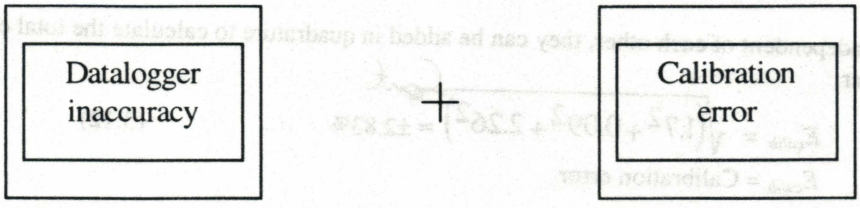

Figure 3.2:- Source of errors in temperature measurement

These errors are independent and random and can thus be added in quadrature to determine the total uncertainty in the measurement of temperature using the 2625A WL datalogger and the thermocouples. This is calculated as:

$$E_{temp} = \sqrt{(1.08^2 + 1^2)} \approx \pm 1.47°F \qquad (3.10)$$

3.5.2 Uncertainties in temperature measurement for thermocouples probes

The temperatures measurements for the inlet and outlet fluid temperatures have been made using the 2625 A WL datalogger. The calibration procedure used for the probes is direct and makes use of the ice point and the boiling point. As no intermediate reference thermocouple has been used, as in the previous case of the surface thermocouples, there is no uncertainty in the measurement due to calibration error. Hence the uncertainty for thermocouple probe measurement is only the datalogger error of ±1.08°F.

3.5.3 Uncertainty in the ΔT measurement

The temperature drop ΔT across the slab is used in the calculation of the heat input. ΔT was determined by using the measurements made by the thermocouple probes installed at the inlet and outlet of the concrete slab. Uncertainty in ΔT was determined directly by an experimental procedure.

The thermocouple probes were placed in an insulated vessel containing water at 95-100°F. This was the typical temperature measured by the inlet and outlet probes during experimentation. After equilibrium between the two probes was attained, the constant difference observed between the two probes was used as the uncertainty in measuring ΔT. Both the thermocouple probes had been adjusted with their respective Mx+B factors before readings were taken. The uncertainty thus obtained was 0.25 °F. Using the typical value of ΔT as 4°F, we obtain the fractional uncertainty as ±6.25%.

i.e. $$E_{\Delta T} = \pm 6.25\%. \qquad (3.11)$$

3.5.4 Uncertainties in flow measurement

The errors associated with the flow measurement are the errors in calibrating the flowmeter and the error due to the DAS 800. These errors give rise to an uncertainty in obtaining the flowrate in terms of gallons per minute for a voltage output. By following the calibration procedure for the flowmeter, we can identify the independent sources of error which contribute to the calibration error of the flowmeter.

While diverting the fluid when the stopwatch was started, it was observed that the fluid was not diverted exactly at the same time the stop watch started. Also some of the fluid spilt out at the time of switching buckets.

This lead to some mass error. During weighing the fluid on the balance there may be some error in balancing the scale. All these errors lead to an uncertainty due to the mass determination of the fluid. For simplicity all these errors were converted to a percentage value.

The maximum time by which the start or stop time was missed was approximately 0.25 seconds. Considering the typical value of the flowrate was measured as 4 gallons per minute, this corresponds to 280g/sec, or 70 g of lost fluid. If we include the error due to balance and the fluid spilt out as 100 g total, we can estimate the total value of lost fluid or excess fluid to be 170g/sec. For a typical weight of a bucket being 10 kg or 10,000 g, this error equals ±1.7%. The error due to the datalogger is given as 0.09%.

During calibration the voltage fluctuated for a given flowrate over the period it was recorded. An average value of this voltage was taken as the value corresponding to the mass of fluid measured. The voltage was observed to fluctuate by 0.034 volts (within ±2σ). For the minimum value measured for calibration of 1.5 volts, this gives an uncertainty of 2.26%.

As all these errors are independent of each other, they can be added in quadrature to calculate the total error in calibrating the flowmeter.

$$E_{calib} = \sqrt{\left(1.7^2 + 0.09^2 + 2.26^2\right)} \approx \pm 2.83\% \qquad (3.12)$$

where E_{calib} = Calibration error

3.5.5 Uncertainties in the heat flux

The heat flux is a derived quantity, and is calculated by using other quantities which have their own individual uncertainties.

The heat flux ($Q_{input\ flux}$) is given as:

$$Q_{input\ flux} = \frac{\dot{m} * Cp * \Delta T}{A} \qquad (3.13)$$

If we assume that area of the slab used has negligible error, then the error in the heat flux is given by

$$Q_{input\ flux} = \dot{m} * C_p * \Delta T \pm \sqrt{\left(E_{\dot{m}}^2 + E_{C_p}^2 + E_{\Delta T}^2\right)} \qquad (3.14)$$

where

$E_{\dot{m}}$ = Error in calculating mass flow rate
$E_{\Delta T}$ = Error in determining temperature drop
E_{Cp}= Error in calculating the specific heat.

Further

$$E_{\dot{m}} = \sqrt{\left(E_{gpm}^2 + E_{\rho}^2\right)} \qquad (3.15)$$

E_{gpm} = Error in calculating mass flow rate
E_{ρ} = Error due to difference in density due to inexact GS-4 quantity mixed with water.

E_{ρ} occurs because our calculation of mass flow rate in the heat flux equation assumes the specific density of GS-4 to be 1.11. The specific gravity of the fluid was measured with a hydrometer, which is presumed accurate to ±0.01, which corresponds to an error of 0.9%. The value of the specific gravity was used as an indicator, to obtain the corresponding concentration of the brine solution of 40% by . The specific heat was calculated by using the curve fit provided in the GS-4 manual. The uncertainty of ±0.01 for determining the specific gravity led to an error in obtaining the required solution concentration. This gave rise to the error in calculating the specific heat. Using the curve fit equations provided in the GS-4 manual, the uncertainty in obtaining C_p was calculated as ±1.29%.

E_{gpm} is the uncertainty due to the volumetric flow rate of the fluid. This quantity is obtained by reading the voltage output of the DAS 800 and using the calibration curve obtained before hand. The error in the DAS 800 is 0.01% and the calibration error as calculated before is ±2.83%. Another source of error arises due to the assumption that the voltage reading does not change considerably over the duration of the test. The observed maximum value by which

the voltage reading was observed to vary over a test period was 0.25 volts. For a reading for 4 volts at which the flow was held constant, this corresponds to an error of 6.3%.

Using the above values

$$E_{gpm} = \pm\sqrt{\left(0.01^2 + 2.83^2 + 6.3^2\right)} \approx \pm 6.9\ \% \qquad (3.16)$$

this gives us $E_{\dot{m}}$ as ±6.96%

$E_{\Delta T}$ is obtained from Equation 3.11 as ±6.25%

The heat flux can thus be calculated as

$$Q_{\text{input flux}} = \dot{m} * C_p * \Delta T \pm \sqrt{\left(6.96^2 + 6.25^2 + 1.29^2\right)} \qquad (3.17)$$

$$Q_{\text{input flux}} = \dot{m} * C_p * \Delta T \pm 9.44\% \qquad (3.18)$$

This gives the percentage uncertainty for determining the heat flux.

A plot of the heat flux, along with its range of uncertainty has been provided in the next chapter.

3.5.6 Uncertainties in the Average slab top surface temperature

The average slab temperature is calculated by using a weighted average of all the relevant thermocouples. The temperatures have been taken at different locations on the slab. Some of these are directly above the pipes on the slab and some have been placed in between the pipes.

Figure 2.6 shows the placement of the surface thermocouples. The temperatures on top of the slab will keep on decreasing as they get closer to the outlet. Figure 3.1 shows the variation of the temperature. An average of the slab surface temperatures does not take this aspect into account. This spatial average leads to an uncertainty in the value of the average slab temperature. Also each of the thermocouple measurements itself contain an uncertainty, as provided by Equation 3.10.

Hence

$$E_{T_{avg}} = \sqrt{\left(E_{temp}^2 + E_{spatial}^2\right)} \qquad (3.19)$$

All the top surface temperatures are found to be within ±2σ of the weighted average calculated.

Hence $E_{spatial}$ was taken as ±2σ. For the typical top surface temperature readings, we obtain

$$E_{spatial} = \pm 5°F \qquad (3.20)$$

Using Equation 3.19 we obtain the error in determining top surface slab temperature as

$$E_{T_{avg}} = \sqrt{\left(1.47^2 + 5^2\right)} = \pm 5.21°F \qquad (3.21)$$

4. Experimental Results

4.1 Overview of experiments performed

The major portion of the experiments were performed during the month of March. Tests began during the last week of February and continued through the month of March and first week of April. Only a few days had temperatures below freezing during this period. Results have hence been presented only for cold nights with air temperatures close to, or below freezing. The low temperatures occurred at night and most of the tests were hence run at night. Also, at night there is no additional heat gain by the slab due to the solar radiation and hence the total potential of this bridge deck deicing system could be tested.

Unfortunately there was no natural freezing precipitation during the test period, nor was there any snowfall. To study the effects of precipitation, it was necessary to make use of an artificial system of producing even precipitation. A hand held bottle spray was used to create a fine mist, which was sprayed at intervals on the slab.

The tests were carried out every night independent of the previous night's test. Each test typically started late at night and continued till early the next morning. In many cases the slab did not cool down from the preceding night's test run to the ambient temperature, before the start of the next test. In such cases, the slab was already preheated, especially the interior of the slab. An initial temperature profile across the cross section of the slab existed before the heat pump was started. During the duration of the entire test period, of approximately one month, the sunrise generally occurred between 6.30 am to 7.00 am in the morning. It was desired to observe the time required for slab temperature to rise above freezing before sunrise, so as to minimize the effect of solar radiation. For most of the cold nights, the average slab surface temperature rose above the freeze line of 32 °F only after sunrise. For three test days presented, the ambient temperature was above freezing, and the deck did not freeze.

Each test run was analyzed independent of the previous night's test. Slight difference in configurations were made for some test runs. The different experimental configurations consisted of:

- bottom of slab insulated or un-insulated
- precipitation applied to the slab surface
- different start times of test runs

4.2 Summary of experimental results

The results obtained for the different nights have been summarized in Table 4.1. The individual results for each night are discussed in the following sections.

	Feb. 28-29	Mar 1-2	Mar 6-7	Mar 7-8
Bottom insulated	No	Yes	Yes	Yes
Precipitation	No	Yes	Yes	Yes
Start time of heat pump	10.30 p.m.	3.15 am	12.00 am	11.30 p.m.
Average air temperature	23	37	16	13
Average slab temp. before start of test (°F)	26	35	23	23
Time to raise slab temp above freezing (hr.)	2.2	N/A	9	10
Average heat input (Btu/hr/ft^2)	195	179	195	197

	Mar 8-9	Mar 9-10	Mar 19-20	Mar 24-25
Bottom insulated	Yes	Yes	Yes	Yes
Precipitation	Yes	No	No	No
Start time of heat pump	3.10 am	2.30 am	12.00 am	8.20 p.m.
Average air temperature	22	36	29	24
Average slab temp. before start of test (°F)	28	39	32	35
Time to raise slab temp above freezing (hr.)	2.5	N/A	N/A	N/A
Average heat input (Btu/hr/ft^2)	205	163	198	181

TABLE 4.1:- Summary Of Experimental Results

4.3 Description of experiments

A brief description of each of the experiments has been provided in this section. Each test has been titled with the two dates between which it was run. An example title of a night's test results would be March 7th and 8th. This test was started on 7th night and continued till 8th morning. In more than one case the test has started after 12.00 am. However to maintain a standard, the same nomenclature has been followed.

A summary plot and a weather plot corresponding to each day has been included with each test day description. The plots provide an overview of the variation of all relevant parameters over the time period of each test. The plots have been made with the absolute time (CST) as the reference.

Summary Plot

The summary plot of each day contains the following information:

- Inlet fluid temperature to the slab (°F)
- Outlet fluid temperature from the slab (°F)
- Heat flux into the slab due to the flow of heated fluid. (Btu/hr.ft^2)
- The Air temperature through the night (°F)
- The Average slab upper surface temperature through the night (°F)

The sudden rise in the heat flux and inlet and outlet fluid temperatures in the plots indicates the start of the heat pump. The heat input in the slab starts to reduce as the test progresses. As the temperature of the slab rises, less heat from the fluid is input to the slab, thereby reducing the input flux. As a reference, a "freeze line" at 32°F, indicates when the slab surface temperature rose above freezing and the time required for this temperature to climb above the freezing temperature. The time at which the sunrise took place has also been provided. Where it is relevant, a note describing the precipitation applied is included in the summary plots. The air temperature is an indication of the ambient conditions. An extremely low air temperature increases the amount of time required for the slab temperature to rise above 32°F. Precipitation in the form of an even mist was added for some tests. For the nights with freezing low temperatures, an ice layer formed on the slab surface. The heat pump was run throughout the night, and shut off only after sunrise. In most cases, the slab top surface temperature rose above freezing only after sunrise with additional solar radiation.

Weather plot

The summary plot of each day contains the following information:

- solar radiation (W / m^2) and
- Wind speed (m / sec)

The solar radiation indicates the time sunrise took place, and the amount of solar radiation. For most tests it is quite relevant, as the solar radiation was responsible for raising slab top temperature above freezing. The wind speed affects the surrounding air temperature by adding an additional 'chill factor', thereby reducing the air temperature to lower values. The weather information was downloaded from the Oklahoma "Mesonet". The weather information is obtained every 15 minutes as compared to the 5 minute recording of the datalogger used for the summary plots.

4.3.1 Individual test days

Descriptions of the tests run for individual days has been provided. Most of the tests were carried out under almost identical conditions, with some minor configuration changes.

4.3.1.1 Day 1 (February 28th and 29th)

The bottom of the slab was left un-insulated. The test was run with precipitation applied every 30 minutes. There was some ice formation and subsequent melting of the ice after the heat pump was started. However because of the decreasing ambient temperature and the constant rate of precipitation, the ice did not melt on all parts of the slab surface till after sunrise. This was the first test and the amount of precipitation was not recorded as the spray effectiveness was being tested. The spike in the heat flux at 4.00 a.m. indicates a drop in inlet fluid temperature.

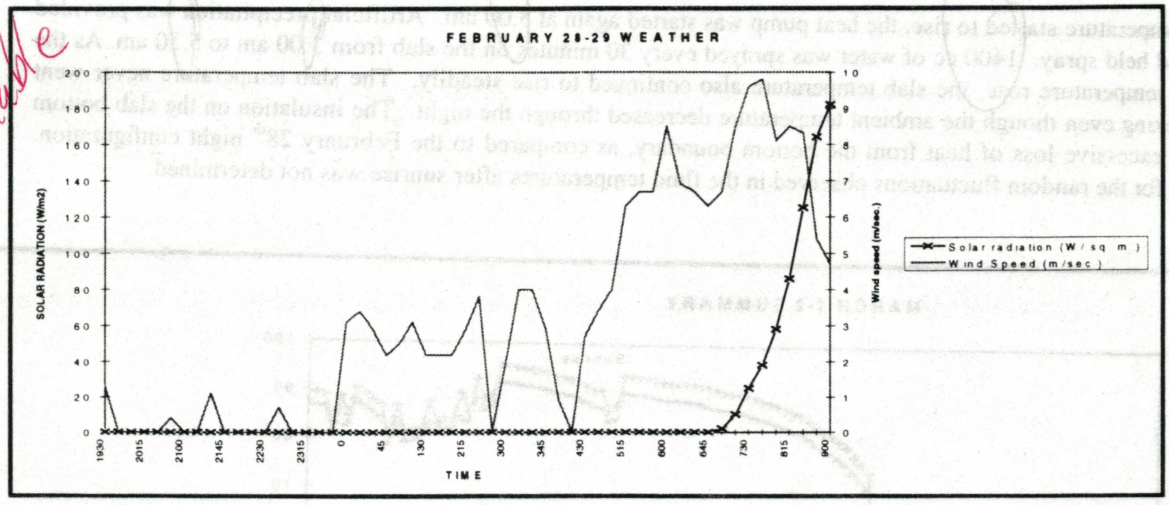

FIGURE 4.1:- Weather Plot for February 28 -29th.

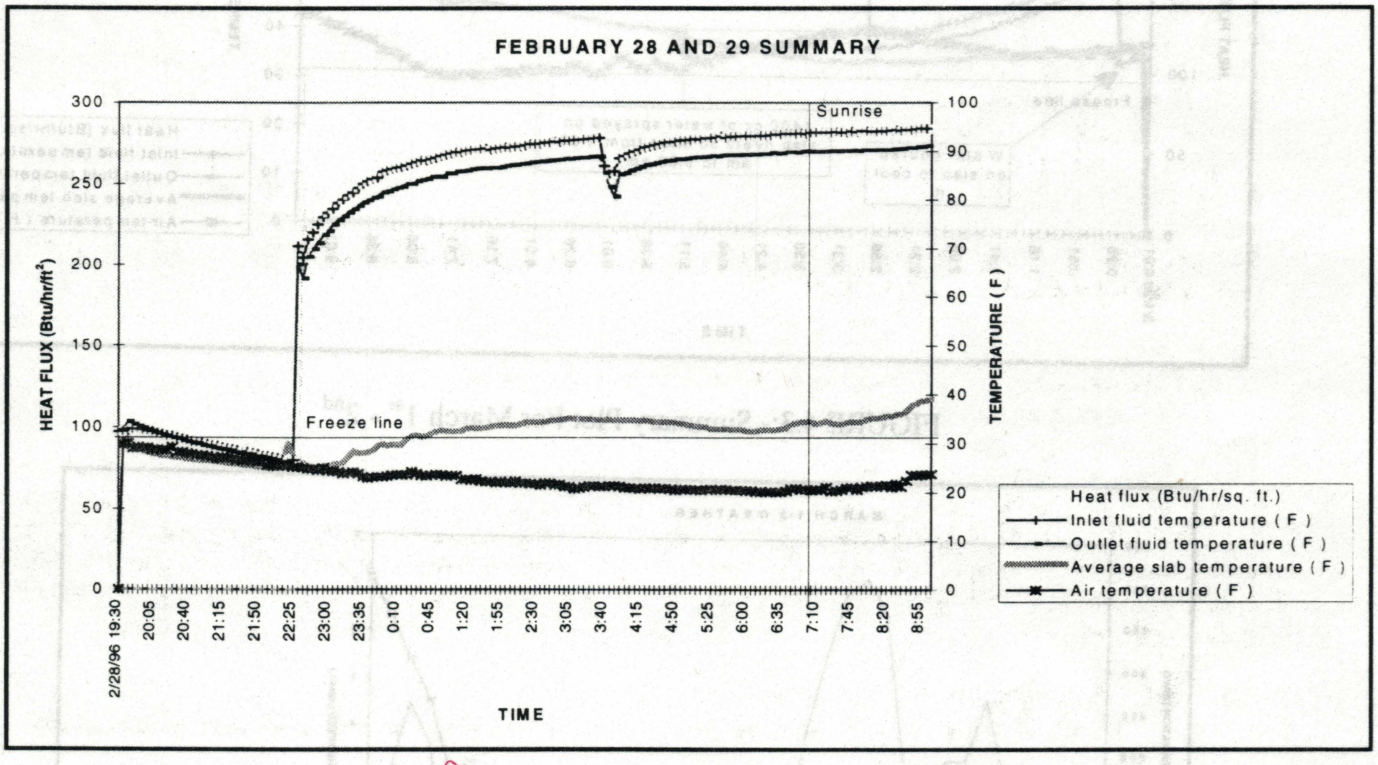

FIGURE 4.2:- Summary Plot For February 28 - 29th

4.3.1.2 Day 2 (March 1st and 2nd)

The bottom of the slab was insulated. All the tests done after this day were carried out with the bottom surface insulated. The weather forecast predicted freezing air temperatures for the night. However temperatures remained above 32°F until after sunrise. At 12.00 am, an attempt was made to cool the slab to the ambient temperature by pouring water on it. The heat pump was started initially at 12.30 am, but was then shut off instantly, to allow the slab to cool further. The slab was preheated due to running the test setup the previous night. As the

ambient temperature started to rise, the heat pump was started again at 3.00 am. Artificial precipitation was provided by the hand held spray. 1400 cc of water was sprayed every 30 minutes on the slab from 3.00 am to 5.30 am. As the inlet fluid temperature rose, the slab temperature also continued to rise steadily. The slab temperature never went below freezing even though the ambient temperature decreased through the night. The insulation on the slab bottom prevented excessive loss of heat from the bottom boundary, as compared to the February 28th night configuration. The cause for the random fluctuations observed in the fluid temperatures after sunrise was not determined.

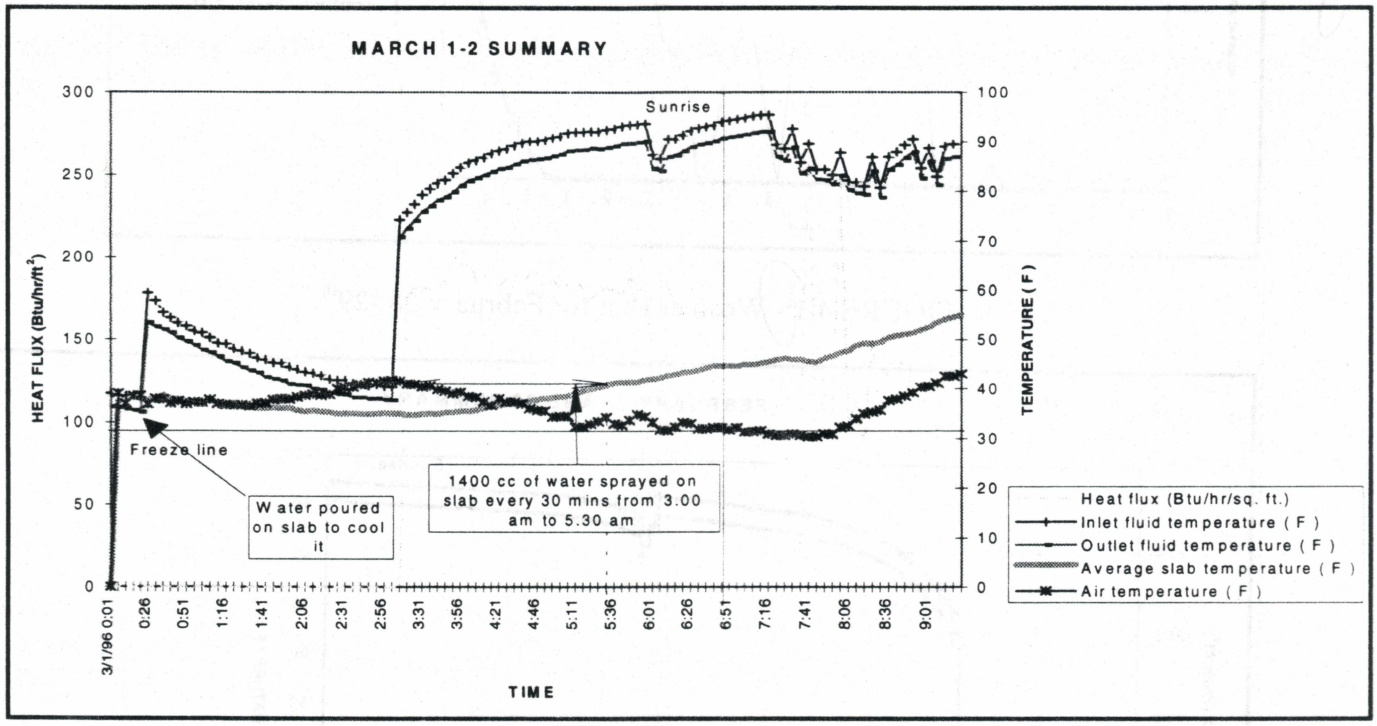

FIGURE 4.3:- Summary Plot For March 1st - 2nd

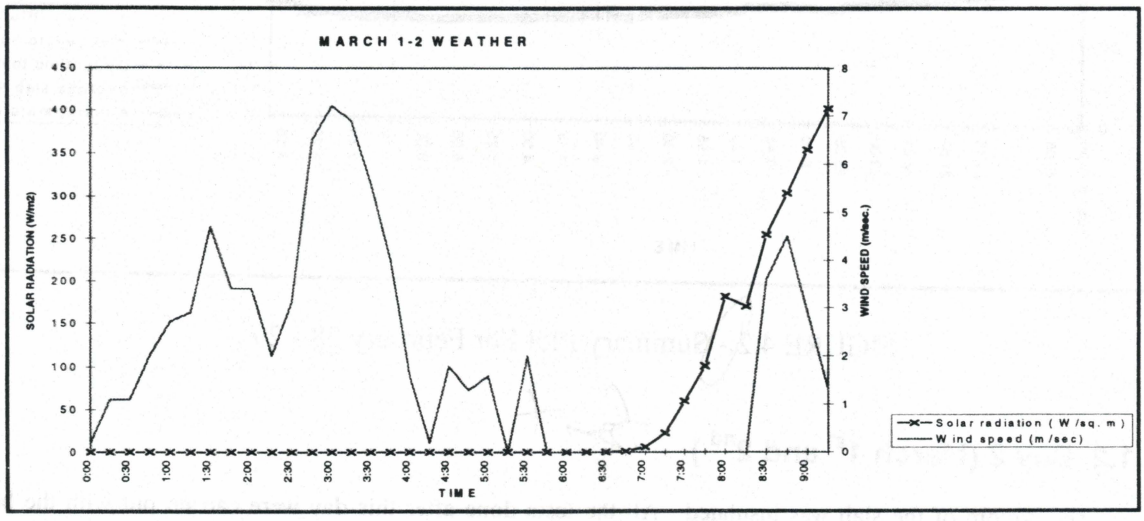

FIGURE 4.4:- Weather Plot For Test Run Of March 1st - 2nd

4.3.1.3 Day 3 (March 6th and 7th)

A low ambient temperature reduced the slab top surface temperature below freezing. Artificial precipitation (5000 cc of spray water) sprayed on the surface at 10.00 p.m. had formed a layer of ice on the slab. The heat pump was started at 12.00 am. One bottle (700 cc) of water was sprayed every 30 minutes after that till 4.00 am. The spikes observed in the slab temperature from 12.00 a.m. to 4.00 a.m. indicate the times slab was sprayed with water. The water temperature was considerably higher, relative to the slab surface temperature. As the surface was sprayed, the thermocouples on the surface were sprayed with this higher temperature water. The slab temperature did not rise above freezing throughout the night. The slab started to warm up only later in the morning after 9.00 am.

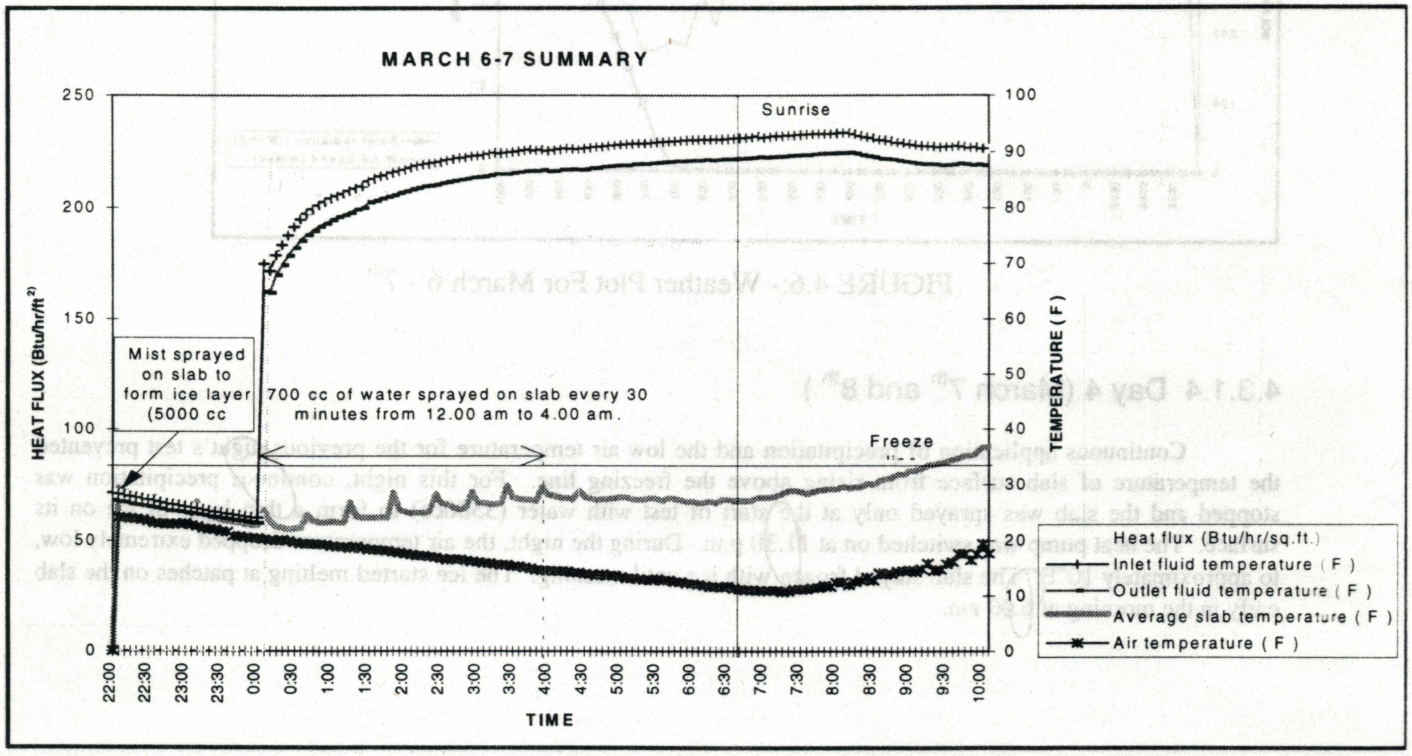

FIGURE 4.5:- Summary Plot For March 6th - 7th

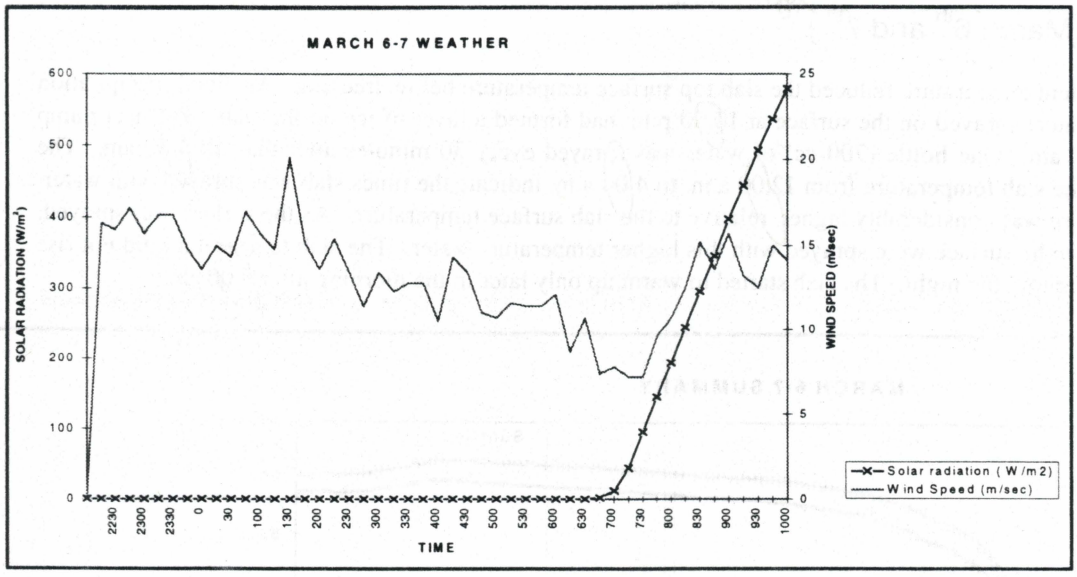

FIGURE 4.6:- Weather Plot For March 6 - 7th

4.3.1.4 Day 4 (March 7th and 8th)

Continuous application of precipitation and the low air temperature for the previous night's test prevented the temperature of slab surface from rising above the freezing line. For this night, continuos precipitation was stopped and the slab was sprayed only at the start of test with water (3500cc) to form a thin layer of ice on its surface. The heat pump was switched on at 11.30 p.m. During the night, the air temperature dropped extremely low, to approximately 10°F. The slab stayed frozen with ice until morning. The ice started melting at patches on the slab early in the morning at 6.00 am.

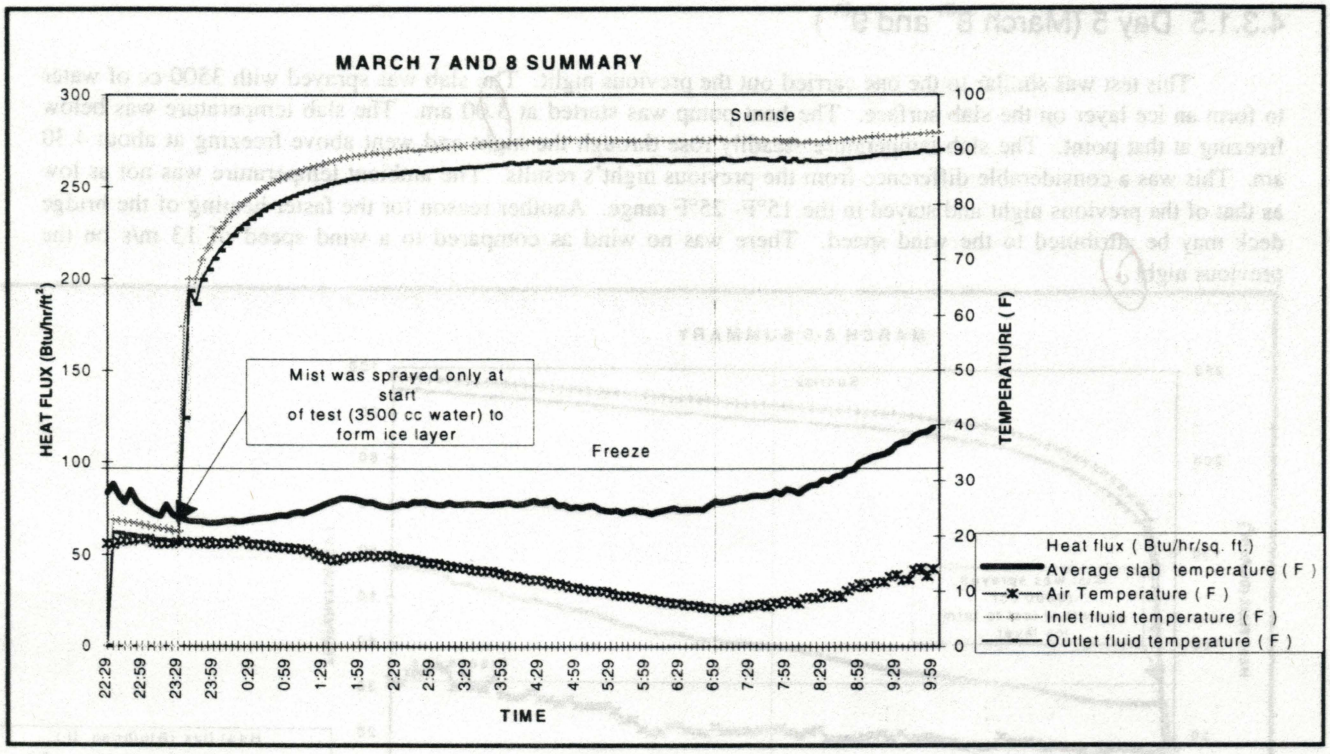

FIGURE 4.7:- Summary Plot For March 7 - 8th

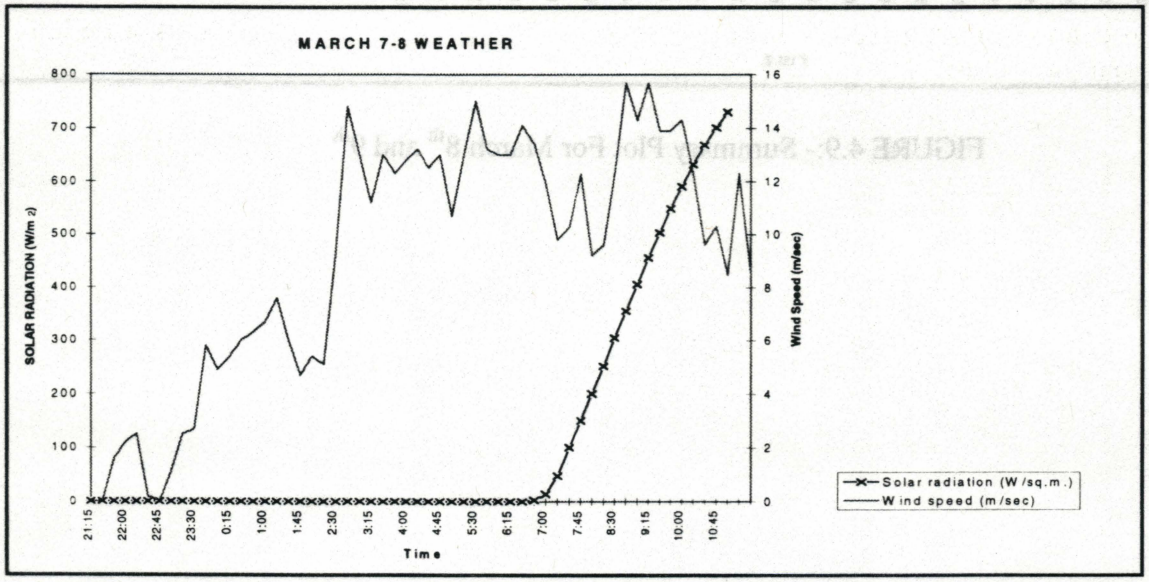

FIGURE 4.8:- Weather Plot For March 7th and 8th

4.3.1.5 Day 5 (March 8th and 9th)

This test was similar to the one carried out the previous night. The slab was sprayed with 3500 cc of water to form an ice layer on the slab surface. The heat pump was started at 3.00 am. The slab temperature was below freezing at that point. The slab temperature steadily rose through the night and went above freezing at about 4.30 am. This was a considerable difference from the previous night's results. The ambient temperature was not as low as that of the previous night and stayed in the 15°F- 25°F range. Another reason for the faster heating of the bridge deck may be attributed to the wind speed. There was no wind as compared to a wind speed of 13 m/s on the previous night.

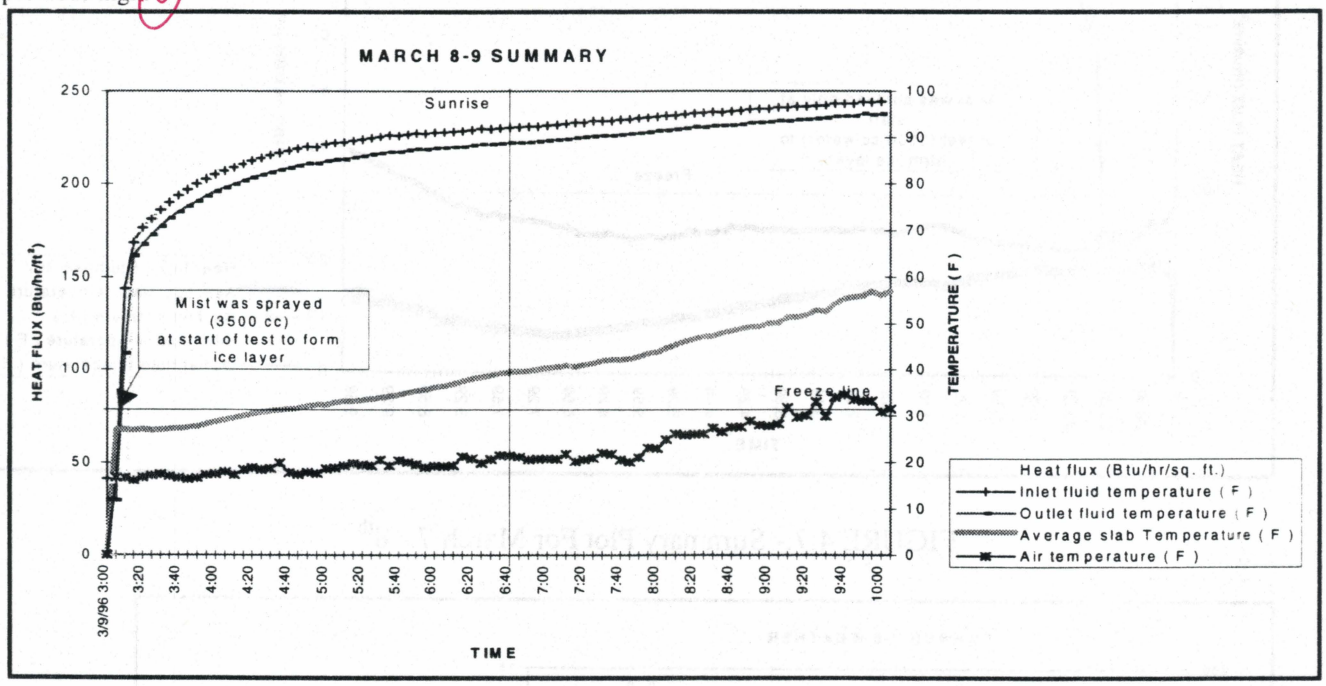

FIGURE 4.9:- Summary Plot For March 8th and 9th

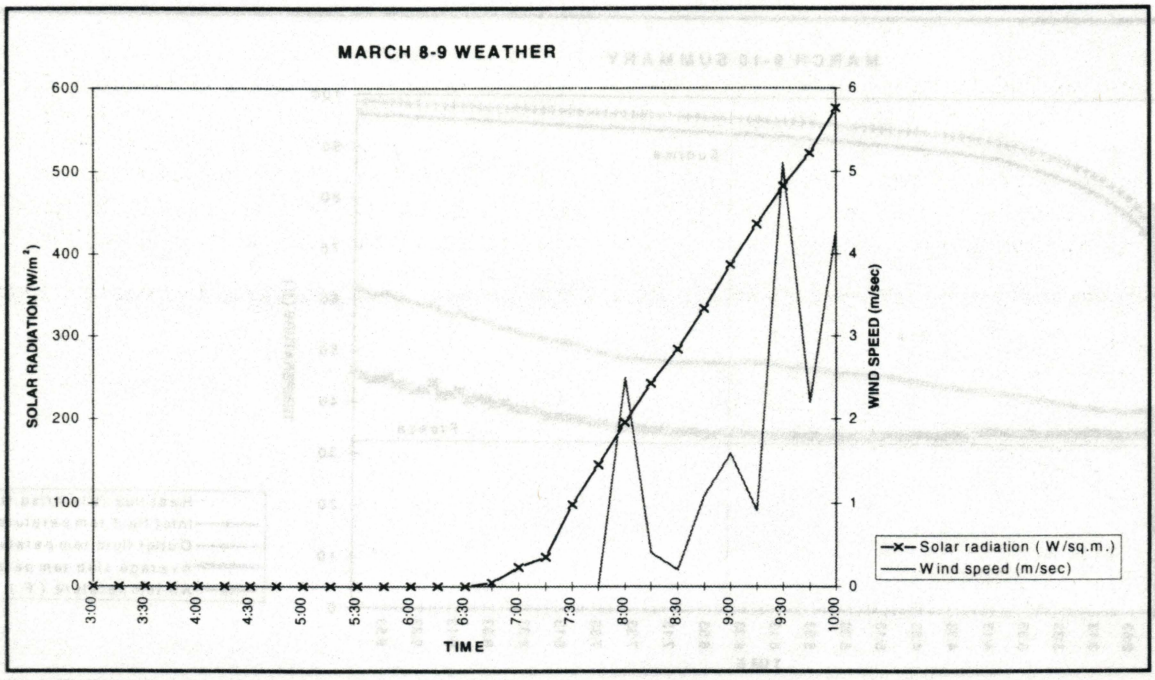

FIGURE 4.10:- Weather Plot For March 8th and 9th

4.3.1.6 Day 6 (March 9th and 10th)

No precipitation was used. The average slab temperature and the air temperature remained above freezing. The slab temperature increased steadily with the air temperature remaining almost constant. The rise in the surface temperature became sharper after sunrise. The heat input flux was the lowest for this test, dropping to as low as 120 Btu/hr./ft^2. A relatively high air temperature and slab temperature were responsible for this low heat input.

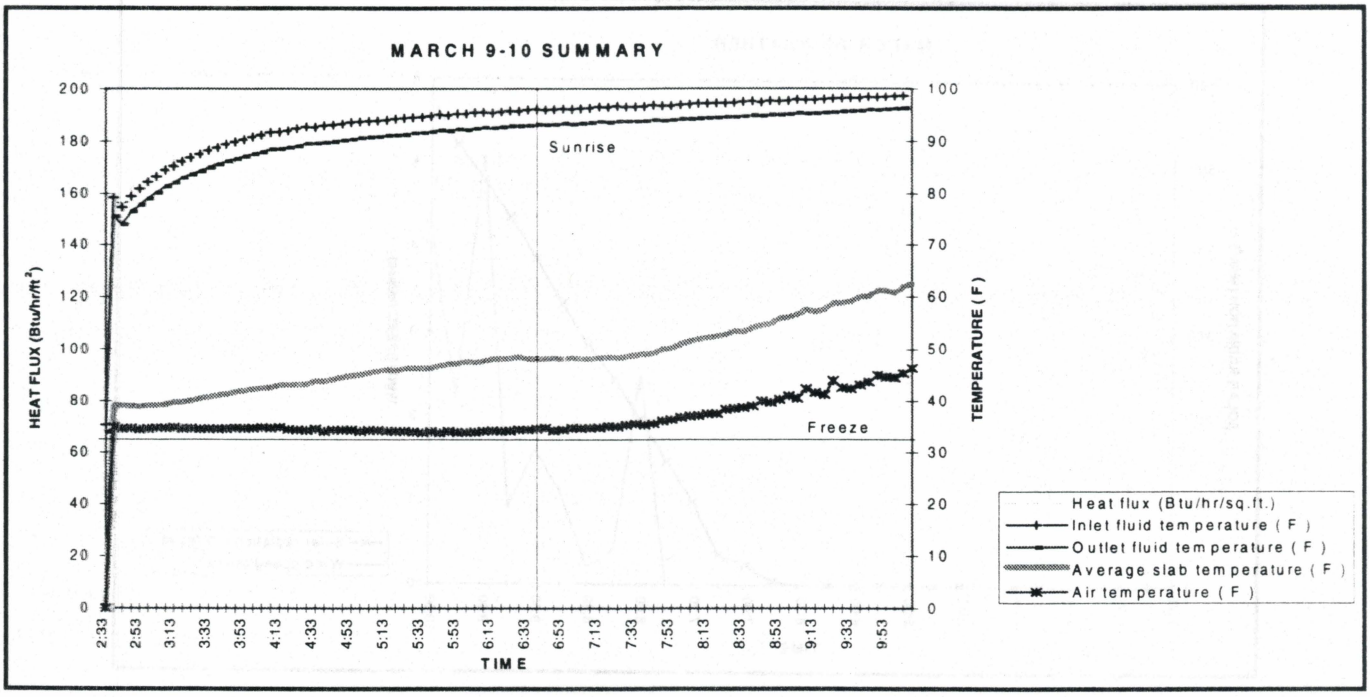

FIGURE 4.11:- Summary Plot For March 9 - 10th

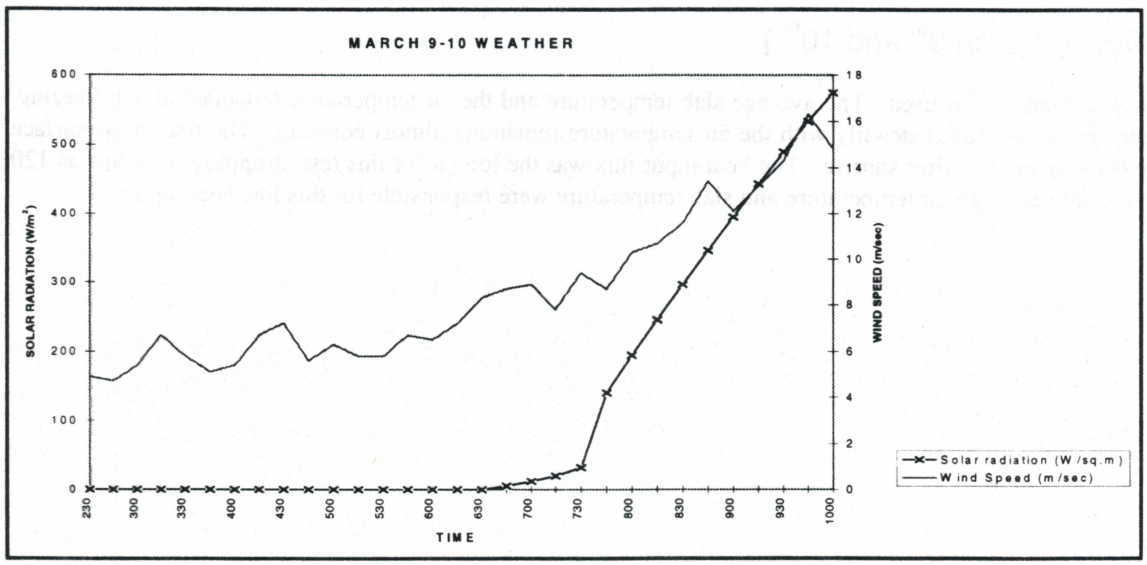

FIGURE 4.12:- Weather Plot For March 9th and 10th

4.3.1.7 Day 7 (March 19th and 20th)

The next test was carried out after a 10 day interval period, due to higher air temperatures in the 50-60°F range for the intermediate days. On this night, the air temperature dropped to 32°F. The slab temperature was also close to freezing. As soon as the heat pump was started, the slab surface temperature rose quickly above the freeze line and the heat input decreased.

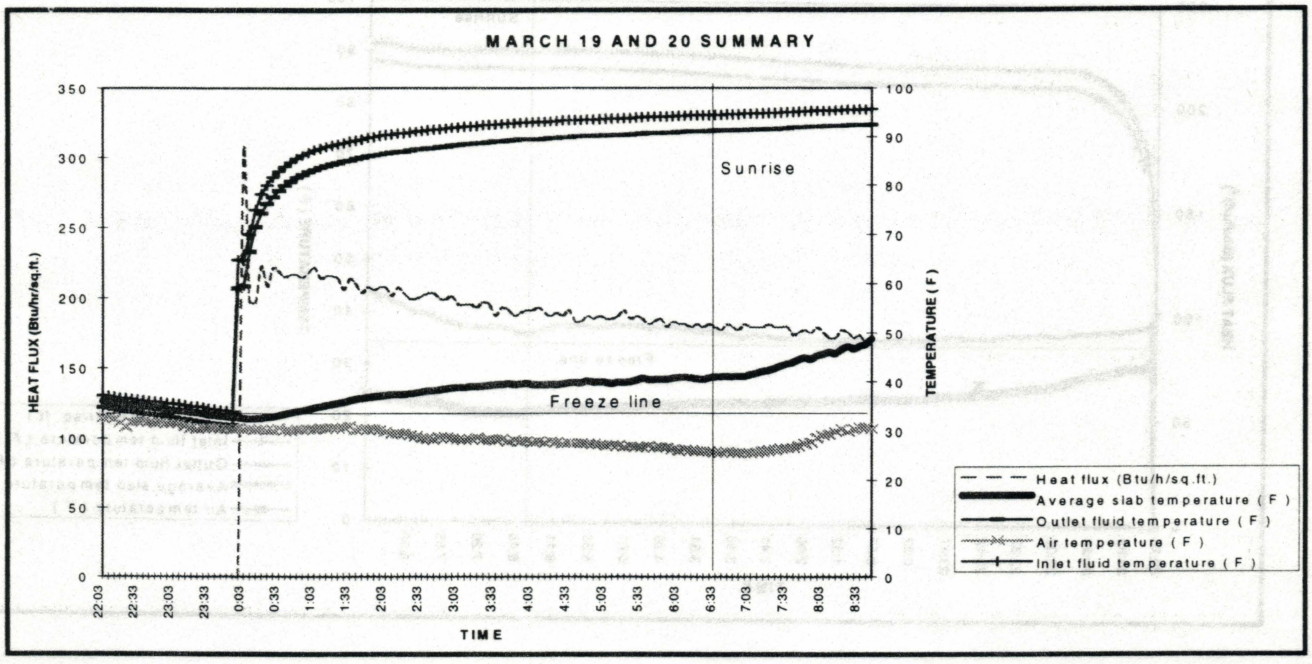

FIGURE 4.13:- Summary Plot For March 19 - 20th

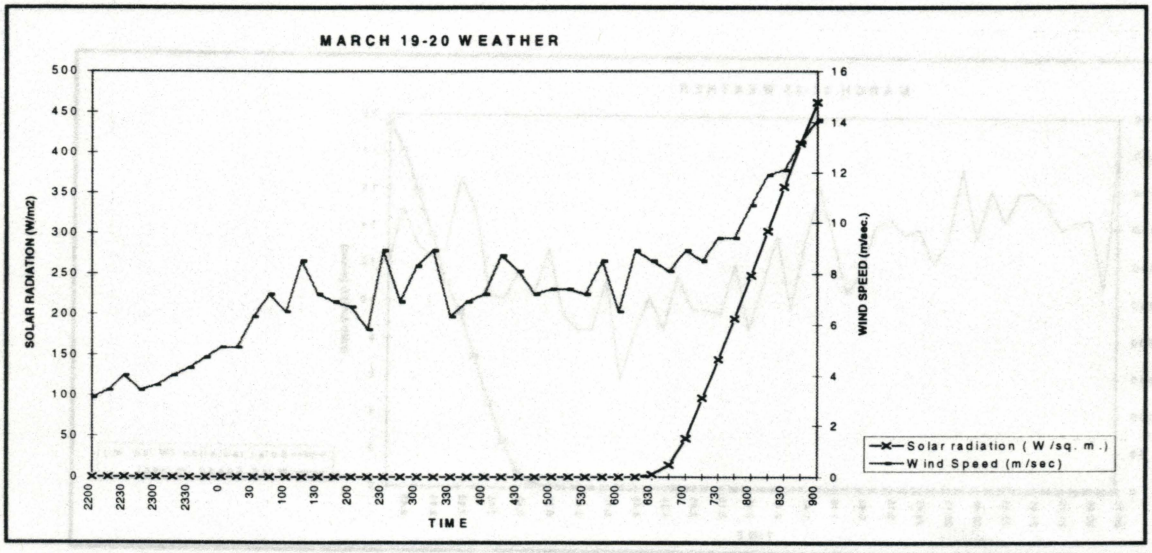

FIGURE 4.14: -Weather Plot For March 19 - 20th

4.3.1.8 Day 8 (March 24th and 25th)

The air temperature dropped below freezing. However as the heat pump had been run the previous day, the slab was sufficiently warmed up, with its surface temperature above freezing. With the heat pump putting in an almost constant heat flux of 180 Btu/hr./ft^2, the slab surface remained at an almost constant temperature just above freezing. The air temperature decreased into the low 20's and a high wind speed of 12 - 15 m/sec prevailed through the night.

why is wind in SI units

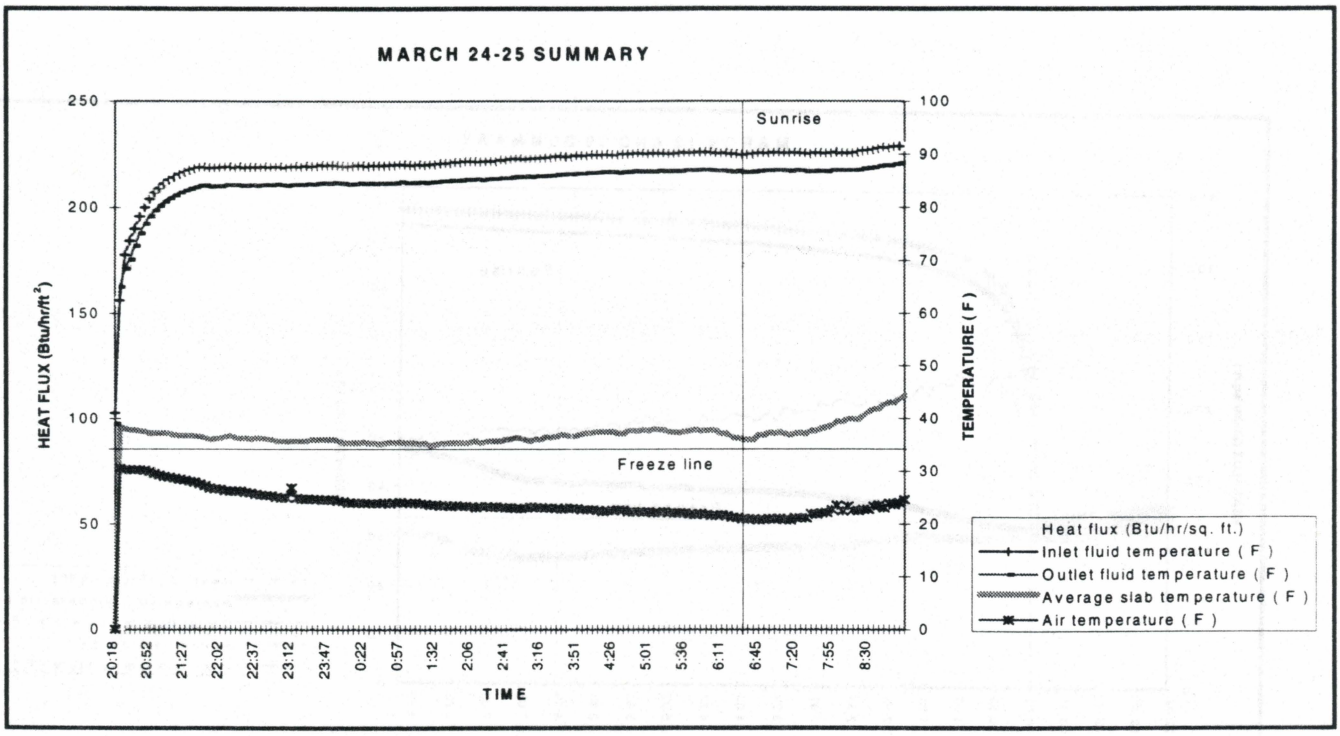

FIGURE 4.15:-Summary Plot For March 24 - 25th

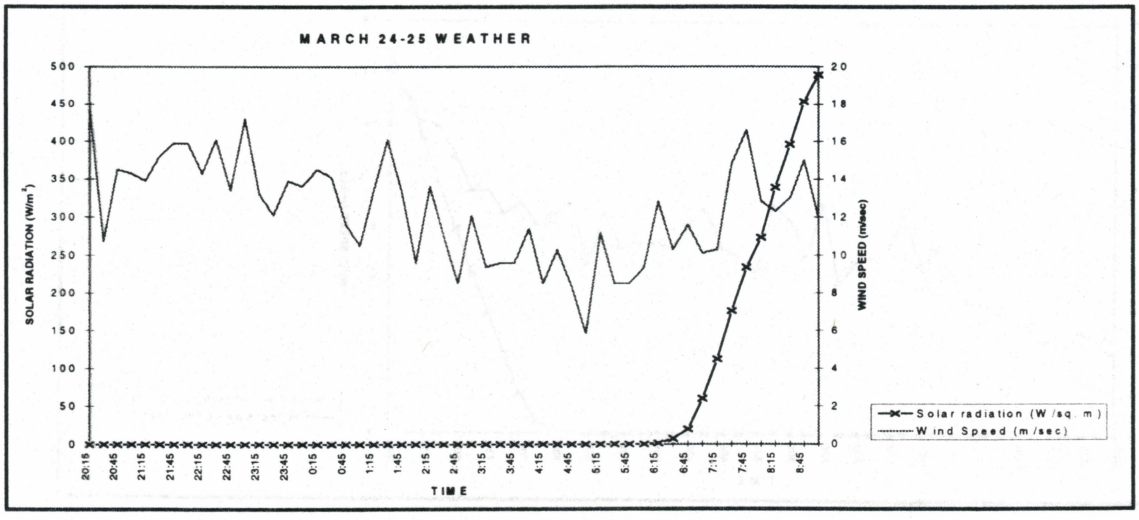

FIGURE 4.16:- Weather Plot For March 24 - 25th

A discussion of the experimental results is presented in Chapter 6.

5. Computer Model and Discussion of Results

The original scope of the project only included an experimental investigation. However, as part of M.S. Thesis research, a numerical model of the bridge deck was developed and a number of simulations were performed which shed further light on the feasibility of the bridge deck deicing system. Only a summary of the work is presented here. For a more comprehensive description, consult Wadivkar (1996).

5.1 Overview of numerical model

The numerical model utilizes a 3-dimensional, explicit, transient finite difference solution for the bridge deck requires the creation of a 3 - dimensional grid. For the simplicity of calculations, the bridge slab with six embedded tubes connected by the U tubes was assumed to be a single length of slab with one long embedded pipe in the slab. This single slab section represents the entire bridge slab and the pipes as if they are uncoiled and straightened out. The slab is assumed to be symmetrical along the longitudinal axis of the pipe. Hence only half of the slab is used in the model. This reduces the number of grid points by half. Figure 5.1 depicts the bridge deck as assumed in the model. A grid mesh divides this section into different nodes in the X, Y and Z directions. In the X-direction, the nodes are assumed to have a spacing of 1 foot. A smaller grid spacing in the X direction increased the total number of grid points, thereby increasing the computer time. A spacing of 0.08 ft in the X direction was initially implemented and the spacing was increased till no change in the results was observed. A 1 foot spacing in the X direction was found to give the same results as those achieved with the spacing of 0.08 feet. Grid independence was observed in results for any spacing below 1 foot. Grid spacing marginally larger than 1 foot did not significantly change the results, however, as the grid used is uniform, there was no node position at the edge. A larger grid spacing of 1.5 or 2 feet affected the results, hence a spacing of 1 foot was maintained.

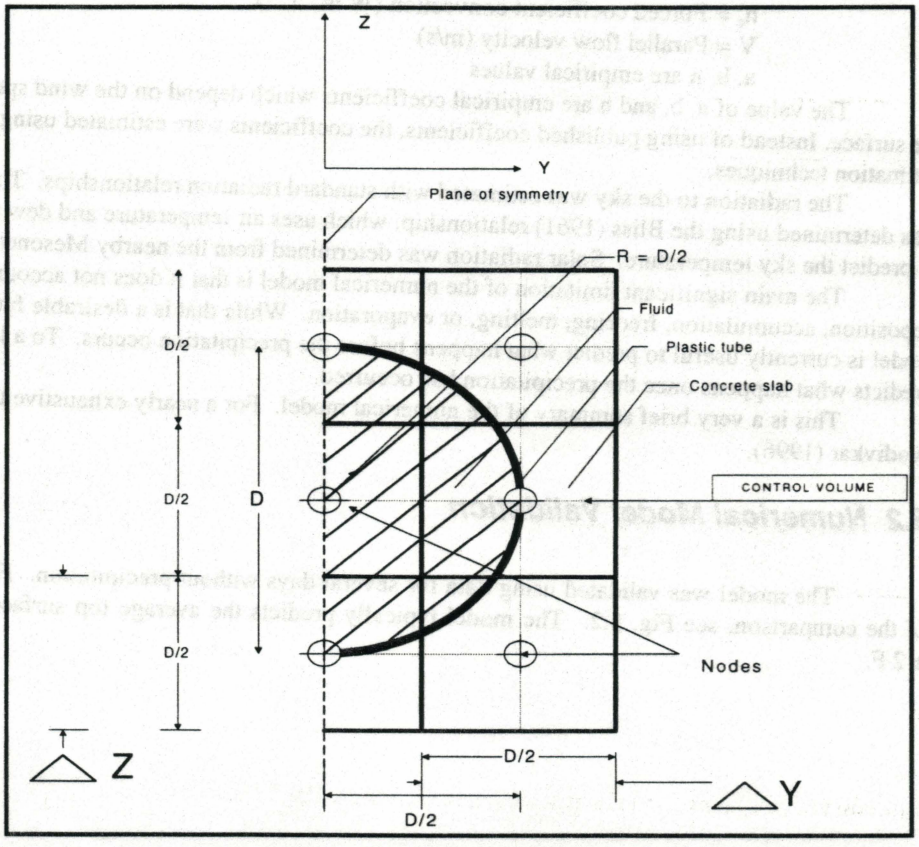

Figure 5.1:-2-D cross sectional view of a fluid pipe node shown with control volumes

Figure 5.1 shows the grid cross-section of the fluid nodes, with the node locations. The cross hatched area is the tube of fluid. Only half of the tube is included, as symmetry is assumed. For simplicity, the outer radius of the plastic pipe is taken as the distance between two nodes, for the Y and Z direction, with one node located at the center of the pipe, the pipe radius is used as the spacing between two nodes. This simplifies the grid geometry, with a node in the center of the pipe and adjacent nodes about the pipe radius. The number of nodes in the Y or Z direction is calculated by truncating the following fraction to an integer.

$$N_{y,z} = S_{y,z} / (D/2) \tag{5.1}$$

where

$N_{y,z}$ = number of nodes in the Y or Z direction
$S_{y,z}$ = slab dimension in the Y or Z direction (ft.)
D = Diameter of tube (ft.)

All the nodes are surrounded by a control volume. Control volumes that contain hydronic tubing are defined as composite cells. A new 'composite' property was defined for such cells calculated by using a weighted average of the properties of the different materials depending on the volume fraction of the material contained in the node.

Explicit finite difference solutions have time steps constrained by stability criteria. For this case, a time step of 12 seconds was used, which corresponded to approximately 90% of the theoretically allowable time step.

The top surface has convective and radiative boundary conditions. The convective heat transfer was estimated with a correlation of the form:

$$h_c = 5.678 * \left(a + b \left(\frac{V}{0.304} \right)^n \right) \tag{5.2}$$

where

h_c = Forced coefficient convection (W $m^{-2}{}^{\circ}C^{-1}$)
V = Parallel flow velocity (m/s)
a, b, n are empirical values

The value of a, b, and n are empirical coefficients which depend on the wind speed and nature of the surface. Instead of using published coefficients, the coefficients were estimated using parameter estimation techniques.

The radiation to the sky was estimated with standard radiation relationships. The sky temperature was determined using the Bliss (1961) relationship, which uses air temperature and dew point temperature to predict the sky temperature. Solar radiation was determined from the nearby Mesonet site.

The main significant limitation of the numerical model is that it does not account for precipitation deposition, accumulation, freezing, melting, or evaporation. While that is a desirable future addition, the model is currently useful to predict what happens before the precipitation occurs. To a lesser accuracy, it predicts what happens once the precipitation has occurred.

This is a very brief summary of the numerical model. For a nearly exhaustive treatment, see Wadivkar (1996).

5.2 Numerical Model Validation

The model was validated using data for several days without precipitation. For a typical example of the comparison, see Fig. 5.2. The model typically predicts the average top surface temperature within ± 2 F.

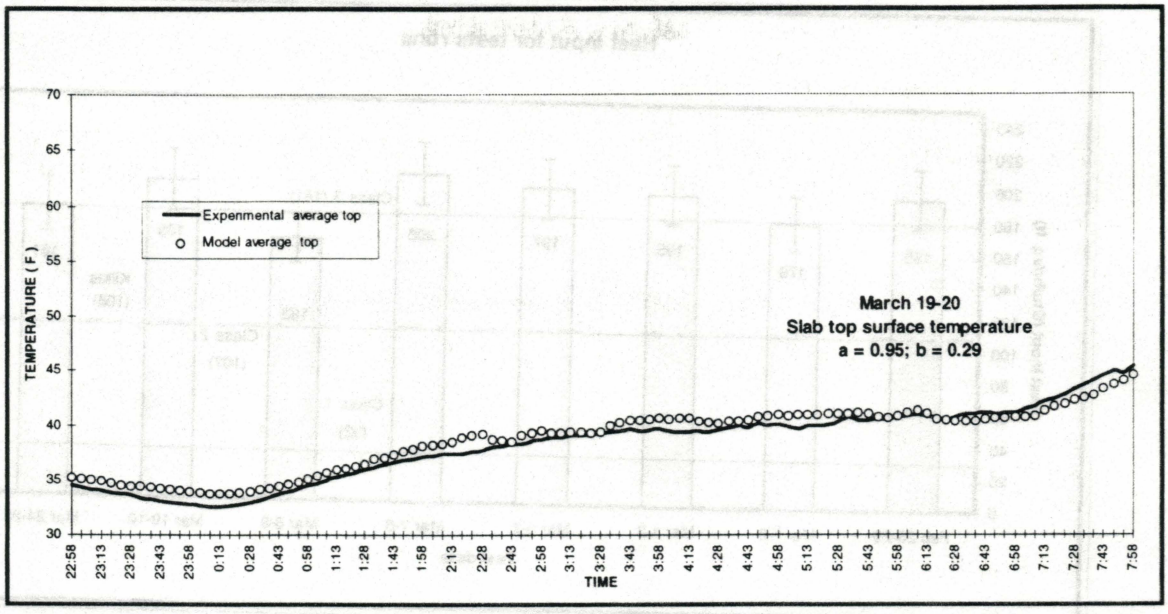

Figure 5.2 Comparison of Numerical Model to Experimental Data

5.3 Simulation

One of the prime objectives of the study was to determine the amount of heat input required and the time of its application to prevent the concrete slab from freezing. It can be seen that the heat input by the ground source heat pump raised the temperature of the slab over the ambient temperature for all days. However, in the case of the days with freezing ambient conditions, when precipitation was applied to the slab surface, this heat input alone was not sufficient to raise the temperature of the slab above freezing. Additional heat input in the form of solar radiation was necessary to raise the slab surface temperature above freezing. Figure 5.3 compares the heat inputs from the heat pump for the eight test days. The heat input noted is the average heat input for the each nightly test run. The heat inputs ranges from 160-205 Btu/hr./ft^2. The low value of 160 Btu/hr./ft^2 was recorded for a day with ambient temperatures relatively higher, than those for the other test days. The average heat input for test runs with air temperatures below freezing was approximately 180 - 200 Btu/hr./ft^2. The heat fluxes have been provided with their error bars (± 9.4 %), as determined in Chapter 3.

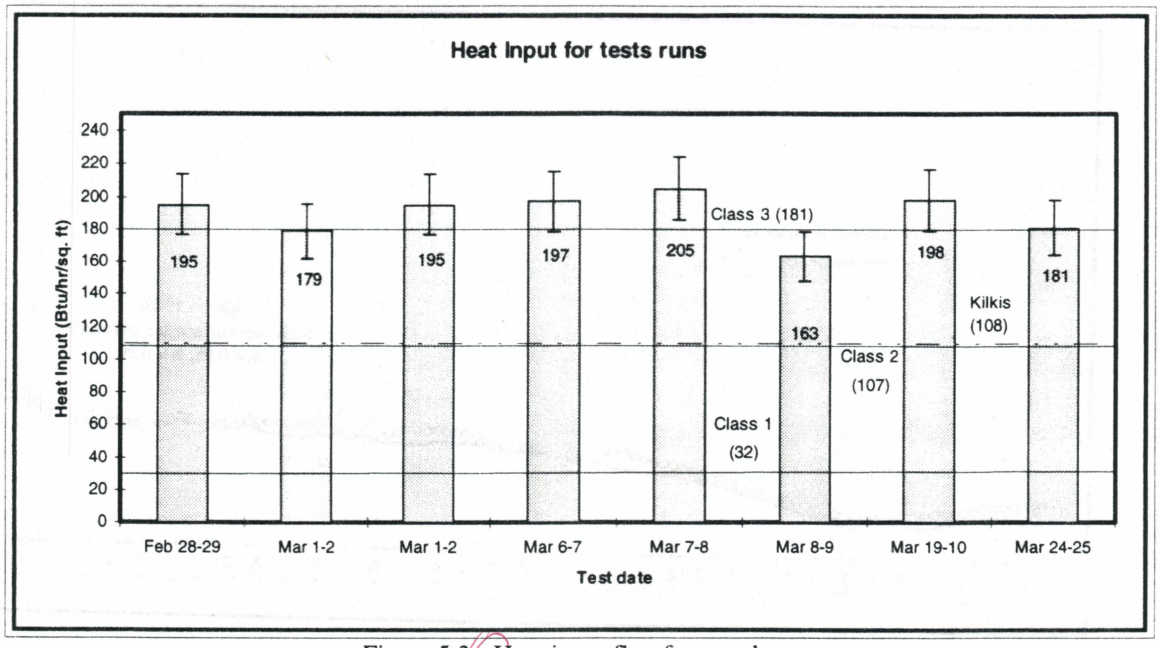

Figure 5.3:- Heat input flux for test days

5.3.1 Heat requirements calculated using ASHRAE and Kilkis models.

Using the ASHRAE and Kilkis models for the day with the most severe weather conditions (March 7th -8th) encountered during experimentation, heating requirements were estimated for "snow melting", with the "snowfall rate" equivalent to the highest rate of artificial precipitation. Table 5.1 presents the results obtained for heat requirements for both the models, along with the input parameters used. The calculated heat inputs for all three snow melting classes by using the ASHRAE guidelines have been depicted in Figure 5.3 by the labeled horizontal lines. The dashed line in Figure 5.3 indicates the heat input requirement for a Class 3 system by applying the Kilkis model to the experimental site.

The three systems are classified on the basis of their performance of snow melting during snowfall. As there was no snowfall during the test period, the bridge deck heating system cannot be classified based on its snow melting performance.

The Kilkis and the ASHRAE models assume idling of the system to maintain the top slab temperature above freezing, before actually using it to melt any snow. The heating requirements in Table 5.1 for snow melting were calculated for extreme conditions with the maximum amount of precipitation applied, which is not the case for all days. It can be seen that, **without idling, as the system was operated,** the Kilkis or the ASHRAE models may underpredict the heat requirements to melt the ice on the surface for some days. Both the models suggest that the heat input to the slab from the heat pump alone was sufficient to melt all the snow from the slab surface, leaving it totally snow free (A_r=1). During experimentation it was observed that the heat input on its own was not sufficient to melt all the ice formed by a high precipitation rate. Additional heat from solar radiation was necessary to raise the slab surface temperatures above freezing.

Input parameters	ASHRAE MODEL	KILKIS MODEL
Rate of snowfall (inch/hr)	0.04	0.04
Air temperature (°F)	13	13
Relative humidity (%)	40.5	40.5
Wind Speed (mph)	16	16
Film temperature (°F)	33	33
Coincident air temperature (°F)	not applicable	18.4
Adjusted wind speed (mph)	not applicable	6
Sensible heat transferred to snow (Btu/hr/ft^2)	1.98	1.41
Heat of fusion (Btu/hr/ft^2)	29.84	29.84
Heat of evaporation (Btu/hr/ft^2)	64.05	18.34*
Convection and radiation heat transfer (Btu/hr/ft^2)	85.87	not applicable
Convective heat transfer (Btu/hr/ft^2)	not applicable	17.86
Radiant heat transfer (Btu/hr/ft^2)	not applicable	40.95
Heating loads		
Idling load (Btu/hr/ft^2)	145	93
Snow melting - Class 1 (Btu/hr/ft^2)	32	93
Snow melting - Class 2 (Btu/hr/ft^2)	107	93
Snow melting - Class 3 (Btu/hr/ft^2)	181	108

* Measured value of 13°F used.

TABLE 5.1:- Heat requirements for snow melting for test site

5.3.2 Idling

The heat requirements calculated by the ASHRAE and the Kilkis models to melt surface ice are based on the system being idled before actual melting begins. The slab would therefore be preheated to a temperature above freezing conditions. In the test runs, the slab was never idled and was always started cold before precipitation. This absence of idling was considered to be a prime reason the slab surface temperature did not rise above freezing conditions during the experimental runs. The numerical model was used to examine the importance of idling in the performance of the existing bridge deck system.

5.3.3 Transient performance of the system

Certain papers in the literature survey revealed that one of the main decisions while running such deicing systems was determining the time period required to start the system prior to the snowfall event, to prevent the bridge deck or road surface from freezing during snowfall. It was required to determine the amount of heat input required along with the time of its application to prevent the freezing of the bridge deck. It is necessary to know the transient response of the system to decide on the above factors. The availability of the transient response of such a deicing system would be useful in the design of 'smart' bridge decks.

5.3.3.1 'Smart' Bridge deck

One of the long term objectives of the study is to build a 'smart' bridge deck (Spitler and Hogue, 1995). Such a system would use the local short term weather forecast to determine the heat input required and the corresponding time period to prevent any icing on the surface. In Oklahoma, the control on such a 'smart' bridge deck can be greatly enhanced by the use of the Oklahoma Mesonet. Data collected by the local Mesonet station can be analyzed and the weather conditions predicted accurately by computers. An automatic signal sent from the Mesonet base station would turn the heating system on and warm the bridge deck well in advance to prevent any icing on the surface. The system would be automatically turned off when the icing risk was past. Such a 'smart' system would need to know the transient response of the heating system.

5.3.3.2 Transient response using computer model.

The transient response of the installed system was studied for different ambient conditions and various input fluxes into the heating system. The limitations to applying the numerical model described in section 5.1 for the purpose of studying the bridge deck transient response were the following:

1. The computer model was developed for 'dry' conditions only. Any precipitation load was not included in the calculations. The model was used to determine response for dry conditions and some 'wet' conditions involving precipitation. If the precipitation load is neglected for 'wet' conditions, the model may under predict the heat input required. However the ensuing study gave a rough estimate of the heat requirements and the response of the system. Future work in developing the computer model would incorporate precipitation loads.
2. Empirical coefficients and exact values for material properties used in the model were obtained by parameter estimation techniques. The values used were obtained by minimizing the sum of the squares of the differences between the model and experimental data from three days. These general values obtained after a parameter estimation were assumed to be consistent for different ambient conditions on different days.

The transient response of the system was studied using weather data from two test days from the Winter of 1995-96. These days were chosen because of the presence of low ambient temperatures and the occurrence of natural precipitation which later froze to form ice on the road surfaces. Transient performance of the system for Day 5 (March 7th and 8th) was also studied using the model, and results compared to experimental data.. Weather data was retrieved from the archives of the Oklahoma 'Mesonet'.

Test Day 1 (December 24-25th 1995)

There was some rainfall on the night of December 24th, which later froze and was converted to ice on the road surfaces. The hypothetical transient response of the installed system under the ambient conditions was studied by running the model by using the day's weather data. A weather plot for the day from 12.00 am December 24th to 11.45 p.m. 25th December is provided in Figure 5.4.

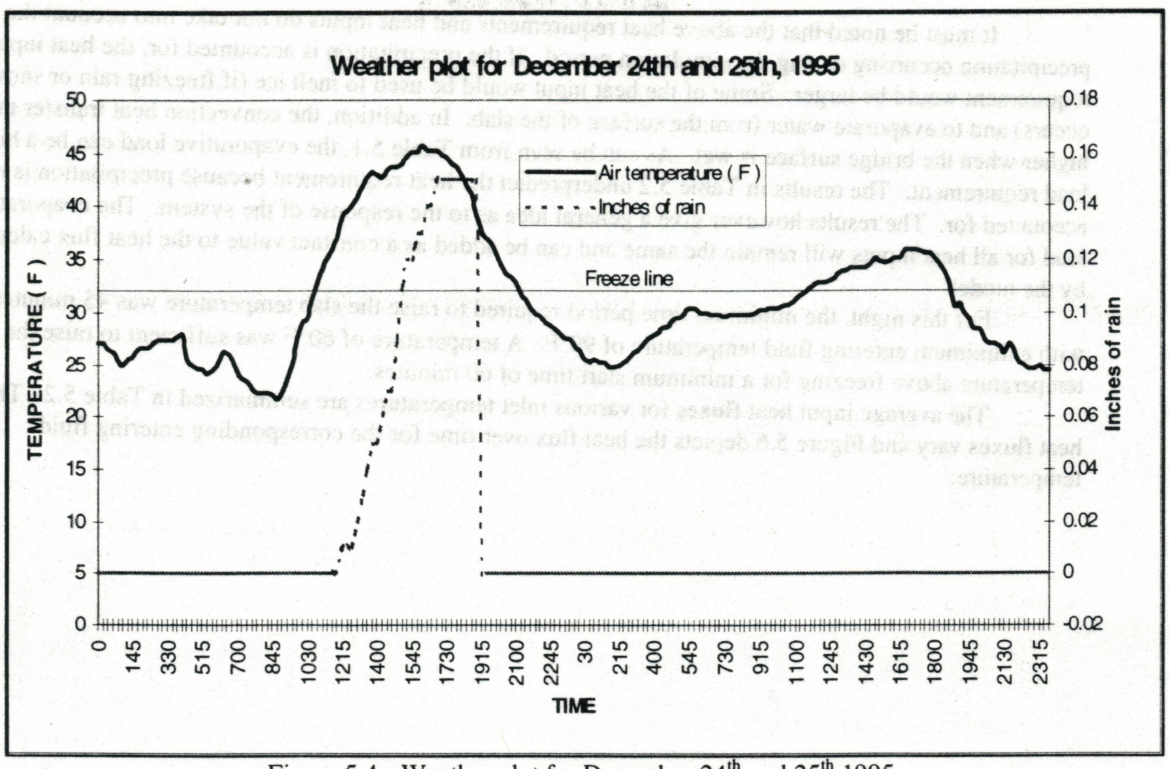

Figure 5.4:- Weather plot for December 24th and 25th 1995

The program BRIDGE3D simulated the slab response to different heat inputs to the slab for the day's weather conditions. The heat input was varied by changing the fluid input temperature to the bridge deck. For the experimental bridge deck higher fluid temperatures could be attained by replacing the present heat pump with a larger capacity heat pump.

Note: It was assumed that the fluid temperature reaches its maximum value as soon as the heating is switched on. In the case of a hydronic system using a heat pump, this would not be true, and the system would take some time to achieve its maximum temperature. However, as determining this time period would require a detailed study of the heating system assumed, it was not considered and an instant temperature rise was assumed.

Figure 5.5 shows the transient response of the slab for different entering fluid temperatures. As a reference, the temperature profile of the unheated slab top surface has also been provided. For each of the different fluid temperatures the critical time period to prevent slab freezing (assuming 33 °F as the cutoff temperature for the top slab surface) was determined by trial runs for each fluid temperature. Latest start times for each fluid temperature is provided in parenthesis in the Figure. Results were calculated every fifteen minutes. Minimum heating time periods to prevent freezing of the slab are presented to the nearest fifteen minute period in Table 5.2.

TEST DAY 1 December 24th and 25th 1995		
Entering Fluid Temperature (° F)	Minimum operation time period before to prevent freezing (minutes)	Average Heat Flux (Btu/hr/ft2)
50	75	70
60	60	110
70	60	151
90	45	233

Table 5.2:- Model results for the transient response of the Bridge deck

It must be noted that the above heat requirements and heat inputs do not take into account the precipitation occurring during the simulation period. If the precipitation is accounted for, the heat inputs requirement would be larger. Some of the heat input would be used to melt ice (if freezing rain or snow occurs) and to evaporate water from the surface of the slab. In addition, the convection heat transfer may be higher when the bridge surface is wet. As can be seen from Table 5.1, the evaporative load can be a high load requirement. The results in Table 5.2 underpredict the heat requirement because precipitation is not accounted for. The results however give a general idea as to the response of the system. The evaporative load for all heat inputs will remain the same and can be added as a constant value to the heat flux calculated by the model.

For this night, the minimum time period required to raise the slab temperature was 45 minutes, with a minimum entering fluid temperature of 90°F. A temperature of 60°F was sufficient to raise the temperature above freezing for a minimum start time of 60 minutes.

The average input heat fluxes for various inlet temperatures are summarized in Table 5.2. The heat fluxes vary and Figure 5.6 depicts the heat flux over time for the corresponding entering fluid temperature.

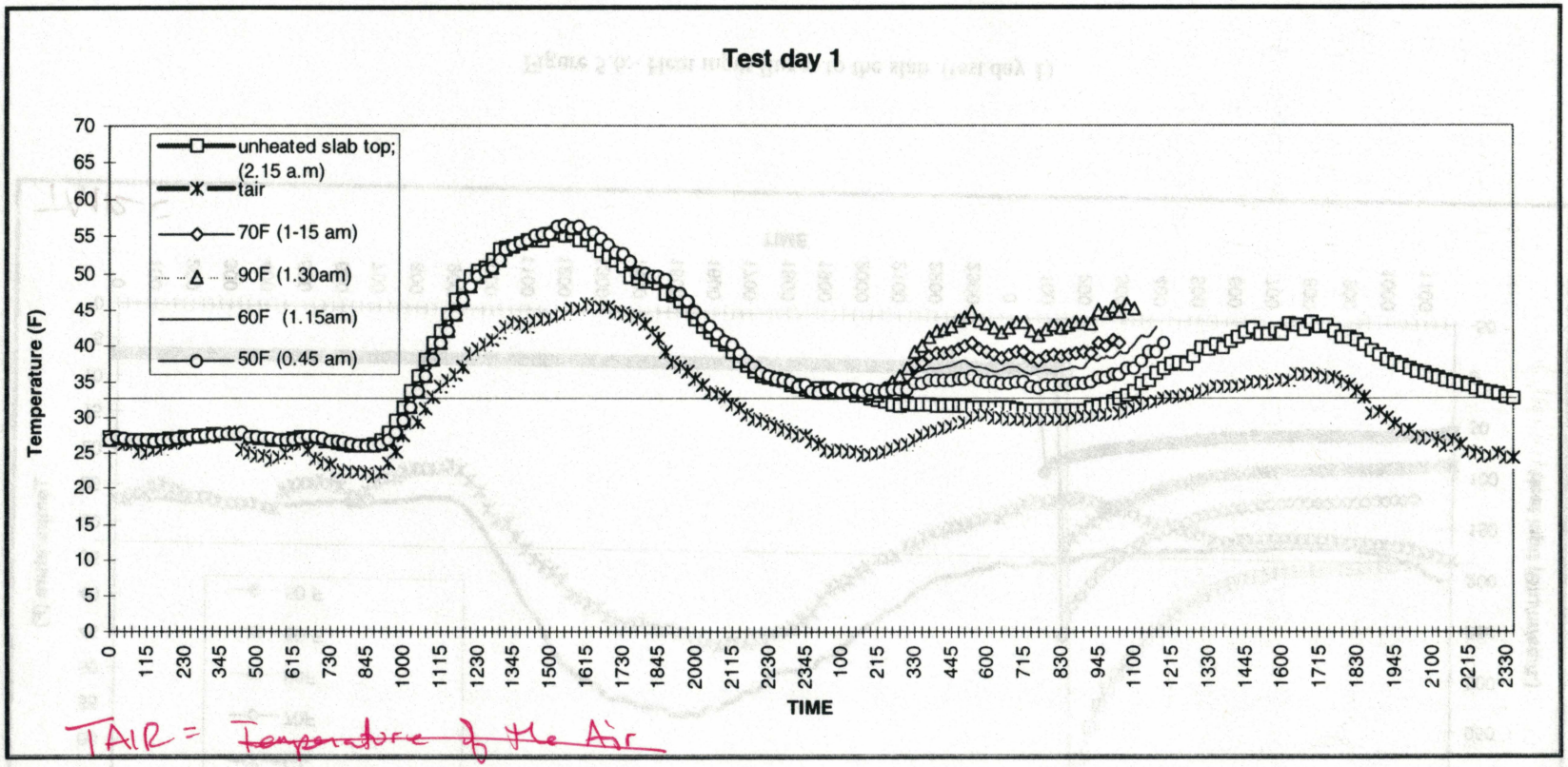

Figure 5.5:- Transient response of slab top surface (test day 1)

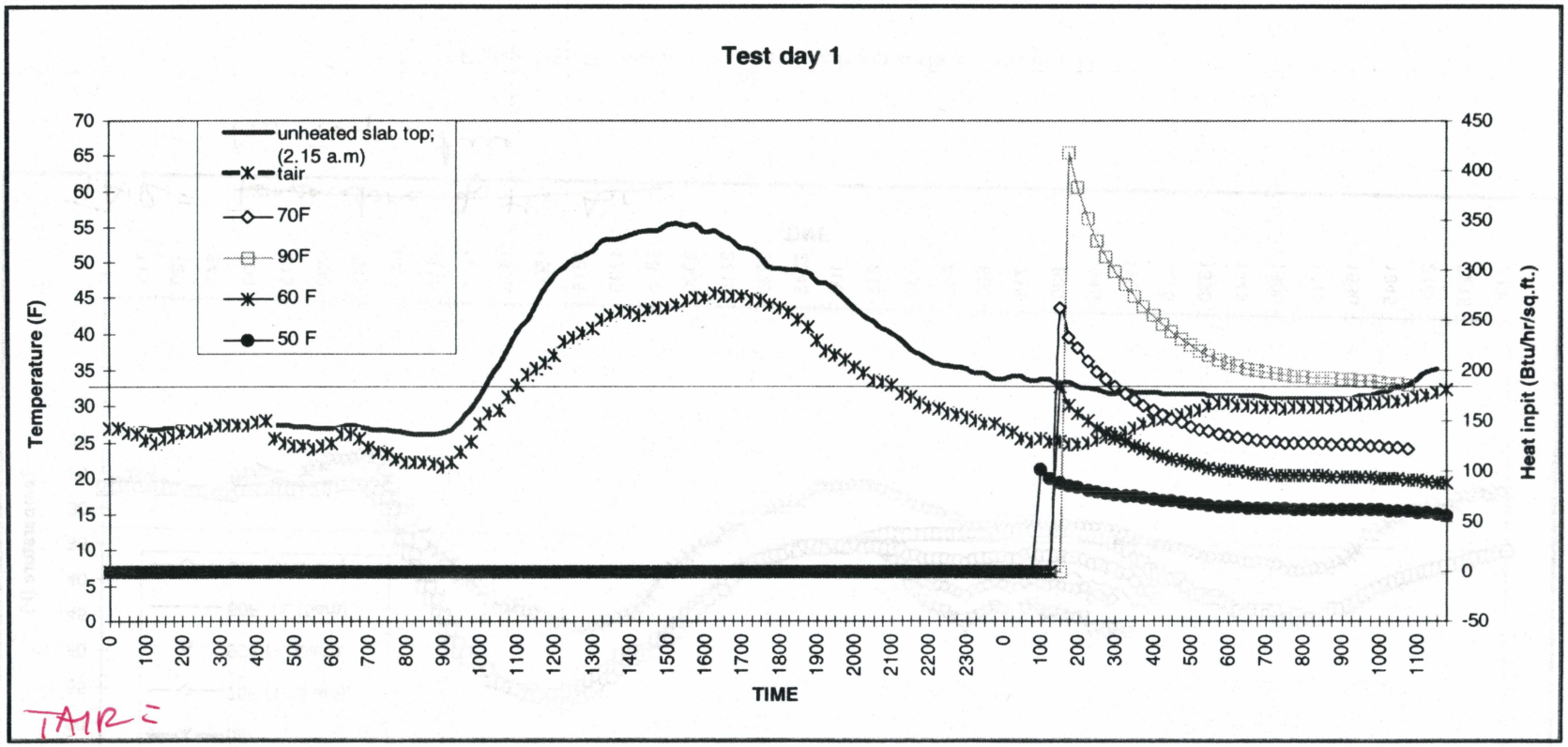

Figure 5.6:- Heat input fluxes to the slab (test day 1)

Test Day 2 (February 5th and 6th)

Similar to the simulation carried out for test day 1, a simulation to determine the transient response of the slab for different entering fluid temperatures and the minimum critical time period required to prevent the slab from reaching a temperature below 33°F was carried out. The weather condition for the period is depicted in Figure 5.7. Rainfall was followed by a drop in the ambient temperature which formed ice on the road surfaces, leading to hazardous road conditions. The response of the slab temperature is presented in Figure 5.8.

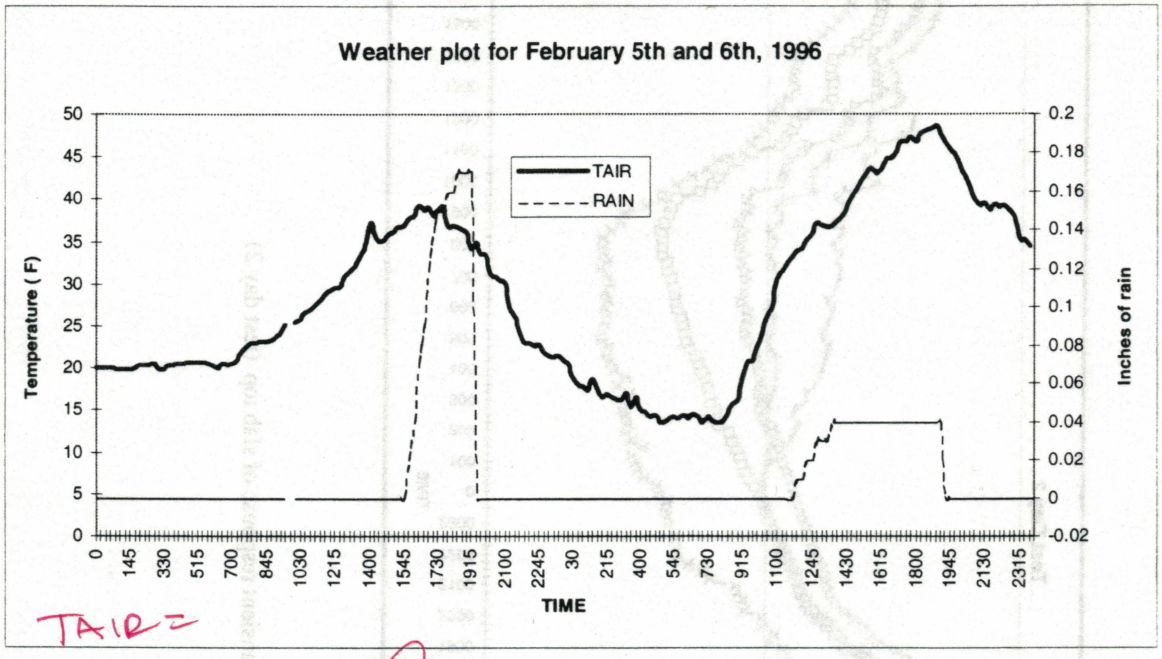

Figure 5.7- Weather plot for February 5th and 6th 1996

TEST DAY 2		
Entering Fluid Temperature (° F)	Minimum operation time period to prevent freezing (minutes)	Average Heat Flux (Btu/hr/ft^2)
50	never rises above freezing	85
60	30	110
70	30	123
80	15	200

TABLE 5.3:- Transient response of the slab

A temperature of 80°F was sufficient to prevent freezing of the slab, if the system was switched on 15 minutes in advance of when freezing would have occurred. Beyond 30 minutes a temperature of minimum 60°F was required. Temperatures below 60°F could not raise temperature above freezing in time. Fluid of 50-55 °F, with an input of 85 Btu/hr/ft ^{2} was circulated but could not raise the slab above freezing inspite of being run for a period of 48 hr. in advance of the specific freezing event. Flux data is provided in Figure 5.9.

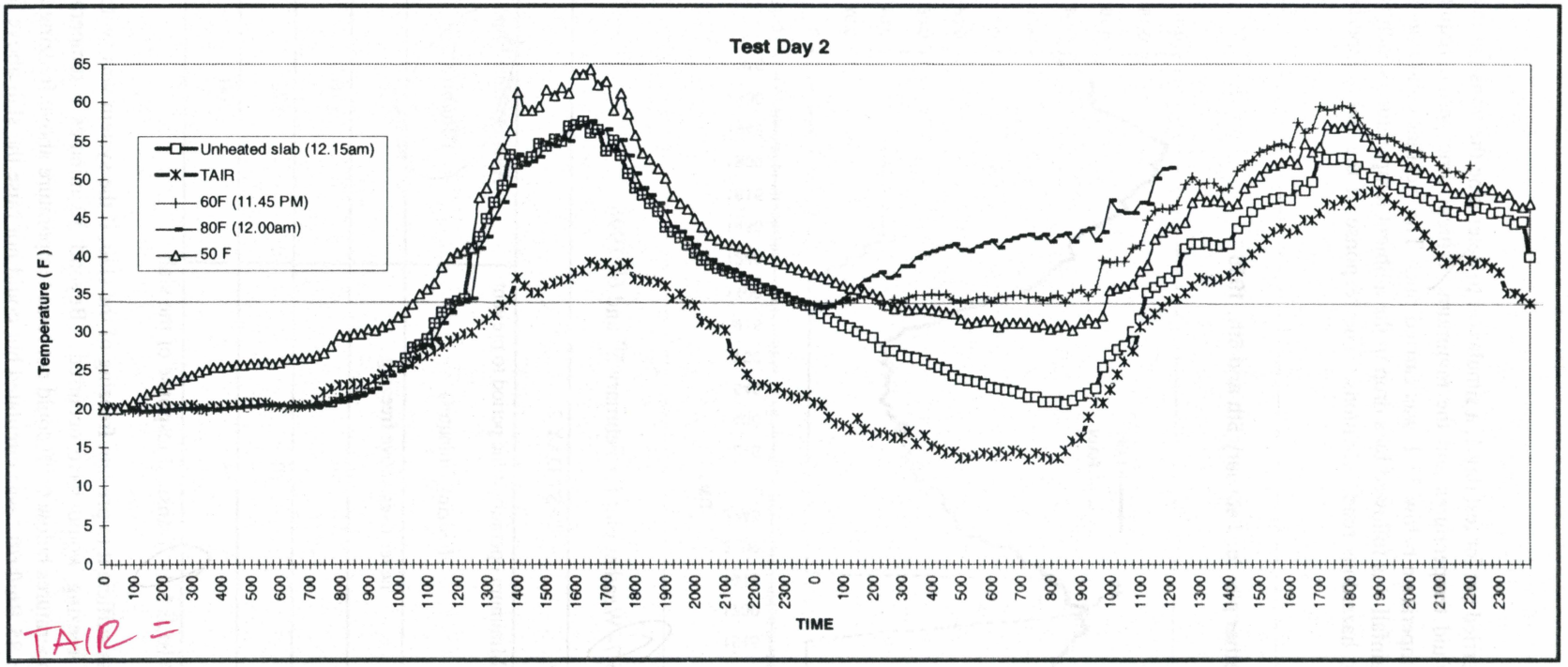

Figure 5.8:- Transient response of slab top (test day 2)

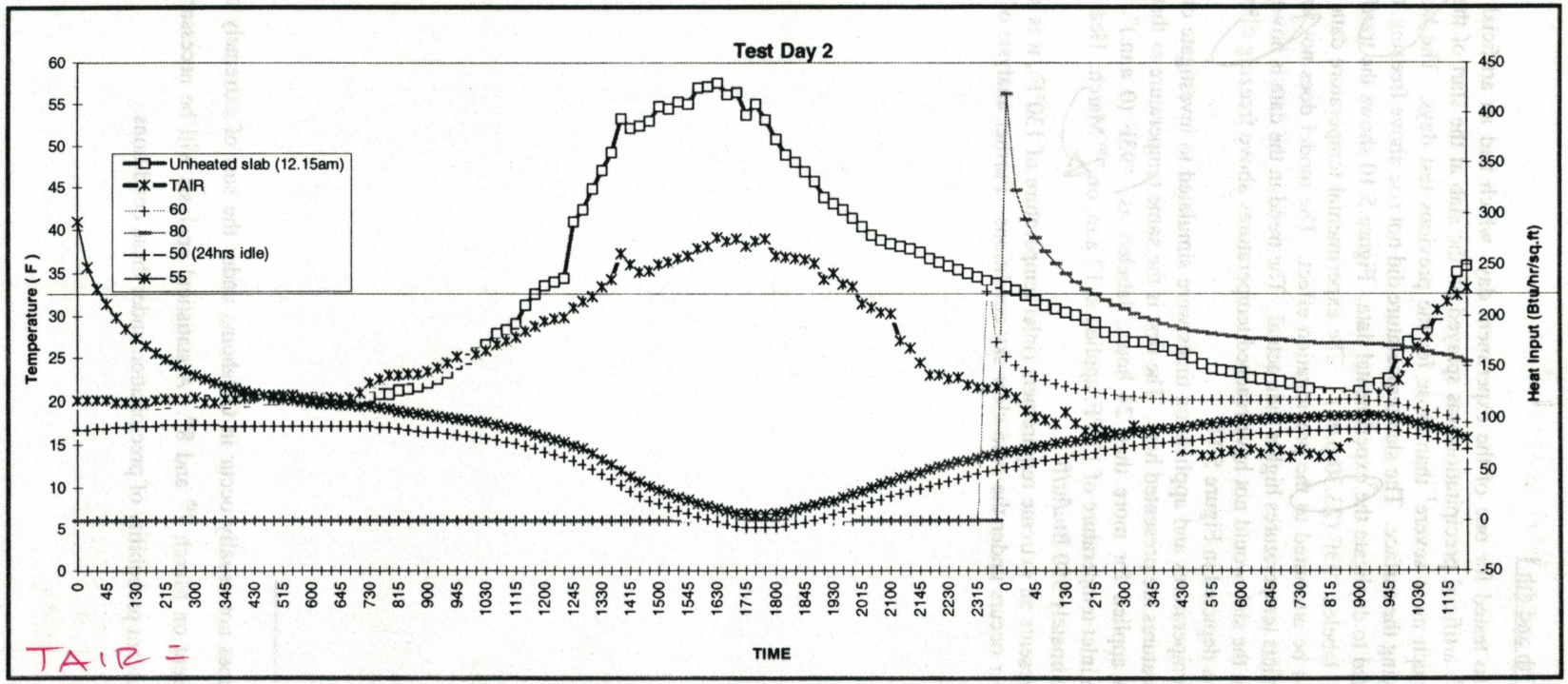

Figure 5.9:- Heat input fluxes to the slab (test day 2)

Test Day 3 (Day 5 - March 7th and 8th)

The model was also tested for one of the experiment days which had an artificial precipitation load. On March 7th and 8th, artificial precipitation was sprayed on the slab at the start of the experiment. Weather conditions were much more severe[1] than those for the previous test days. The heat pump was started two hours after spraying the surface. The slab temperature did not rise above freezing, till sunrise.

The model attempted to duplicate the experimental data. Figure 5.10 shows the transient response of the slab using the model, labeled "93F (23.30 p.m.)". The experimental temperature data is lower than the model results, this could be attributed to the precipitation effect. The model does not account for the precipitation and hence predicts temperatures higher than actual. The trend in the data is however the same. The model also predicts that the slab would not have reached temperatures above freezing till sunrise. Heat input due to the heat pump is depicted in Figure 5.11.

A range of input temperatures and application times were simulated to investigate other operating strategies. Only two temperatures are presented here. The first is the same temperature as that of the actual inlet temperature, but was applied for more than 24 hours, labeled as "93F (0 a.m.)". The second simulation plotted, is for an inlet temperature of 130°F, applied at 12 a.m. on 7th March. Heat input flux for this temperature was approximately 350 Btu/hr/ft^2.

Although this represents an extreme requirement (inlet temperature of 130°F), it is not at all clear if freezing precipitation ever occurs under the cold clear sky conditions. Further analysis of the historical weather data is needed.

[1] Freezing precipitation does not usually occur in Oklahoma under the sort of extremely cold conditions (clear sky) that were present on March 7th and 8th. A statistical analysis will be necessary to determine weather there is any significant probability of precipitation under these conditions.

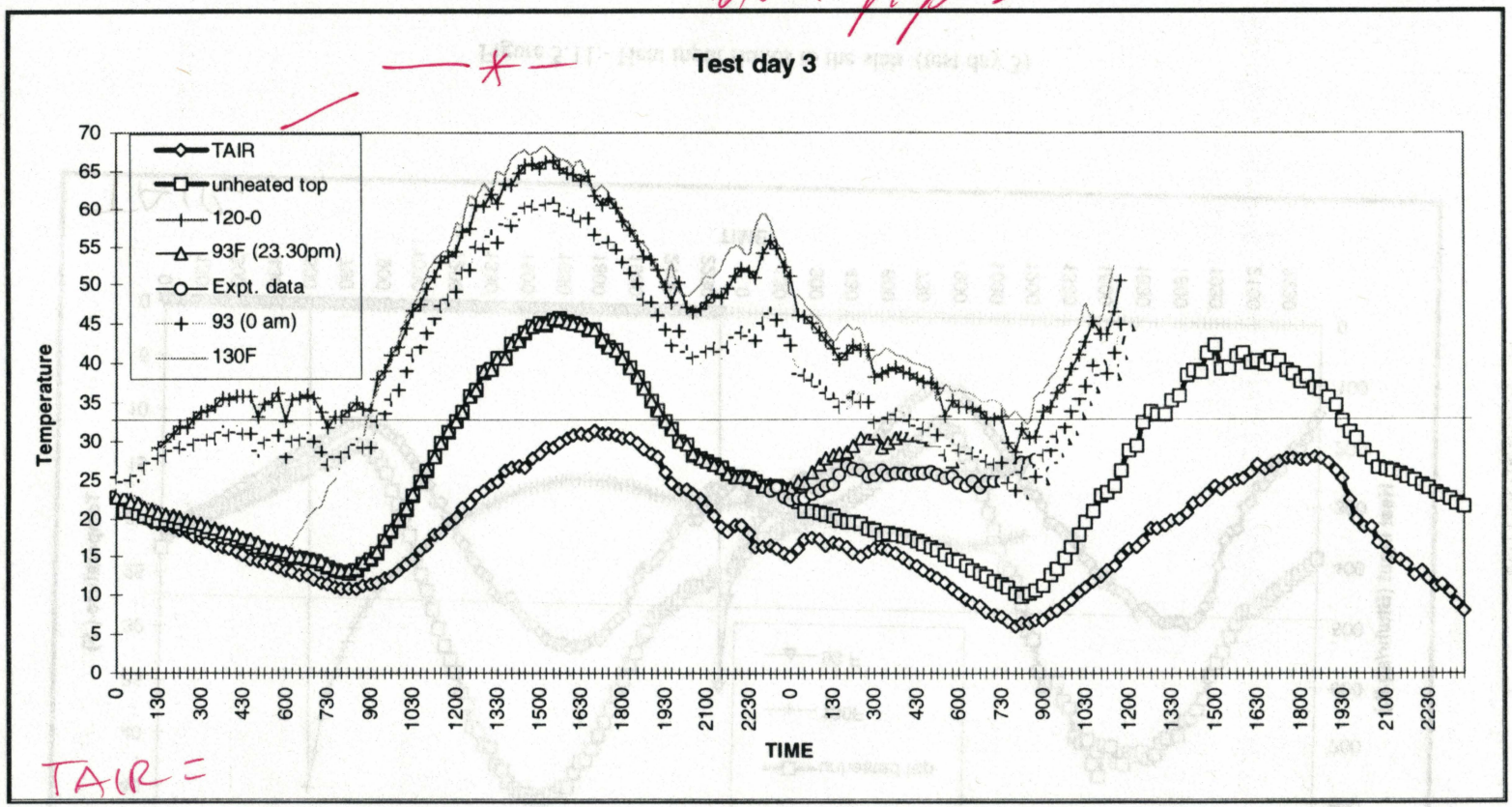

Figure 5.10:- Transient response of slab top surface (test day 3)

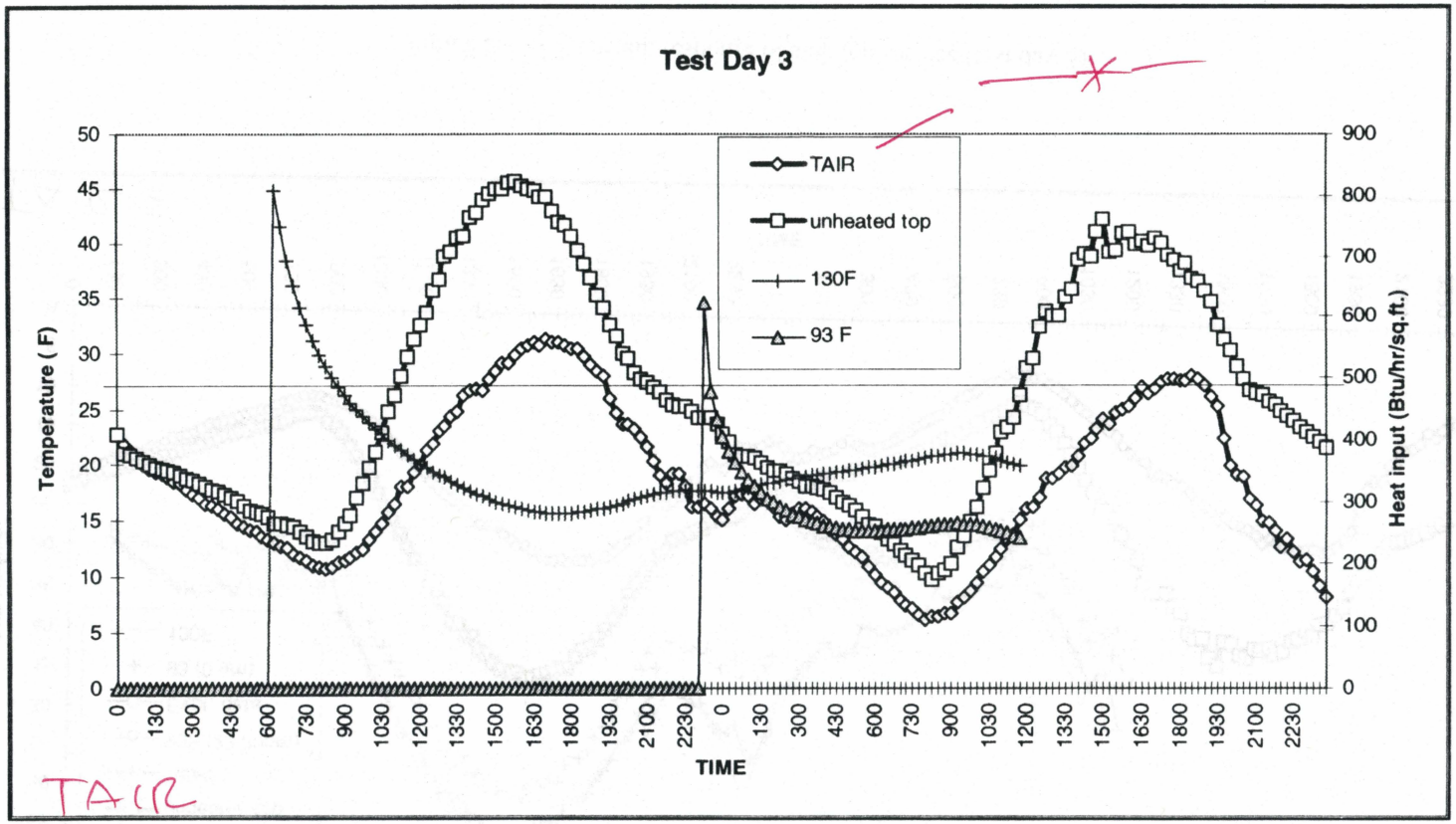

Figure 5.11:- Heat input fluxes to the slab (test day 3)

5.3.3.3 Heat loss calculated by BRIDGE3D and ASHRAE

The heat flux as calculated by the ASHRAE model required for a day like test day 3 would be approximately 225 Btu/hr/ft^2. This heat flux is of course valid for snow melting incidence, whilst there was no snowfall on test day 3. However these would provide an upper bound for the heat input requirement as the precipitation load for test day 3 does not exist. Simulation for test day 3 shows that a heat input of 350 Btu/hr/ft^2 was required to keep surface temperature above freezing. The reason for this could be attributed to the convection and radiation losses, as calculated by both models (ASHRAE and BRIDGE3D). Further investigation of these differences should be made. Figure 5.12 provides a comparison of the convective and radiative losses as calculated by the ASHRAE relations and the computer model BRIDGE3D for test day 3.

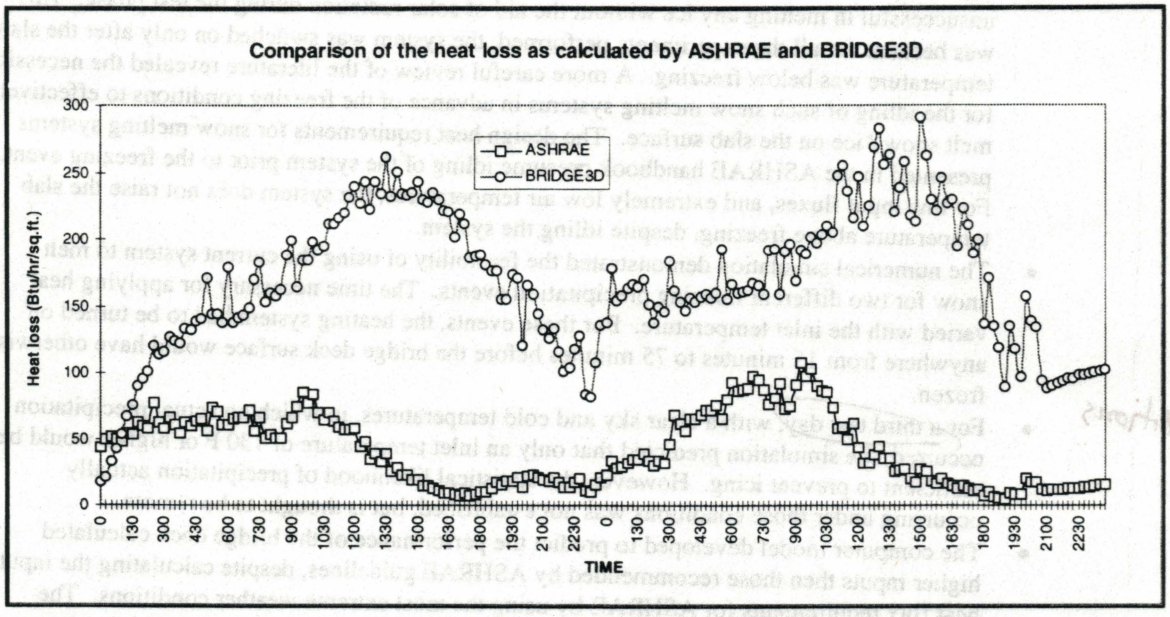

Figure 5.12:- Heat loss comparison between ASHRAE and BRIDGE3D

6. CONCLUSIONS AND RECOMMENDATIONS

An experimental facility was constructed to study the feasibility of using ground source heat pumps for bridge deck deicing. The test bridge deck built was essentially a concrete slab insulated on all sides, except the top to represent the middle section of a bridge deck. Due to the time spent initially on building the experiment and putting it into operation, the snow season for the year was missed. Experiments were hence performed by simulating artificial precipitation by using a hand held spray. A very detailed numerical model was developed and validated using the experimental data. Based on the experiments run and subsequent simulations performed, using the numerical model, the following conclusions can be made about the bridge deck deicing system:

- The bridge deck deicing system, as built, appears to be a feasible system, however it was unsuccessful in melting any ice without the aid of solar radiation during the test phase. This was because for all the experiments performed, the system was switched on only after the slab temperature was below freezing. A more careful review of the literature revealed the necessity for the idling of such snow melting systems in advance of the freezing conditions to effectively melt snow / ice on the slab surface. The design heat requirements for snow melting systems presented in the ASHRAE handbook presume idling of the system prior to the freezing event. For low input fluxes, and extremely low air temperatures, the system does not raise the slab temperature above freezing, despite idling the system.
- The numerical simulation demonstrated the feasibility of using the current system to melt snow for two different freezing precipitation events. The time necessary for applying heat varied with the inlet temperature. For these events, the heating system had to be turned on anywhere from 15 minutes to 75 minutes before the bridge deck surface would have otherwise frozen.
- For a third test day, with a clear sky and cold temperatures, in which no actual precipitation occurred, the simulation predicted that only an inlet temperature of 130 F or higher would be sufficient to prevent icing. However, the statistical likelihood of precipitation actually occurring under those conditions was not established, but is thought to be remote.
- The computer model developed to predict the performance of the bridge deck calculated higher inputs then those recommended by ASHRAE guidelines, despite calculating the input heat flux requirements for ASHRAE by using the most extreme weather conditions. The computer model predicted the transient response of the system and calculated higher input requirements for the system than those developed by ASHRAE. Convection and radiation losses as calculated by ASHRAE were found to be much lower than those computed by the numerical model.

The experimental facility and numerical model were used to investigate the feasibility of a bridge deck deicing system. While several aspects of the feasibility were established, there are some additional questions which need to be addressed. The absence of snow and other weather conditions precluded further experimental investigations. The following recommendations for a further study can be made:

- Perform some experiments while idling the system and running it prior to the application of precipitation.
- A statistical study of the weather should be made to determine the day with the most severe weather conditions under which natural precipitation occurs. The system should be sized with the requirements calculated by using these weather conditions.
- Only about 30-40 % of the heat output delivered by the heat pump went to the slab. There was considerable amount of heat loss to the ground and also to the atmosphere. This limited the input heat flux for the experimental facility. A higher inlet temperature can be achieved by using a higher capacity heat pump, or adding an auxiliary heater, or reducing the underground pipe heat loss by insulating the pipes.
- The insulation thickness for the bottom of the bridge slab insulation was small. The insulation thickness and air tightness should be improved to reduce unnecessary weather losses.

- The instrumentation and experimental procedure should be modified for more accurate results. Specific improvements that need to be made include grounding the thermocouples wire shields and taking voltage readings from the flow meter continuously throughout the experiment and not at discrete intervals. More careful calibration of inlet and outlet thermal probes is necessary and more internal slab temperatures should be acquired.
- The computer model should be modified to incorporate precipitation.
- Further validation and improvement of the model by acquiring more experimental data under a wider range of conditions.

7. REFERENCES

Adlam, T.N. (1950). *Snow melting*. New York. The Industrial Press.

ASHRAE. (1993). *ASHRAE Handbook*. Fundamentals. American Society of Heating, Refrigeration and Air - Conditioning Engineers, Inc. Atlanta.

ASHRAE. (1995). *ASHRAE Handbook*. Heating, Ventilating, and Air - Conditioning Applications. American Society of Heating, Refrigeration and Air - Conditioning Engineers, Inc. Atlanta.

Babaei, K., and Hawkins, N. M. (1987). *Evaluation of Bridge Deck Protective Strategies, National Cooperative Highway Research Program*. Report No. 297, Transportation Research Board, Sept.

Bent, S. (1992) *A Numerical Model for Prediction of Road Temperature and Ice*. Journal of Applied Metrology, Vol. 31, No. 12, Dec. 1992.

Blackburn, R. R., Glennon, J. C., Glautz, W. D., and St. Johns, A. D. (1978). *Economic Evaluation of Ice and Frost on Bridge Decks, National Cooperative Highway Research Program*. Report No. 182, Transportation Research Board.

Brinkman, C.P. (1975). *Space Age Technology for Deicing Hazardous Highway locations*. Public Roads, Vol. 39, No. 3., pp. 89-95.

Chapman, W. P., Katunich, S. (1956). *Heat requirements of Snow Melting Systems*. ASHRAE Transactions, Vol. 62, pp. 359-372.

Clarke, J.A. (1985) *Energy Simulation in Building Design*. University of Strathclyde, Glasgow, Scotland. Adam Hilger Ltd.

Croft, D., Lilley, D. (1977) Heat Transfer Calculations using Finite Difference Equations. Essex. Applied Science Publishers.

"Deicer Plays Vital Role in Winter Bridge Maintenance." (1994). *Public Works*, July, pp. .33-34.

"Deicing Agents: A Primer." (1991). Dow Chemical Co., Midland, Michigan. *Public Works*, 122(8), July, pp. 50-51.

Fleeg, E. (1990). *Minnesota DOT Tests Deicing Alternatives*. Public Works, 121(8), July, pp. 58-59.

Havens., J. H., Vernon, A. W., Rahal, A. S., Deen, R. C. (1979) *Heating Bridge Decks by Electrical Resistance*. Snow Removal and Ice Control Research, Special Report 185, -Transportation Research Board.

Isaka, H. et al., (1990). *Prediction of road surface temperature*. Proceedings of the 5th International Road Weather Conference, March 13. Standing International Road Weather Commission.

Jones, F. (Oklahoma State University) (1996). Personal Phone Conversation. Sept. 26.

Kempe, C. (1990). *An estimation of the value of special weather forecasts in a pilot project for road authorities in Sweden*. Proceedings of the Technical Conference on Economic and Social Benefits of Meteorological and Hydrological Services, Geneva. March 26-30. World Meteorological Organization.

Kilkis, I.B, (1994). *Design of Embedded snow melting systems. Part 1: Heat requirements - An Overall Assessment and Recommendations*. ASHRAE Transactions, 1994, part 1, pp. 423-441.

Lee, R. C., Nydahl, J. E., and Pell, K. M. (1986). *Design and Implementation of a Water Powered Heat Pipe System for Bridge Heating*. Report No. FHWA-WY-86-002, Dec.

Leal M.R., *A Mathematical Model for the Heating of a Plane Slab by Embedded Cylindrical Sources*. Ph.D. Dissertation, Mechanical Engineering Department, Kansas State University, 1971.

Leal, M.R., Miller, P.L. (1972). *An Analysis of the transient temperature distribution in pavement heating installations*. ASHRAE Transactions 78(2). pp. 61-66.

Liao., C. J,., (1996). *Untitled MS. Thesis*. Oklahoma State University.

Long, D. C., and Baldwin, J. S. (1980). *Snow and Ice Removal From Pavement Using Stored Earth Energy*. Report No. FHWA-TS-80-227.

Malloy, D. (Oklahoma Department of Transportation) (1994). Phone conversation with T. D. Hogue, Mar. 8.

Nydahl, J., Pell, K., Lee, R., and Sackos, J. (1984). *Evaluation of an Earth Heated Bridge Deck.* Report No. FHWA-WY-84-001, Apr.

Nysten, E. (1980) *Determination and forecasting of road surface temperature in the COST-30 automatic road station (CARS).* Unpublished, copy available in the National Meteorological Library, Bracknell.

O' Dell, B. (1994). *3-D Heat Conduction Transfer Model.* Class Project for MAE 5873. Oklahoma State University.

Oklahoma Mesonet, The. (1993). Pamphlet published by the Oklahoma Mesonet network, Norman, OK.

Parmenter, B. S., Thornes, J. E., (1986). *The use of a computer model to predict the formation of ice on road surfaces.* Research Report 71, Transport and Road Research Laboratory.

Pell, K. M. (University of Wyoming) (1994). Phone conversation with T. D. Hogue, Feb. 18.

Ponting, M. (1984) *Weather Prediction Systems.* Journal of the Institution of Highways and Transportation, November., pp. 24-31.

Press , W.H., Flannery, B.P., Teukolsky, S.A., Vetterling, W.T. (1986). Numerical Recipes. Cambridge University Press.

Rayer, P.J. (1987). *The Meteorological Office forecast road surface temperature model.* Meteorological Magazine, 116, pp. 180-191.

Shao, J. (1990). A winter road surface temperature prediction model with comparison to others. Ph.D. thesis. University of Birmingham.

Spitler, J. D., Hogue, T. D. (1995). *Prevention of Bridge Deck Icing Using Geothermal Heat.* Research Proposal. Oklahoma State University.

Stephenson, T. E. (1988). *Wisconsin's winter weather system.* In. Proceedings of the 4th International Conference on Weather and Road Safety, Florence. November 8-10. Standing International Road Weather Commission.

Schnurr, N. M., Rogers, D.B. (1970). Heat Transfer Design Data for Optimization of Snow Melting System, ASHRAE Transactions, vol. 76, Part 2, pp. 257-263.

Taylor, J. R. (1982). *An Introduction to Error Analysis- The Study of Uncertainties in Physical Measurements.* University Science Books, Mill Valley, California.

Thompson, N. (1988). *The Meteorological Office road surface temperature prediction model.* In. Proceedings of the 4th International Conference on Weather and Road Safety, Florence. November 8-10. Standing International Road Weather Commission.

Thornes, J. E., (1984) *The prediction of ice formation on motorways.* Ph.D. thesis. University of Birmingham

Thornes, J.E., Shao, J. (1991) *A comparison of UK road ice prediction models.* Meteorological Magazine, 120, pp. 51-57.

Trent, D.S., Welty, J.R. (1974). *A summary of numerical methods for solving transient heat conduction problems.* Corvallis, Oregon. Oregon State University Engineering Experiment Station.

Winters, F. (1977). *Pavement Heating, 1969-1975, Final Report.* Division of Research and Development. New Jersey Department of Transportation.

Williams, G.P. (1976). *Design heat requirements for embedded snow-melting systems in cold climates.* National Research Record No. 576. Washington, D.C: Transportation Research Board.

Williamson, P. J.(1967). *The estimation of heat outputs for road heating installations.* RRL Report No. LR 77. Crowthroe Road Research Laboratory.

Wright, B.W. (1988). *A comparison of Numerical Methods for the Prediction of Two- Dimensional Heat Transfer in an Electrothermal Deicer Pad.* National Aeronautics and Space Administration.

8. APPENDIX

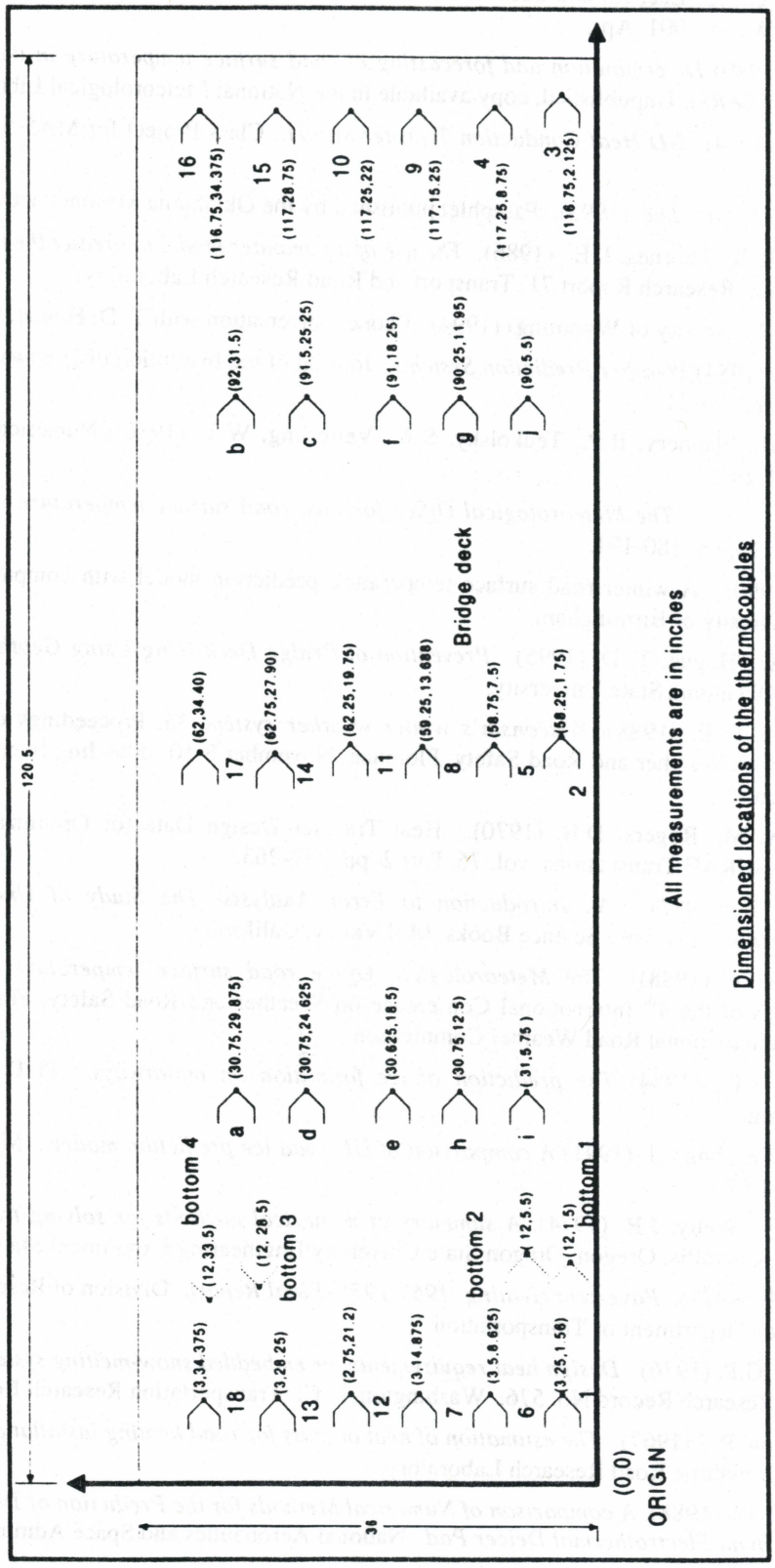
120.5
36
(0,0)
ORIGIN
bottom 4
bottom 3
bottom 2
bottom 1
Bridge deck
(3.34.375)
18
(12.33.5)
(3.28.25)
13
(12. 28 5)
(2.75.21 2)
12
(3.14.875)
7
(3 5.8 625)
6
(12.5.5)
(3 25.1 58)
1
(12.1.5)
(30.75.29 875)
a
(30.75.24 625)
d
(30.625.18.5)
e
(30.75.12 5)
h
(31.5.75)
i
(62.34.40)
17
(62.75.27 90)
14
(62.25.19.75)
11
(59.25.13.688)
8
(58.75.7.5)
5
(58.25.1 75)
2
(92.31.5)
b
(91.5.25 25)
c
(91,18 25)
f
(90.25.11.95)
g
(90.5.5)
j
16
(116.75.34.375)
15
(117.28 75)
10
(117.25.22)
9
(117.15 25)
4
(117.25.8.75)
3
(116.75.2.125)
All measurements are in inches
Dimensioned locations of the thermocouples

THERMAL STRESS PREDICTIONS FOR GEOTHERMALLY HEATED BRIDGE DECKS

By

Chen-Jui Liao

Timothy D. Hogue

Prepared for
State of Oklahoma
Department of Transportation
September, 1996

THERMAL STRESS PREDICTIONS FOR GEOTHERMALLY HEATED BRIDGE DECKS

By Chen-Jui Liao and Timothy D. Hogue

ABSTRACT

An active geothermal deck heating system has been developed to eliminate ice on bridge decks. A test section with the deck heating system was built to represent a section of actual bridge decks. The test section was elevated above the ground and placed at an outdoor location to simulate realistic heat transfer conditions near bridge sites. Fluid temperatures at the inlet and outlet of embedded piping of the test section were measured by thermocouples.

An actual concrete bridge superstructure was modeled using a three-dimensional bridge superstructure model subjected to input temperature load parameters. Temperature gradients from several possible flow patterns of the deck heating system were developed as temperature loads. Thermal stresses in the bridge deck due to the deck heating system were predicted by the computer program STAAD-III.

With the predicted thermal stresses, higher thermal stresses are induced when the fluid flow patterns of the active geothermal deck heating system are not installed in the same flow direction. More restraints at bridge supports, more thermal stresses will occur in the bridge deck. In addition, higher thermal stresses are induced when temperature differences along the longitudinal direction of the bridge deck are increased. The maximum compressive thermal stress of 500 psi was assessed when the most feasible fluid flow patterns of the deck heating system were assumed to be applied to the bridge deck.

TABLE OF CONTENTS

Can these be lined up better

Chapter Page

CHAPTER I

INTRODUCTION

Preferential Icing of Bridge Decks

Travel is hazardous in the late fall and winter seasons during periods of snow, sleet and freezing rain. Perhaps the greatest danger along the roadway is the frequent occurrence of preferential icing of bridges where bridge decks become icy and slick while adjacent roadways remain clear and free of snow and ice. Several accidents occur due to drivers losing control of their vehicles when they suddenly enter such an icy and slippery section of roadway [6].

Removal of Bridge Deck Ice

The conventional removal of bridge deck ice includes plowing; blading; application of gritty materials; and spreading of deicing chemicals. Mobilized snow eliminating equipment is operated to remove localized ice and slush remaining on the bridge during and after a snow storm [6]. The bridge deck surfaces are treated with sand, or a mixture of salt and sand, and then plowed [3]. Common deicing chemicals cause corrosion of bridge deck reinforcement and vehicles [9] and are ineffective if temperatures fall below 25 °F [7]. The environmental contamination and traffic disruption of the conventional responses are still controversial.

The alternatives include use of high conductive materials and high resistance wires embedded in bridge decks [14]. These deck heating methods are technologically successful but economically unfeasible due to limitations of high initial and operating costs and non-renewable energy sources [6, 14].

Brief Overview of Deck Heating System

Heat within the earth's crust is plentiful throughout the United States [15]. An active geothermal heating system composed of a pump that forces earth-heated fluid flowing through piping to heat bridge decks is considered in this research. The term "active" means the deck heating system is controlled to operate only when needed to prevent ice formation on bridge decks.

A prototype of the deck heating system was tested by a test section. Temperature changes between the inlet and outlet of the prototype were measured by thermocouples. Several different fluid flow patterns are developed to be temperature loads according to temperature changes in the prototype. This research focuses on predicting thermally induced stresses (thermal stresses) in bridge decks due to the different flow patterns of the deck heating system.

Project Objectives

The primary objective of this research is to predict thermal stresses in bridge decks due to the active geothermal deck heating system. Because of the complexity of temperature distribution in the bridge deck, finite element analysis program is used to assist the prediction of the thermal stresses. Once the thermal stresses are assessed, potential detriment in the bridge deck will be examined by a three-dimensional bridge superstructure model.

Project Scope

In Chapter II, currently available techniques about removal of bridge deck icing are categorized in two responses: conventional and alternative methods. The development of the active geothermal heating system is presented. In addition, several literature about thermal stresses in concrete and bridge superstructures are reviewed.

Temperature responses in a typical bridge deck due to the active deck heating system was tested by using a test section. The test section was placed at an outdoor location so that realistic heat transfer conditions near real bridge sites would be simulated. Instrumentation for measuring temperature responses of the test section are also discussed in Chapter III.

In Chapter IV, a three-dimensional finite element model of an actual concrete girder bridge superstructure is used for predicting thermal stresses in the bridge deck due to several possible fluid flow patterns of the deck heating system. The different fluid flow patterns are based on the field temperature measurements obtained from the test section. Service loads (i.e. dead loads, live loads, wind loads, and snow loads, etc.) are not discussed in this research.

The prediction of thermal stresses in the bridge deck implemented by the structural analysis computer program STAAD-III is presented in Chapter V. Temperature load parameters applied to the bridge superstructure model are limited on the use of temperature gradients developed from the possible fluid flow patterns in the deck along the bridge span.

CHAPTER II

RESEARCH BACKGROUND AND DEVELOPMENT

Bridge Deck Icing

Preferential icing of bridge decks is a condition where ice forms on decks while adjacent roadways remain clear and free of snow and ice. This condition usually occurs in the late fall and winter seasons, especially during periods of sleet, freezing rain, and snow. Some drivers lose control of their vehicles and cause accidents when they cross the preferentially iced bridges.

Snow and Ice Removal on Bridge Decks

(1). Conventional Responses

(a). Mechanical Methods

Snow plowing is a mechanical method to remove snow and ice on bridge decks during and after a snow storm. A snow plow's blade may impact deck joints due to a different elevation of adjacent spans.

(b). Abrasive Methods

Bridge decks are frequently treated with sand, cinders, or other gritty materials and then plowed to reduce the accumulation of snow. Friction effect among vehicle wheels, gritty materials and deck surfaces causes heat to melt snow. However, snow removal becomes more difficult when snow changes to ice [6].

(c). Chemical Methods

There are several deicing chemicals in widespread use today: sodium chloride (NaCl), calcium chloride ($CaCl_2$), and magnesium chloride ($MgCl_2$) [3]. They are used to prevent a strong bond from forming between ice and deck surface since they lower the freezing point of water.

Sodium chloride is a popular salt due to its low cost and easily accessible material for government deicing crews [9]. However, ice will not be melted by sodium chloride if temperatures fall below about 25 °F.

Calcium chloride is found to be effective down to the lower temperature of 20 °F [8]. However, calcium chloride is considerably more expensive [7] and more corrosive than sodium chloride [26].

Magnesium chloride is tested by the Wisconsin Department of Transportation (WDOT). The WDOT found that snow is melted well by magnesium chloride if the temperature is above 20 °F. However, magnesium chloride is better than neither sodium chloride [3] nor calcium chloride [8], if the temperature is below 20 °F.

Metals are corroded by many deicing agents. Bridge steel reinforcement and vehicles are corroded since chloride and acids are released from deicing agents. Corroding results in high equipment and maintenance labor costs. Some vegetation near bridges is also contaminated due to excessive spreading the deicing agents [21]. Corrosion protection measures include the use of epoxy-coated bars, galvanized bars, greater concrete cover above the top layer of reinforcing steel bars, concrete surface treatments, and noncorrosive deicing products [4, 9, 25].

Epoxy-coating is to provide steel rebar a barrier to water and prevention of corrosion. Galvanizing is to provide rebar a relatively hard surface. Epoxy-coating is more popular than galvanizing since the Federal Highway Administration (FHWA) endorsed the practice of epoxy-coating and classified galvanizing as experimental in the mid 1970s [25]. Recently, the New York State Thruway Authority adopted galvanizing instead of epoxy-coating because of the harder galvanized surface of rebar and consequent better bond strength between concrete and rebar [25]. The effectiveness of epoxy-coating and galvanizing is still controversial.

Some noncorrosive deicing agents are being developed. The Minnesota Department of Transportation (Mn/DOT) found that 80 percent of rust on deck reinforcing rebar can be prevented using CG-90, an anticorrosive deicer introduced by the Cargill chemical company [9]. Officials in the Mn/DOT hope to find a cost-effective and noncorrosive product since the cost of the CG-90 product is several times than that of sodium chloride [9].

The New York State Energy Research and Development Authority developed calcium magnesium acetate (CMA), a chemical agent which has a less sever impact on the environment. However, practical use of CMA is hampered by its high cost and by availability of the product [3].

Hinrichs designed a fixed-type deicer system which was installed on railings of bridges. The fixed-type deicier system can automatically spread deicing agents over bridge decks. The system is not an effective way to remove ice due to a limited spreading area on bridge decks [6].

(2). Alternative Responses

(a). Weather Sensors and Weather Forecast System

Recently, ODOT has tried to apply road-weather sensors in combination with a weather forecast system to apply deicing agents on roadways and bridge decks. The application of deicing agents is planned and conducted much more efficiently since ODOT can pinpoint when and where to begin anti-icing operations. However, cost of road-weather sensors are considered to be high in the initial installation.

(b). Embedded Materials and Devices

The alternatives include use of high conductive materials and high resistance wires embedded in bridge decks [14]. Fluid heated by fuel is circulated through embedded piping to heat bridge decks. These deck heating methods are technologically successful but economically unfeasible due to limitations of high initial and operating costs and non-renewable energy sources [6, 14].

High resistance wires and high conductive materials are embedded in bridge decks so that snow on decks is melted. Their effects show that there are no disadvantages in corrosion of bridge reinforcing steel, contamination of bridge adjacent vegetation, and disruption of traffic. However, These methods are considered to be expensive since they cost a lot in construction and maintenance and use large amounts of energy in operation [6, 14].

Therefore, the utilization of cheap, renewable, and waste heat sources becomes attractive to replace that of non-renewable and expensive energy sources. Natural heat from the earth or waste heat from power plants and steel shops are feasible substitutes [14]. Geothermal heat is the most attractive energy source among of these substitutes because it is plentiful and available throughout the world [14].

Research in Wyoming [14], West Virginia [15], and Japan [24] has demonstrated that a "heat pipe" deck heating system eliminates preferential icing of bridges. The deck heating systems developed in Wyoming and West Virginia researches are briefly described as follows.

Lee et al. [14] developed a heat pipe system that consisted of evaporator pipes embedded into the ground near a bridge and filled with working fluid. The working fluid was evaporated by the heat of the earth and the vapor traveled upward into condenser pipes embedded in the bridge deck. The vapor then distributed its thermal energy to the deck, gradually condensing in the process. Finally, the condensed fluid flowed back by gravity down into the evaporator to complete the cycle. This system is a passive system in that it operates without need of pumps, control system, external power, or any human intervention. The evaporation-condensation cycle is in operation whenever the bridge deck is cooler than the earth. There is no operating cost. However, the diameter of embedded pipes or the depth of buried evaporator pipes must be increased to compensate for the excessive heat loss.

Ammonia is an appropriate working fluid for the passive system due to its excellent thermal properties and low cost. However, the leakage of ammonia is a potential problem because of its toxicity [14].

The inside of each heat pipe must be carefully cleaned so that fluid flow resulting from the evaporation-condensation cycle is unimpeded. Embedded pipes in bridge decks must also have the correct slope so that condensed liquid can flow back to the evaporators. In the research cited, some pipes became fouled or were improperly installed. Such pipes, once imbedded, cannot be repaired and ice may accumulate over them. In addition, due to the complications of preparing and constructing the system, the installation cost of the heat pipes is prohibitive—around 60 % of the cost of the combined bridge and heating system [18].

(c). Active Geothermal Heating System for Prevention of Bridge Deck Preferential Icing

Nydahl et al. [18] in their Wyoming research showed that ice on bridge decks was melted well by using geothermally heated fluid through embedded steel piping in the decks. Geothermal heat is also plentiful in America, costs much less than other fuels, and less impact to environment due to no toxicity. Therefore, geothermal heat is used to heat working fluid through piping and deliver heat to bridge decks in this research. Active geothermal deck heating system holds the promise of being economical. The term "active" means the system is controlled and operated in combination with weather forecast system. Therefore, heat keeps from loss and any operating costs of conveying heat to the deck are minimized.

In Figure 1, a schematic view of an active geothermal deck heating system is presented. An electric-powered pump circulates geothermally heated fluid through piping to the bridge deck. Fluid flow is forced by pump pressure so no particular slope for the embedded pipes is necessary.

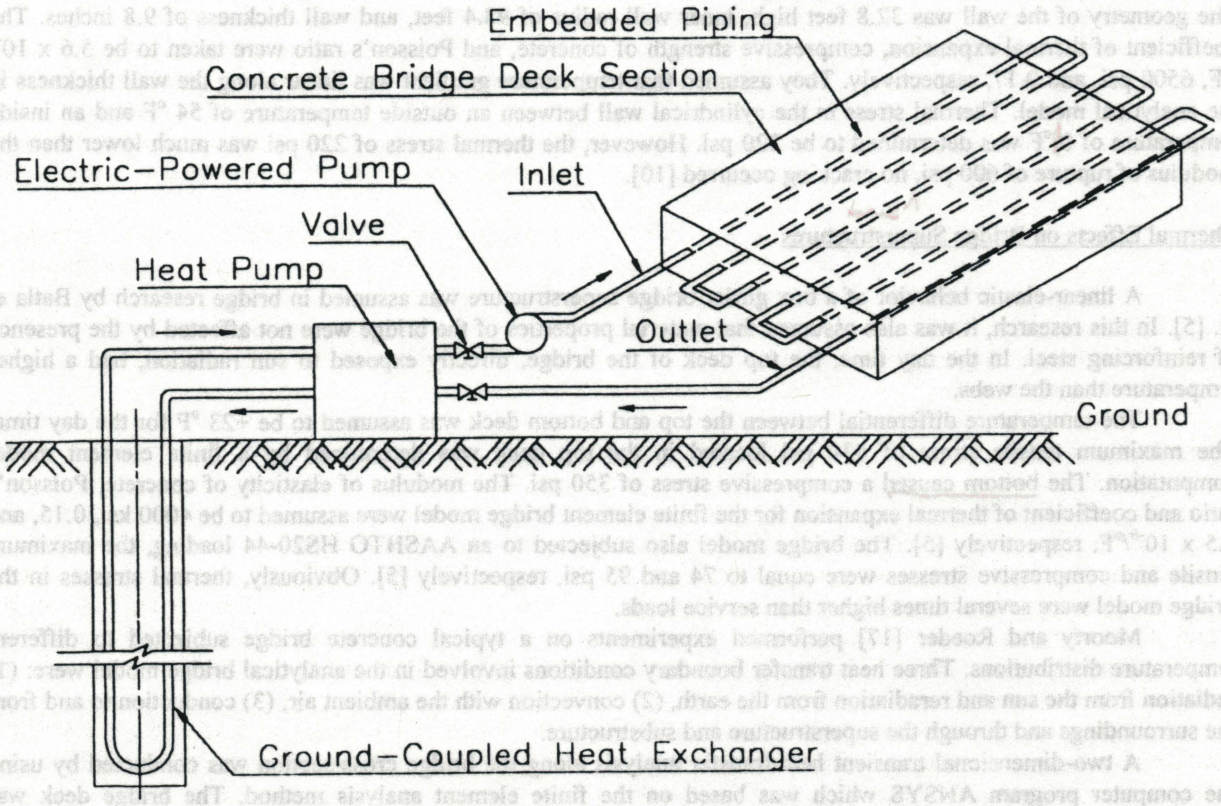

Figure 1. Schematic Diagram of Active Geothermal Deck Heating System.

An electric-powered ground-source heat pump is also incorporated into the system. The heat pump provides additional heat to the hydraulic fluid to remove accumulated ice on bridge decks even when the weather is extremely cold.

To maximize efficiency, the active system proposed could be integrated with weather forecast algorithm utilizing the Oklahoma Mesonet. The Oklahoma Mesonet consists of 108 automated observing stations scattered throughout the state [20]. The active deck heating system would be switched on by a telemetry sent from the Mesonet data collection center based on local Mesonet station data. A bridge deck could then be warmed before snow fell on it. Thus, preferential icing would be prevented.

Can't make this statement.
efforts to eliminate preferential...

The utilization of the active geothermal deck heating system would take full advantage of currently available heating systems and telemetric technologies. Driving on bridge decks would be safer and corroding on bridges and vehicles would be minimized.

corrosion

Thermal Effects on Concrete Structures

Internal stresses in a structural element due to temperature variation are developed given that the element is suitably restrained. Heat effects on concrete or bridge decks have been studied by several researchers and will be reviewed in the following sections.

Ghali and Elliott [10] developed a analytical model of a cylindrical concrete tank wall to predict thermal stresses in the cylindrical wall. The top edge of the wall was free and the bottom edge was completely restrained. The geometry of the wall was 32.8 feet high, inner wall radius of 98.4 feet, and wall thickness of 9.8 inches. The coefficient of thermal expansion, compressive strength of concrete, and Poisson's ratio were taken to be 5.6×10^{-6} /°F, 6500 psi, and 0.17, respectively. They assumed that temperature gradient was linear along the wall thickness in the analytical model. Thermal stress in the cylindrical wall between an outside temperature of 54 °F and an inside temperature of 0 °F was determined to be 220 psi. However, the thermal stress of 220 psi was much lower than the modulus of rupture of 600 psi, no cracking occurred [10].

and

Thermal Effects on Bridge Superstructures

A linear-elastic behavior of a box girder bridge superstructure was assumed in bridge research by Batla et al. [5]. In this research, it was also assumed that material properties of the bridge were not affected by the presence of reinforcing steel. In the day time, the top deck of the bridge, directly exposed to sun radiation, had a higher temperature than the webs.

The temperature differential between the top and bottom deck was assumed to be +23 °F for the day time. The maximum tensile stress of 430 psi located in the top deck was determined by a finite element model computation. The bottom caused a compressive stress of 350 psi. The modulus of elasticity of concrete, Poisson's ratio and coefficient of thermal expansion for the finite element bridge model were assumed to be 4000 ksi, 0.15, and 6.5×10^{-6}/°F, respectively [5]. The bridge model also subjected to an AASHTO HS20-44 loading, the maximum tensile and compressive stresses were equal to 74 and 95 psi, respectively [5]. Obviously, thermal stresses in the bridge model were several times higher than service loads.

max stress in the bottom of the deck.. & the bottom did not cause this

Moorty and Roeder [17] performed experiments on a typical concrete bridge subjected to different temperature distributions. Three heat transfer boundary conditions involved in the analytical bridge model were: (1) radiation from the sun and reradiation from the earth, (2) convection with the ambient air, (3) conduction to and from the surroundings and through the superstructure and substructure.

A two-dimensional transient heat-transfer analysis along the bridge cross-section was conducted by using the computer program ANSYS which was based on the finite element analysis method. The bridge deck was modeled using isoparametric quadrilateral thermal shell elements. The bridge superstructure was supported by a pin bearing plate placed at one end and a rocker bearing plate at the other end [17].

The initial temperature of the bridge was assumed to be uniform and equal to the ambient temperature. The results showed that longitudinal displacements gradually increased along the span but uniformly cross the depth. The transverse displacements symmetrically distributed about the center. However, no thermal stress were discussed in their study [17].

Husley and Emanuel [12] found that thermal stresses in slab-girder concrete bridges were affected by daily temperature fluctuations, and material properties and geometry of the bridges. They assumed that there was no temperature differential along the cross-section of the bridge superstructures. Frictionless bearings were applied to supports in the interior and last abutments. A pinned bearing plate was applied to support in the first abutment. In their analytical model with coefficient of thermal expansion of 4×10^{-6}/°F, they found that thermal stress at the bottom was equal to 497 psi in the midnight during the summer. However, the maximum thermal stress was found to be 4460 psi at the bottom in the afternoon. This compressive thermal stress was much higher than the modulus of rupture. The bridge superstructure was considered in a dangerous condition [12].

due to . . .

Mirambell and Aquado [16] selected a concrete box girder bridge to investigate environmentally induced thermal stresses in the bridge superstructure. They found that the temperature distribution in the bridge superstructure was nonlinear. Model parameters included environmental heat transfer boundary conditions around the bridge, material properties, location, and geometry of the bridge. If the depth-width ratio of the superstructure

was increased one time, the compressive thermal stress at the bottom was found to be 0.2 MPa (0.30 psi) due to a temperature differential of 10 °C from the top to the bottom along the depth.

Priestley [22] used an approximate method to analyze deformation of a concrete box-girder bridge when temperature gradient data was not sufficient. In the concrete box-girder bridge, the temperature uniformly raised on the top deck was assumed to be higher than that of other portions. If the bridge was unrestrained, the deformation of the top deck would vary with the variation of temperature inside the section.

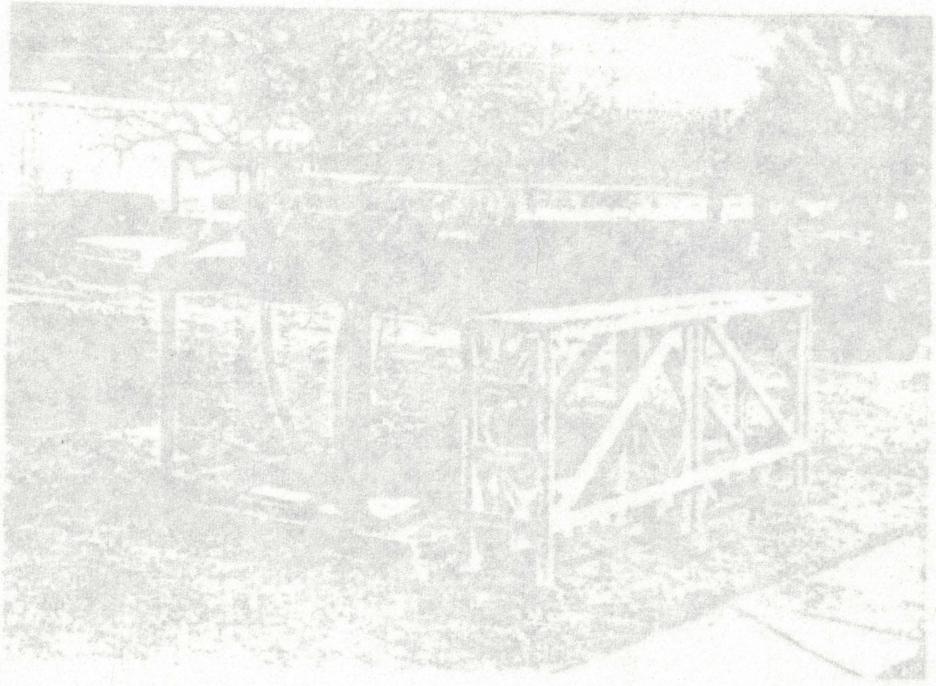

CHAPTER III

PROTOTYPE OF ACTIVE GEOTHERAML DECK HEATING SYSTEM

A prototype of the active geothermal deck heating system applied on bridge decks was modeled by using a test section. Temperature responses of the test section due to the deck heating system were measured. A photograph of the prototype is shown in Figure 2.

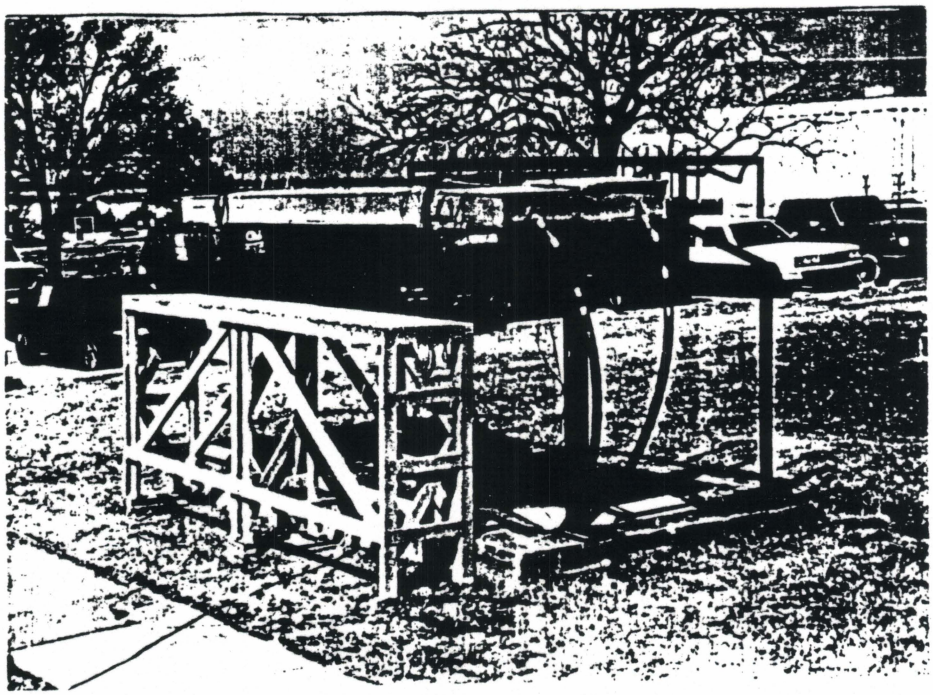

Figure 2. Prototype of Deck Heating System.

In the photograph, the prototype consisted of the test section which was encased by plywood along the edges and supported by a prefabricated steel frame. A wooden truss placed in the front of the steel frame was used for the researchers to inspect instrumentation on the test section.

Test Section

The test section dimensions were selected to represent a small section of a real concrete bridge deck. The dimensions for the test section are 10-ft length by 3-ft width by 8-inch thickness. The 10-ft length is about one forth of a typical 40-ft-wide clear roadway. The 3-ft width is considered to accommodate 6 pipes with equal space of 6.5 inches so that heat through the six pipes would be dissipated to any point of the test section. The value 8 in. is a typical deck thickness of concrete girder bridges.

The details of the test section are illustrated by a schematic diagram in Appendix A. The strength of concrete and the arrangement of reinforcing steel in this test section are patterned after the specification and design details of a typical Oklahoma highway bridge [19].

Figure 3 shows that there are six polybutylene pipes with 7/8-in. outside diameter and 12-ft length embedded in a parallel direction. The embedded polybutylene pipes were elevated 3.44 in. above the bottom since available space was limited by reinforcement within the test section.

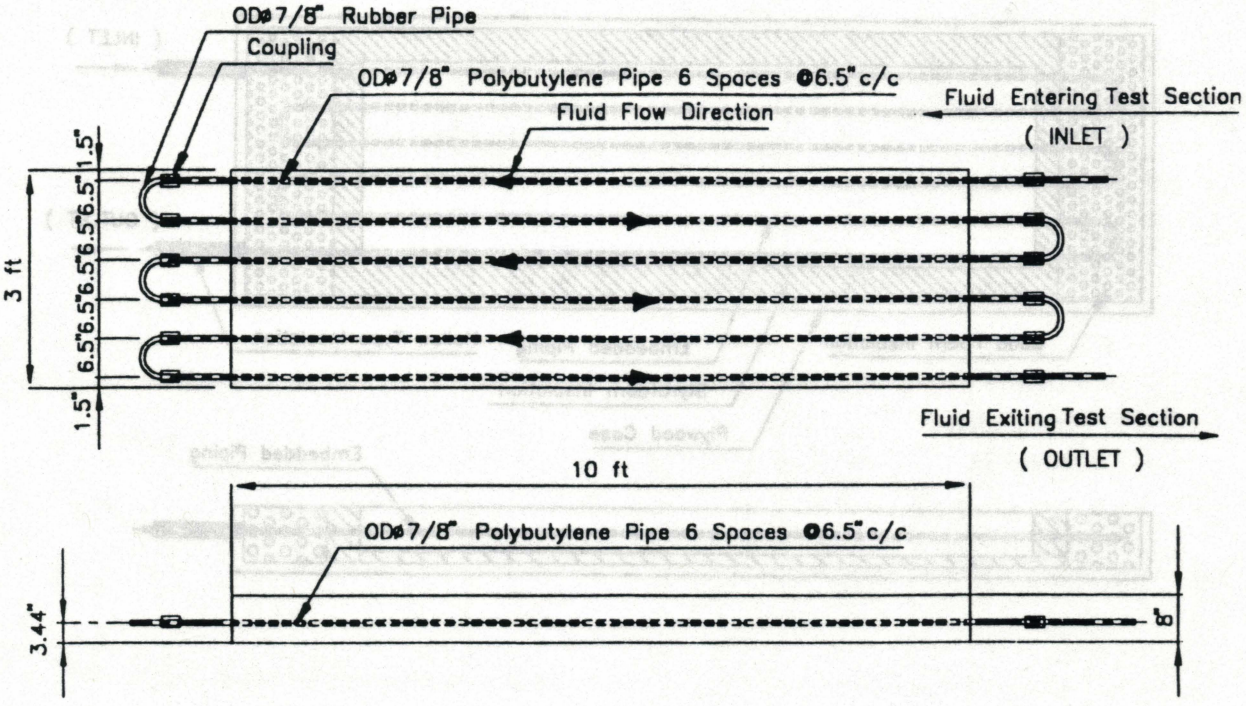

Figure 3. Schematic Diagram of Piping and Fluid Flow Pattern of Test Section.

The embedded pipes were placed at equal spacing of 6.5 in. center-to-center resembling reinforcement spacing used in typical bridge decks. Therefore, the embedded pipes can be directly tied with top reinforcing steel without additional chair to support them.

The ends of each 12-ft-long polybutylene pipe were connected with flexible rubber pipes by coupling so that a loop of the test section piping was formed. Figure 3 also shows the piping and a fluid flow pattern of the test section. The geothermally heated fluid was pumped through the piping of test section entering the inlet, through the piping, and leaving from the outlet. Thus, the fluid flow pattern of the test section was established to represent the prototype deck heating system which would be applied to a real bridge situation.

Once the test section was cast and cured, it was placed on the top of the prefabricated steel frame at an outdoor location. The details of the steel frame are illustrated by a schematic diagram in Appendix B.

In order to simulate a continuous region of a real bridge deck with little heat flux transfer, all edges of the test section were insulated by Styrofoam [27], a foamed polystyrene which has been used for various applications in the temperature range from about -22 °F to 212 °F [11]. A schematic diagram of the test section insulation is illustrated by Figure 4.

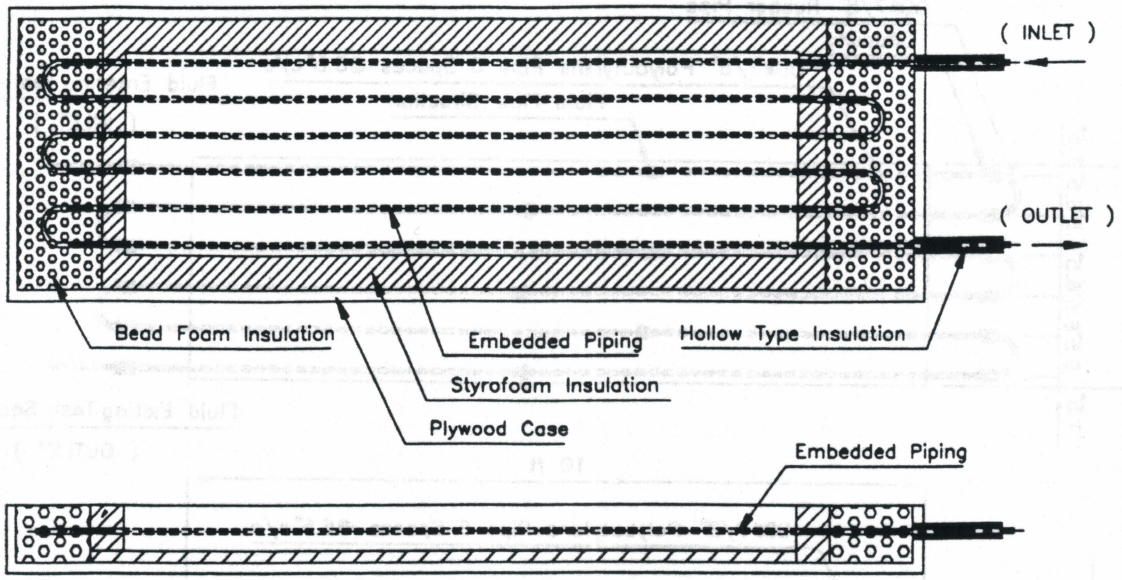

Figure 4. Schematic Diagram of Test Section Insulation.

The bottom of the test section was insulated by Styrofoam to reserve heat for energy savings and examine the benefits such insulation might provide in an actual application. In addition, the piping outside the test section was filled with bead foam insulation which was encased by plywood. Hollow-shaped insulation was used to wrap along the other piping outside the plywood case. The top was directly exposed to air so that realistic heat transfer conditions near an actual bridge deck was simulated.

Data Acquisition

The investigation of temperature changes in the test section due to the prototype heating system is one objective of this project. Field temperature measurements were completed by two devices: (1) thermocouples; (2) a data acquisition system. The two devices are described as followings:

(1) Thermocouples

A thermocouple was used to measure temperature changes of the test section. After surface preparation, thirty-two thermocouples were bonded on the top and bottom of the test section with a thin layer of epoxy and hydraulic cement. Temperature distributions over the top and bottom were recorded. Figure 5 shows the locations of

thermocouples on the test section: twenty-eight on the top, four on the bottom, and two inserted in the inlet and outlet of the embedded piping.

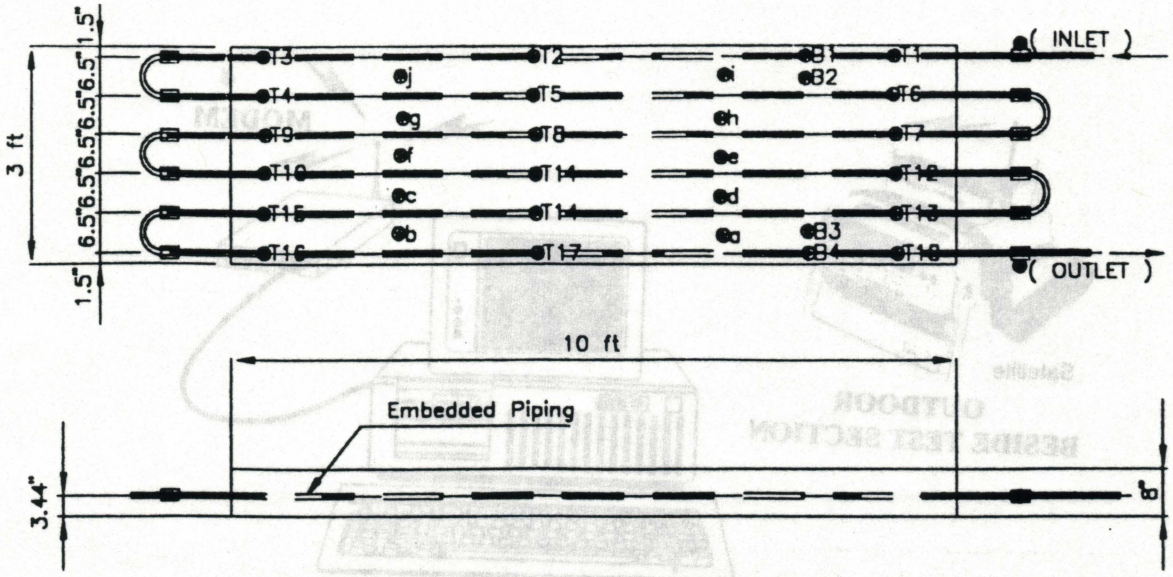

Note: (1) Mark ● represents thermocouple.
(2) T and B indicate the location of thermocouples on the top and bottom, respectively.
(3) The lower case of english letters indicate the location of thermocouples at the center of pipe spacing on the top of the test section.

Figure 5. Locations of Thermocouples on Test Section.

Two thermocouples were respectively inserted into the inlet and outlet of the embedded piping to detect the fluid temperature change after fluid flowing through the piping. One thermocouple was hung 1 in. above the test section to measure ambient temperature variation. Terrain temperature below the test section was also measured.

(2) Data Acquisition System

A data acquisition system was used for remote site data acquisition which consisted of a wireless base station and a remote satellite shown in Figure 6. The wireless base station was located inside the monitoring station and consisted of a computer and a wireless modem. A program called Wireless Logger which allowed the computer to store data from the remote satellite and process data with a spreadsheet was installed in the computer.

The remote satellite placed near the test section consisted of a modem and a data logger called Hydra which collected data from thermocouples. The modem enabled data collection and transmission to the indoor base station from the outdoor satellite.

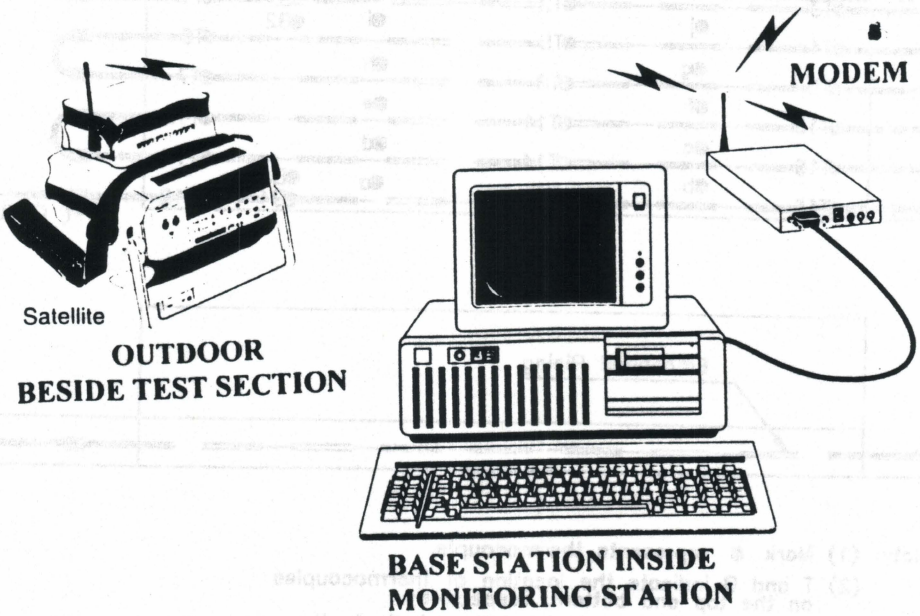

Figure 6. Data Acquisition System.

Field Temperature Measurements

Temperature measurements were completed by other researchers from the School of Mechanical and Aerospace Engineering at Oklahoma State University. Field tests were conducted from March 16 to April 6. In order to simulate a low-temperature environment, all tests were performed from the late night to the early morning. Therefore, field temperature measurements were not affected by radiation from the sun and reradiation from the earth. Heat transfer and reradiation from the steel frame or other substructures were assumed negligible.

Air temperatures at Stillwater during the test period, as shown in Figure 7, were obtained from the Oklahoma Mesonet data. The air temperatures on March 20, 21, 22, 25, and 26 were found below the water freezing point of 32 °F.

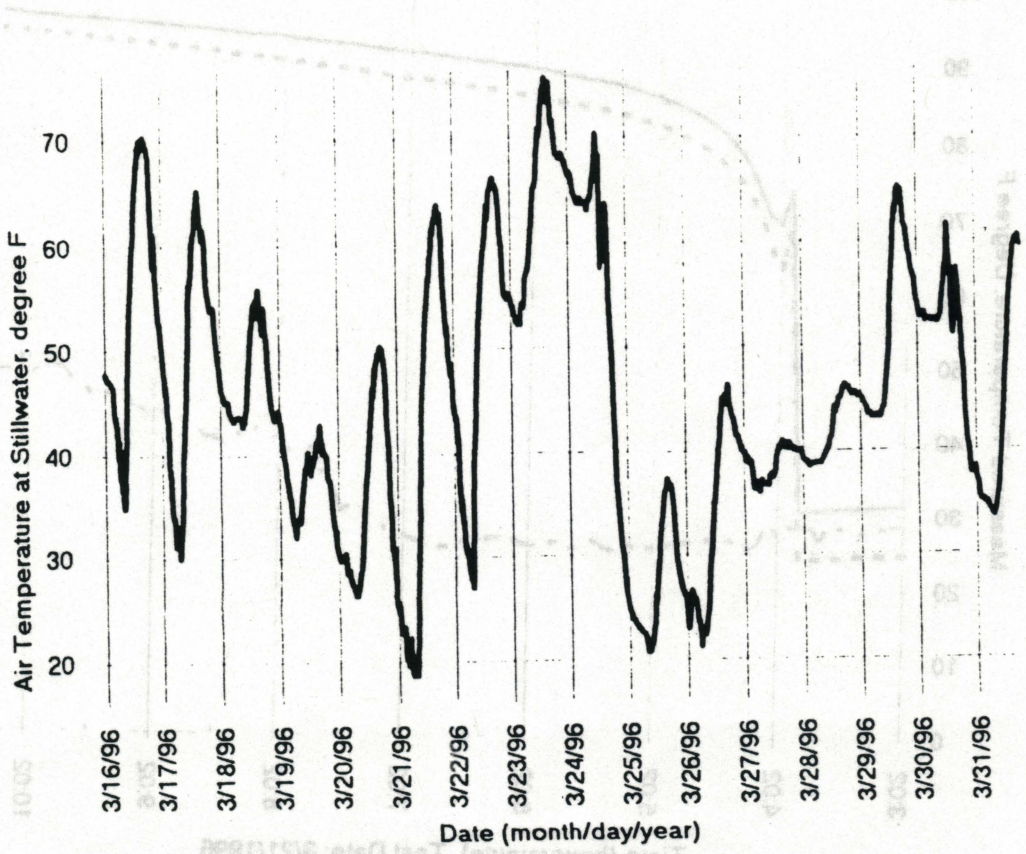

Figure 7. Air Temperatures Obtained from Oklahoma Mesonet Data.

No precipitation of snow was found during these days. However, tests while air temperatures below 32 °F were considered to represent typical temperature responses of the test section when the prototype deck heating system was switched on.

From the temperature measurements on 21 March 1996, which was the coldest day during the test period, the highest fluid temperature at the inlet of the embedded piping was measured about 96 °F after the prototype deck heating system had been switched on about 6 hours. The ambient temperature and the fluid temperature at the inlet and outlet of the test section piping is shown as Figure 8.

The maximum fluid temperature loss between the inlet and outlet of the embedded piping was found to be about 3 °F. Therefore, the average rate of fluid temperature loss through the 60-ft-long piping was determined to be 0.05 °F/ft at the constant fluid flow rate of 3.24 ft/sec [27]. However, the rate of 0.05 °F/ft was applicable when the bottom of the test section was insulated.

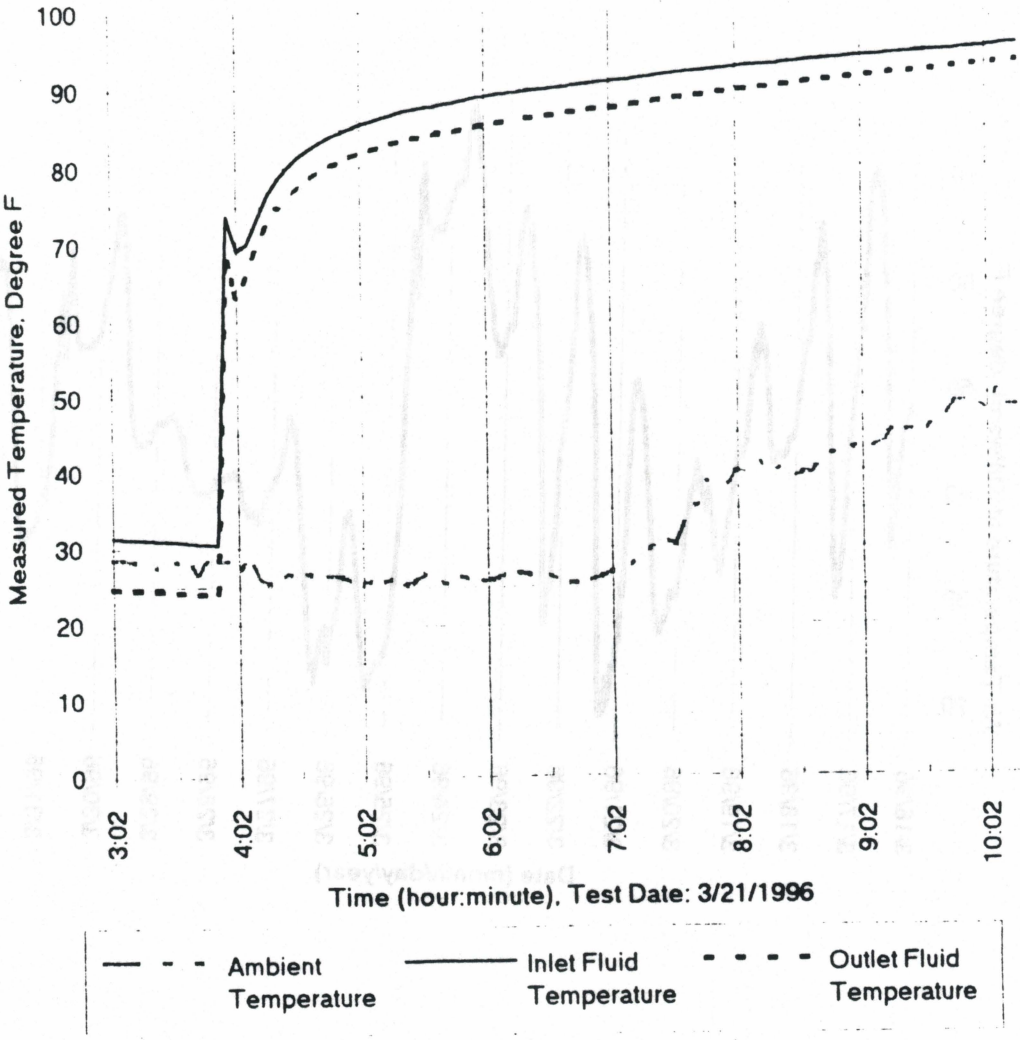

Figure 8. Field Temperature Measurements on March 21, 1996.

In Figure 8, measured temperatures at the inlet and outlet before 4:20 am were suddenly jumped and dropped within ten minutes. The two temperature spikes were caused by a segment of the piping temperature already heated by a warmer room temperature for a while [27]. The segment of piping was connected to the pump and heat pump because they had been placed inside the monitoring station. Fluid temperature differentials around the spikes were unstable and neglected in this study.

CHAPTER IV

FINITE ELEMENT MODELING

Introduction

Thermal stresses due to the deck heating system in an actual concrete girder bridge deck are assessed using a finite element analysis program. In order to predict the thermal stresses, a 3D bridge superstructure model of the actual concrete girder bridge superstructure is developed in this Chapter.

In addition, the finite element bridge superstructure model requires a complete description of the geometric and elastic properties of the actual bridge superstructure being modeled, and the boundary conditions to be applied. Three different support features, while modeling the bridge superstructure model, are also presented in this chapter.

Description Of Concrete Girder Bridge

An actual concrete girder bridge with a 100-ft-long span and a 41-ft-8-inch-wide roadway is schematically shown in Figure 9. The superstructure of the actual bridge is elevated above the ground 40 feet and supported by abutments.

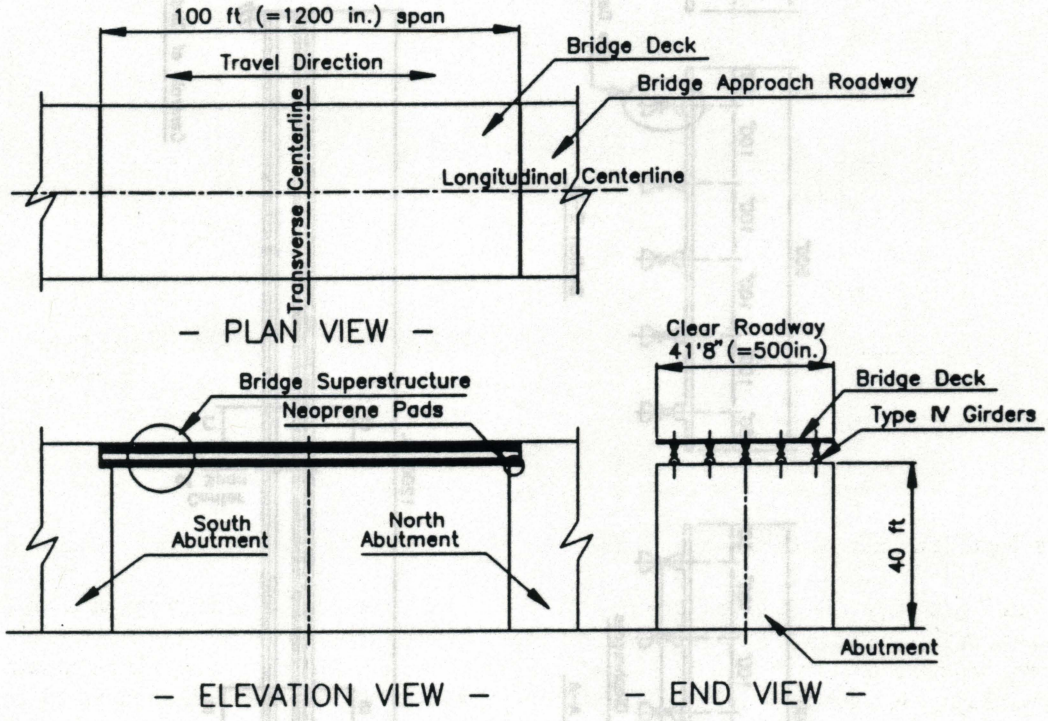

Figure 9. Concrete Girder Bridge.

The bridge superstructure consists of a continuous 8-inch thickness, cast-in-place concrete deck acting compositively with five Type IV AASHTO prestressed concrete I-girders. The Haunch between the deck and girders is 3 inches in thickness. The centroid of the prestressed girder is 24.73 inches above the bottom of its depth [1].

Figure 10 presents the configuration and dimensions of the superstructure. Diaphragms are cast in the ends of the prestressed girders and monolithic with the deck. Diaphragms are also cast in the ends and mid-spans between each pair girders to provide stability and to stiffen this superstructure.

The continuous deck is connected to the girders by bent dowels which are embedded into the girders. The bent caps provide pinned joint connections between the deck and girders. The effect of side barriers on the deck are not considered in this study. Neoprene bearing pads, placed between the abutments and girders, allow relatively free movement of the superstructure.

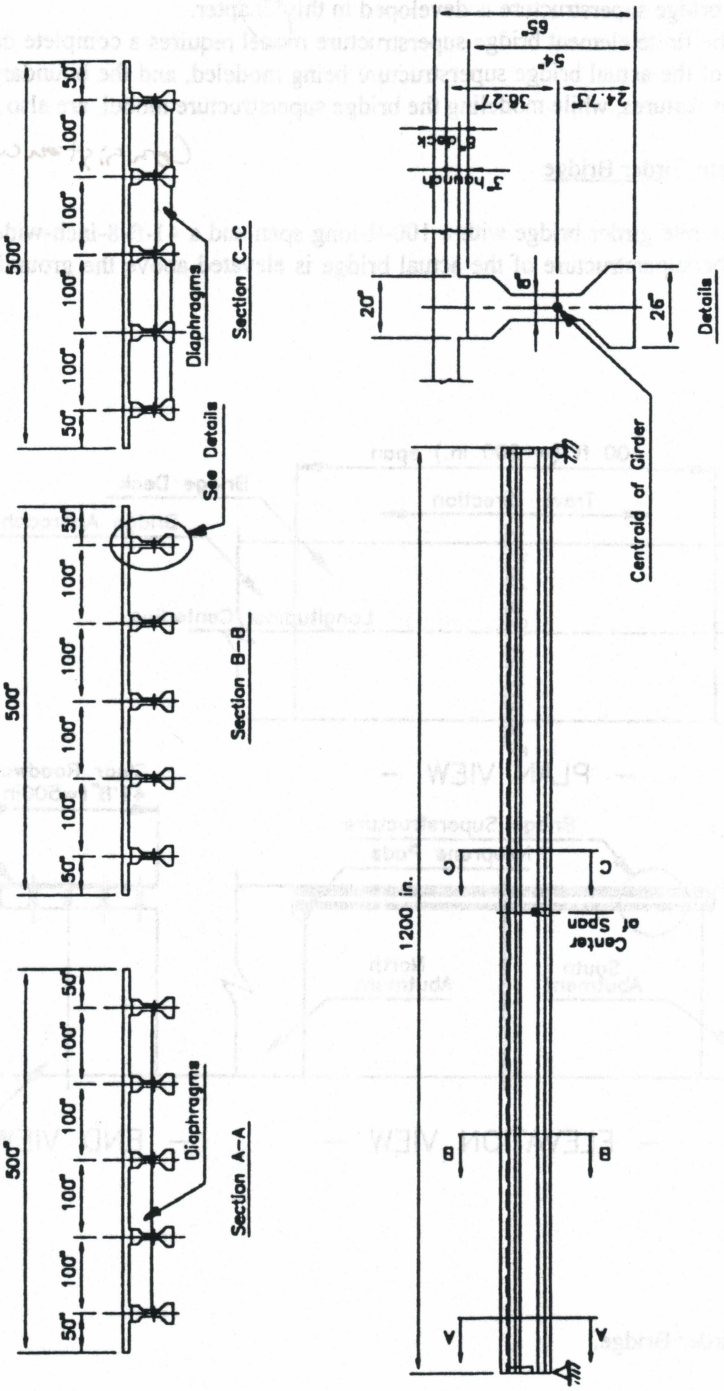

Figure 10. Superstructure of Concrete Girder Bridge.

Finite Element Software

The 3D finite element model of the concrete girder bridge superstructure is presented using a commercial computer program, STAAD-III [23]. STAAD-III is installed on a personal computer (PC) and runs on the Disk Operating System (DOS). It is a finite element analysis software used in the analysis of structural engineering problems and also equipped with design, graphics, and visualization capabilities.

STAAD-III deals with beam and frame elements, even shell finite element which is based on hybrid finite element formulations [23]. The shell element can be used to model "surface structures" such as bridge decks. Temperature loads due to a uniform increase or decrease of temperature and to a difference in temperature between top and bottom surfaces of the element can be imposed as an element load. Therefore, a nonlinear temperature difference along the bridge deck depth is not applicable to be the element load. In addition, the element aspect ratio cannot be excessive for the shell element. The aspect ratio is recommended to be on the order of 1:1 and preferably less than 4:1 [23].

Description Of Bridge Superstructure Model

The general configuration and size of an actual concrete girder bridge and bridge superstructure as illustrated in Figure 9 and 10 have been described in the previous section. The 3D bridge superstructure model, as shown in Figure 11, is based on this bridge superstructure. The bridge width, depth, and length are respectively assigned along the X-axis, Y-axis, and Z-axis in the Cartesian coordinate system.

The bridge superstructure model with 1200-by-500-by-8-inch continuous bridge deck is used to model the bridge deck portion. The bridge deck portion is modeled using four-noded shell elements which have six degrees of freedom for each node. The program STAAD-III automatically generates fifth node at the center of the four-noded shell element.

The bridge deck is composed of two hundred shell elements. Each shell element with a 60-by-50-inch dimension is selected to qualify the requirement of the aspect ratio. The aspect ratio for these shell elements is equal to 1.2:1 which is within the value recommended in STAAD-III documentation. All shell elements with 8-inch thickness are used to represent the bridge deck thickness and the centroid of the shell element thickness is placed at the centroid of the bridge deck thickness.

The five Type IV AASHTO prestressed concrete I-girders have a moment of inertia of 260730 $in.^4$ [1] and a length of 1200 inches. The girders are modeled using space frame elements. Each girder is composed by ten 120-inch-long space frame elements. The space frame elements are located along the centroid of the girders which is a 24.73-inch height above the bottom of the girders.

In order to simulate the composite action between the deck and girders, eleven rigid-link members with a 36.27-inch length for each girder are selected to connect the shell and space frame elements. These connections between the shell and space frame elements are allowable in STAAD-III. The length of each rigid-link member includes the thickness of the haunches and one half of the deck thickness. In order to simply the geometry of the bridge model, the haunches are not modeled by shell or other elements since their thickness compared with the bridge deck thickness are relatively small. In addition, ten 24.73-inch-long rigid-link members are used as rigid connections from the supports to the centroid of the girders at the ends of the bridge spans.

Diaphragms cast at the ends and mid-spans of the girders are modeled using the master/slave function which is provided in STAAD-III. All joints connected to the girders are slaved about the Z-axis which gives the girders without any rotation with respect to the Z-axis. Therefore, the stabilization of the superstructure is provided by the master/slave function.

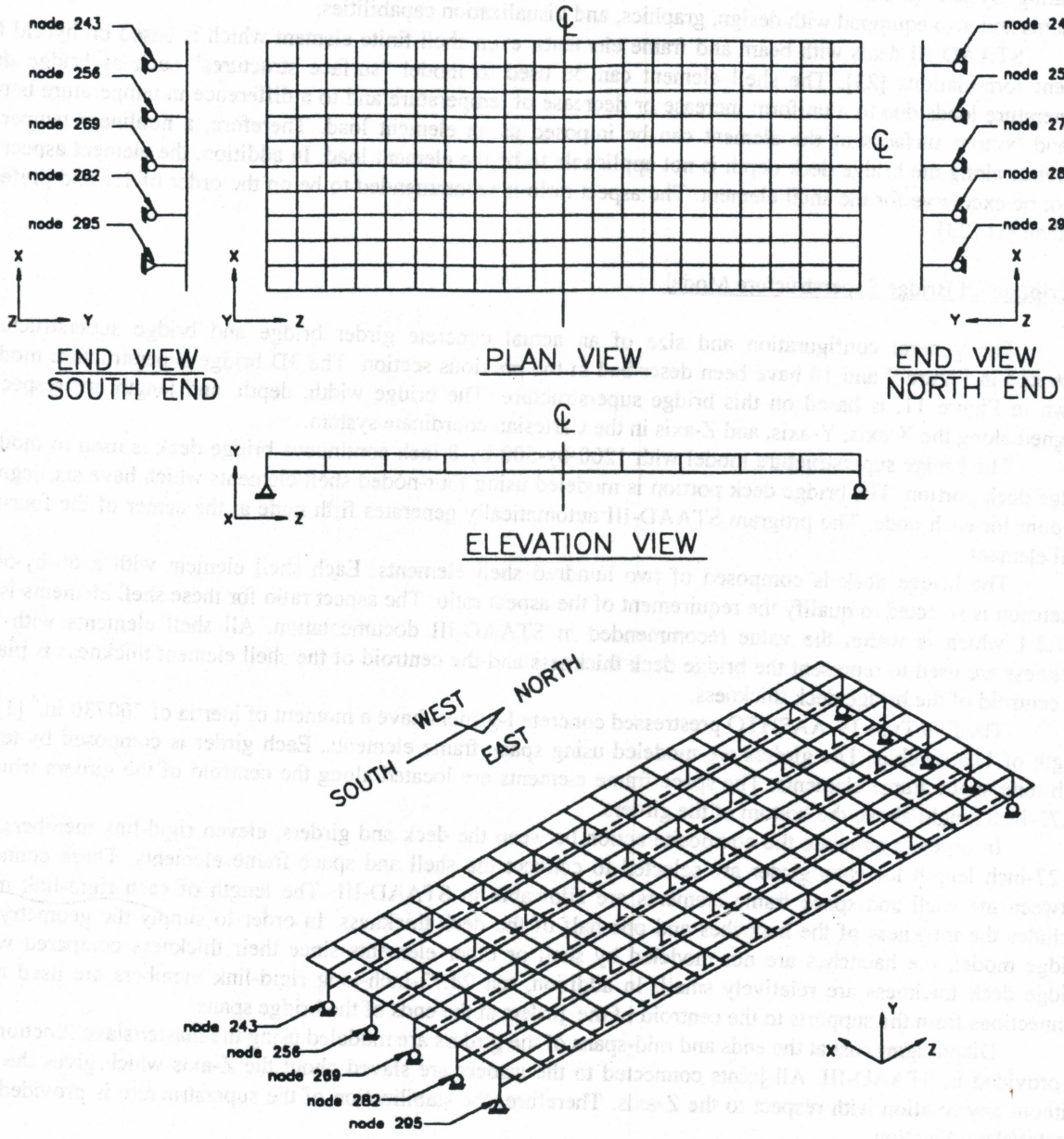

Figure 11. 3-D Bridge Superstructure Model.

Support Features

In order to simulate actual bridge support conditions, the support of the bridge superstructure model is modeled by three support features: Case I PINNED-ROLLER support, Case II FIXED-ROLLER support, and Case III FIXED-FIXED support. A PINNED support is support which has translational, but not rotational restraints. A FIXED support has both translational and rotational restraints. A ROLLER support is one specified condition of the PINNED support which is restrained along the Y-axis in this bridge model.

In the three support features, all nodes located at supports are restrained to move along the vertical axis (Y-axis). Support nodes 295 and 296 are restrained in the X-axis for the purpose of the model stability. In addition, all support nodes at the south ends of the girders are restrained to move in the Z-axis for the model stability as well.

The support Case I PINNED-ROLLER, as illustrated in Figure 12, is considered to use when the south and north ends of the girders are free to rotate about the X-axis. Therefore, the degrees of freedom is considered to reach the maximum values for the actual bridge superstructure supports when the bridge model is modeled using the support Case I.

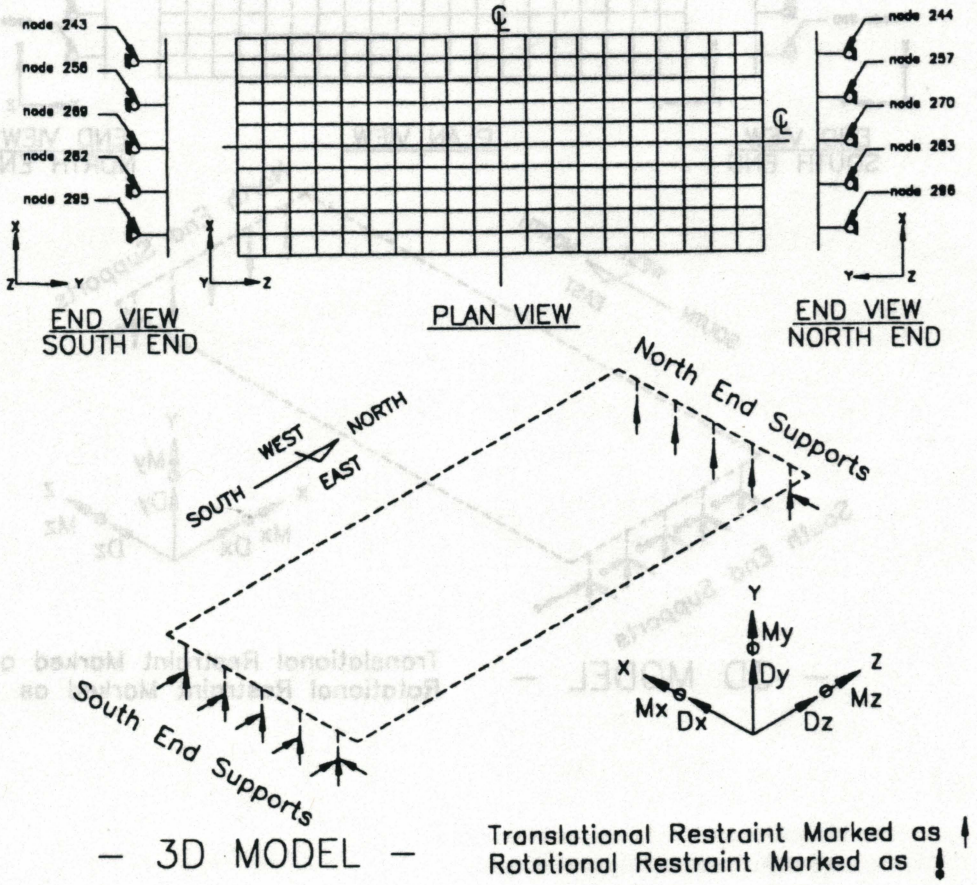

Figure 12. Case I PINNED-ROLLER Support.

The support Case II FIXED-ROLLER shown in Figure 13 is used as the support nodes at the south ends of the girders are restrained to rotate about the X-axis. However, the support nodes at the north ends are free to rotate about the X-axis.

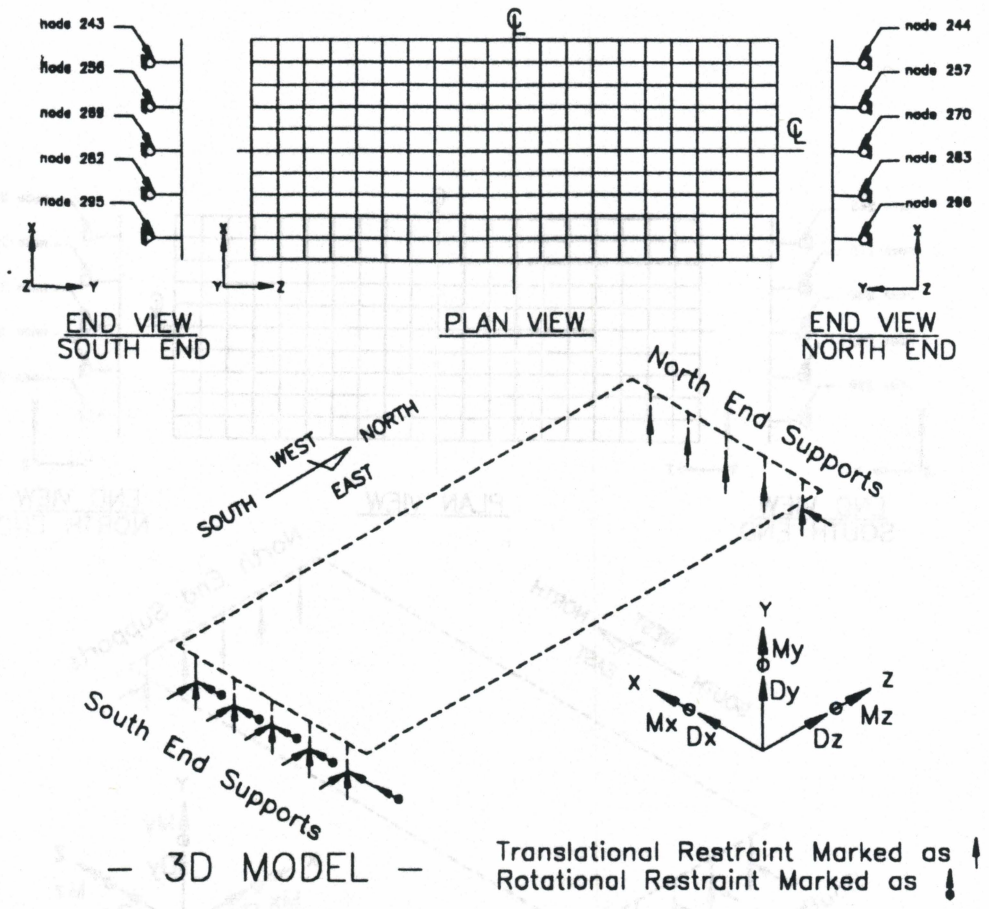

Figure 13. Case II FIXED-ROLLER Support.

The support Case III FIXED-FIXED, as shown in Figure 14, is considered when the support nodes at the ends of the girders are restrained to rotate about the X-axis. The support Cases II and III with less degrees of freedom are used for the bridge model due to more constraints at the support nodes.

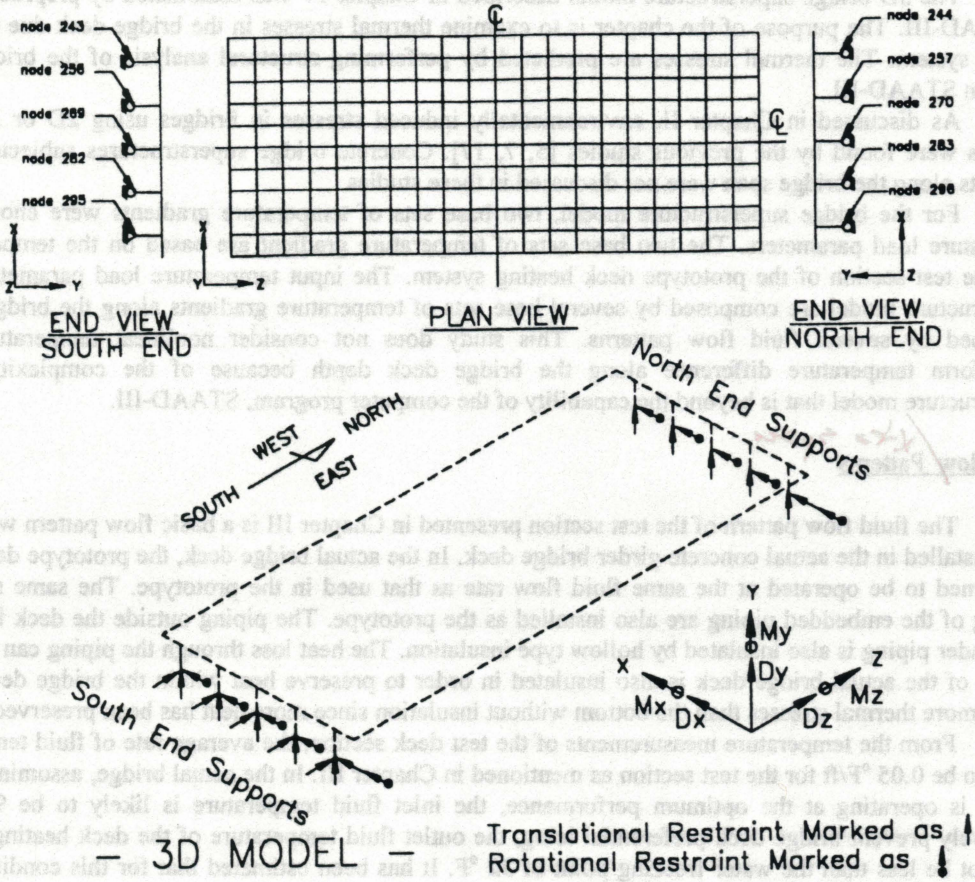

Figure 14. Case III FIXED-FIXED Support.

The material properties of the deck and girders are used based on typical highway concrete girder bridge specifications used in Oklahoma: the compressive strength of concrete f_c' of 4000 psi for concrete deck and 6000 psi for concrete girders [19]. According to the ACI code, the modulus of elasticity E_c for normal weight concrete is taken as the following equation [2]:

$$E_c = 57{,}000\sqrt{f_c'}$$

Therefore, E_c = 3605 ksi and E_c = 4415 ksi are determined to be used for the deck and girders of the bridge superstructure, respectively. Possion's ratio and coefficient of thermal expansion for the concrete bridge superstructure are taken as 0.17 and 6.6 x 10^{-6}/°F, respectively. Both values are close to those values used in the past researches [5, 10] when the bridge superstructure was subjected to temperature loads. In addition, the properties of materials of the bridge superstructure are assumed to be homogeneous and isotropic.

CHAPTER V

STUDY OF THERMAL STRESSES IN BRIDGE DECK

Introduction

The 3D bridge superstructure model described in Chapter IV was established by preprocessing procedures in STAAD-III. The purpose of the chapter is to examine thermal stresses in the bridge deck due to the active deck heating system. The thermal stresses are predicted by performing structural analysis of the bridge superstructure model in STAAD-III.

As discussed in Chapter II, environmentally induced stresses in bridges using 2D or 3D finite element methods were found by the previous studies [5, 7, 17]. Concrete bridge superstructures subjected to temperature gradients along the bridge span were not discussed in these studies.

For the bridge superstructure model, two base sets of temperature gradients were chosen as base input temperature load parameters. The two base sets of temperature gradient are based on the temperatures measured from the test section of the prototype deck heating system. The input temperature load parameters for the bridge superstructure model are composed by several base sets of temperature gradients along the bridge deck which are developed by several fluid flow patterns. This study does not consider nonlinear temperature gradients and nonuniform temperature difference along the bridge deck depth because of the complexity for the bridge superstructure model that is beyond the capability of the computer program, STAAD-III.

Fluid Flow Patterns

The fluid flow pattern of the test section presented in Chapter III is a basic flow pattern which is considered to be installed in the actual concrete girder bridge deck. In the actual bridge deck, the prototype deck heating system is assumed to be operated at the same fluid flow rate as that used in the prototype. The same size, location, and spacing of the embedded piping are also installed as the prototype. The piping outside the deck including coupling and header piping is also insulated by hollow type insulation. The heat loss through the piping can be prevented. The bottom of the actual bridge deck is also insulated in order to preserve heat within the bridge deck. This condition causes more thermal stresses than the bottom without insulation since more heat has been preserved in the deck.

From the temperature measurements of the test deck section, the average rate of fluid temperature loss was found to be 0.05 °F/ft for the test section as mentioned in Chapter III. In the actual bridge, assuming the deck heating system is operating at the optimum performance, the inlet fluid temperature is likely to be 96 °F. In order to effectively prevent bridge deck preferential icing, the outlet fluid temperature of the deck heating system should at least not be less than the water freezing point of 32 °F. It has been estimated that for this condition to be insured, more than one set of pipe loops must be installed in the deck.

Each pipe loop has a complete deck heating system which is composed by heat pump, pump, embedded piping, header piping, and coupling as identical as the prototype deck heating system. Based on the average rate of fluid temperature loss 0.05 °F/ft, the inlet fluid temperature of 96 °F, and the outlet fluid temperature of 32 °F, the total traveling length of embedded piping for each loop must be limited to be at most 1280 ft. Therefore, two base loops A and B are considered to be installed in the bridge deck.

In Figure 15, the embedded piping for Loop A is developed to be symmetrical about the longitudinal centerline of the clear roadway. The inlet and outlet of the embedded piping are located at the same edge. Fluid enters the inlet, flows through the embedded piping, and finally leaves the deck. Loop A covers an area about one half of the roadway by 20-foot length. Loop B, as illustrated in Figure 16, covers the entire roadway width with the length of 10 feet. The inlet and outlet are located at the same edge. The embedded piping for the two loops is installed along the transverse direction which is perpendicular to the travel direction.

For each base loop, the total embedded piping length is 720 feet. Therefore, the outlet fluid temperature of 60 °F can be determined by using the average temperature loss rate of 0.05 °F/ft. A fluid temperature difference between the inlet and outlet is equal to 36 °F for each loop.

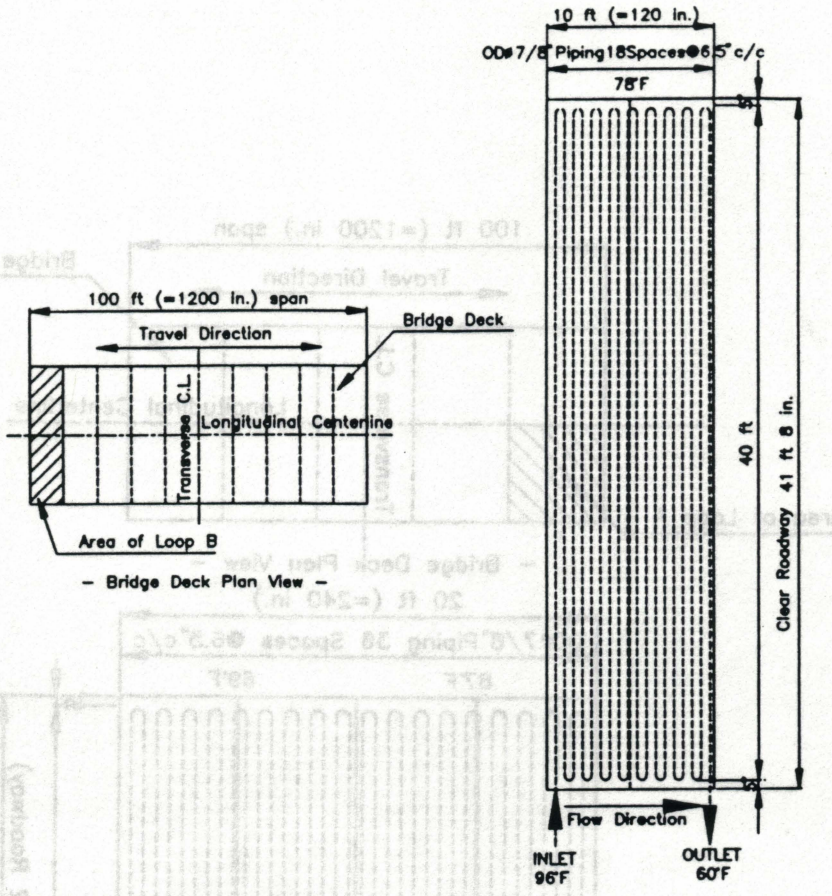

Figure 16. Embedded Piping: Loop B.

In order to cover the vast and continuous bridge deck, ten sets of Loops A and B are necessary to be installed in the bridge deck. Several possible fluid flow patterns are developed by the ten sets of Loops A and B with different flow directions.

There are six possible fluid flow patterns composed by the base Loop A, numbered from Patterns A-1 to A-6, as illustrated in Figures 17 through 22, respectively. Figure 17 shows the fluid flow pattern A-1 where ten sets of Loop A have the same fluid flow direction from the left to the right. A horizontal arrow mark represents the fluid flow direction. Two vertical arrow marks with "IN" represents the inlet of the loop and "OUT" for the outlet.

In Figure 18, the flow direction of Pattern A-2 is in a counterflow fashion where the opposite flow direction is arranged at both sides of the longitudinal centerline. Patterns A-3, A-4, A-5, and A-6, as illustrated in Figures 19 through 22, are other possible fluid flow patterns.

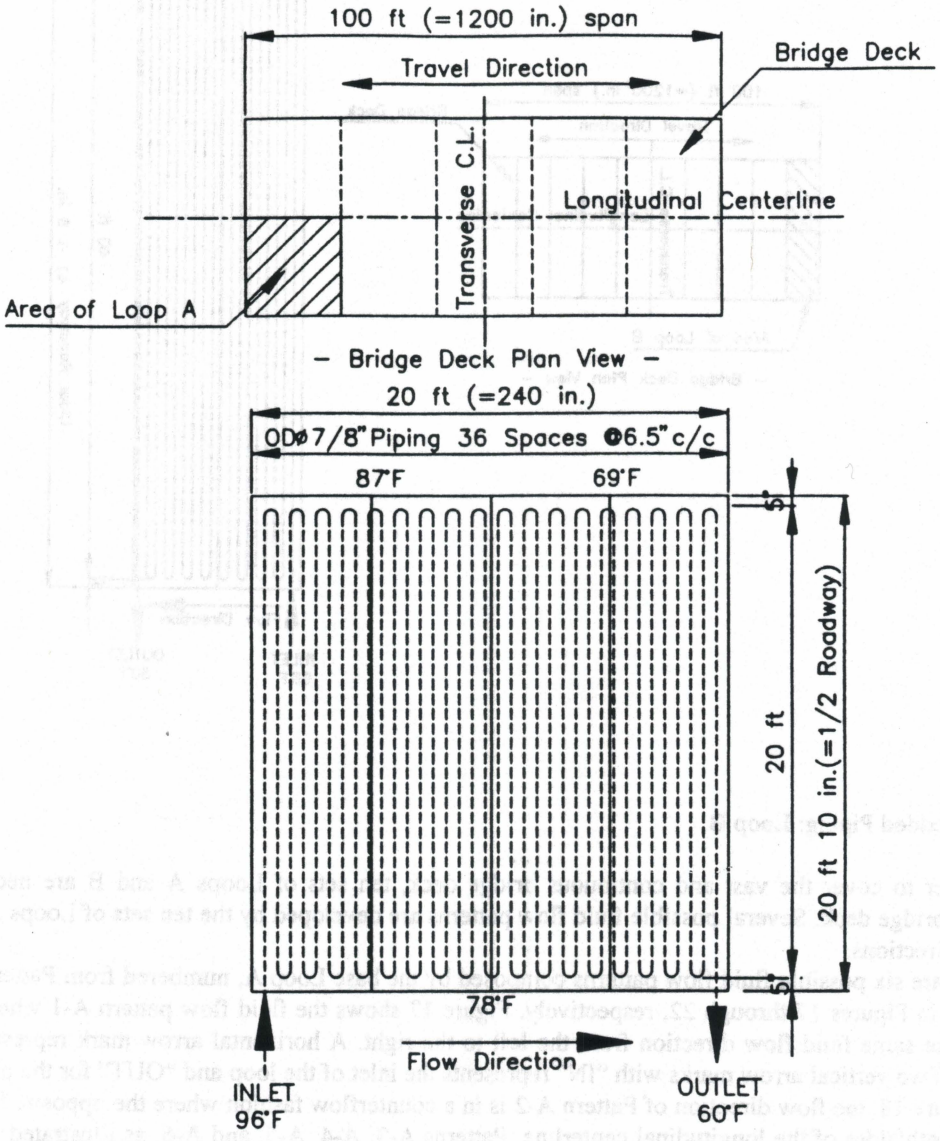

Figure 15. Embedded Piping: Loop A.

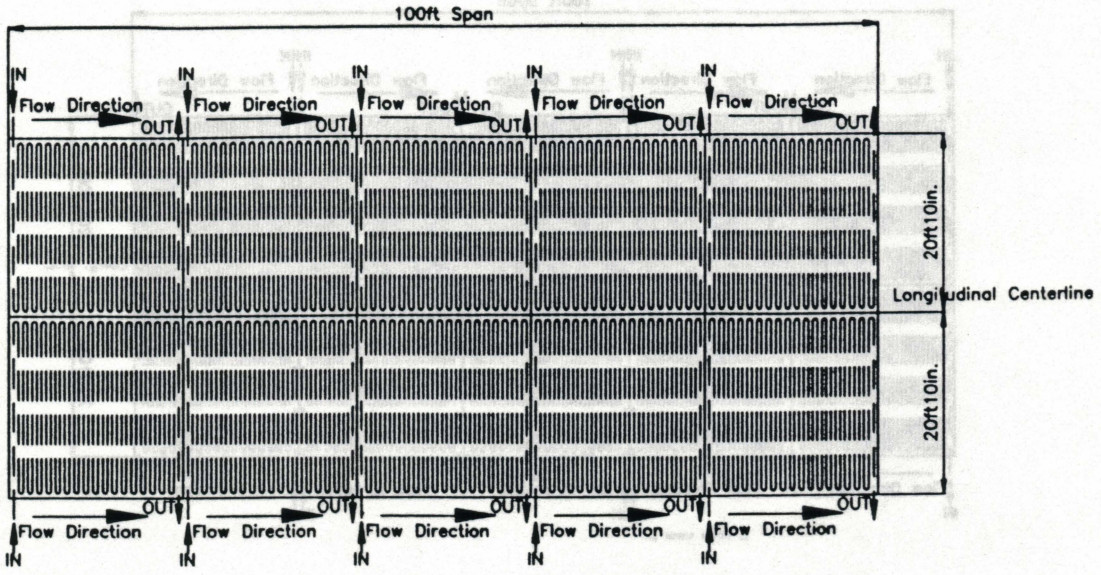

Figure 17. Fluid Flow Pattern A-1.

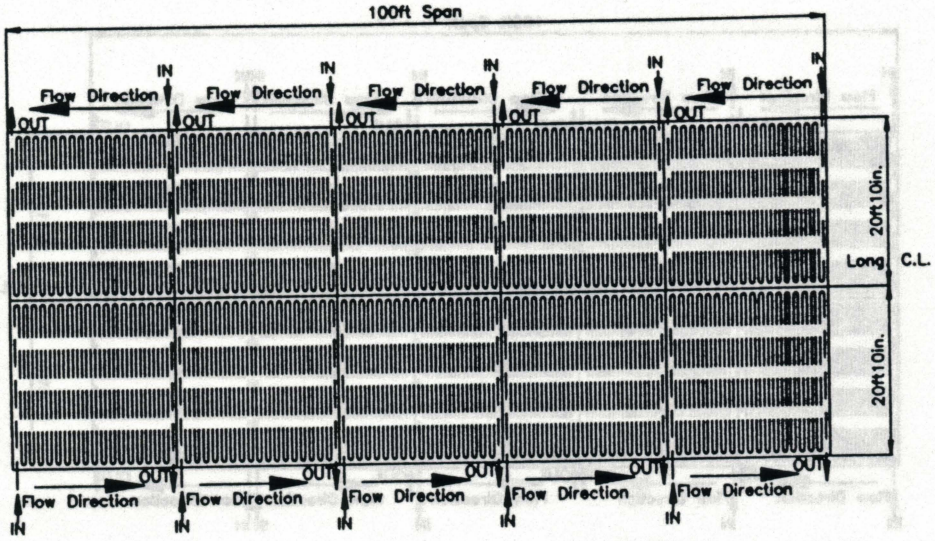

Figure 18. Fluid Flow Pattern A-2.

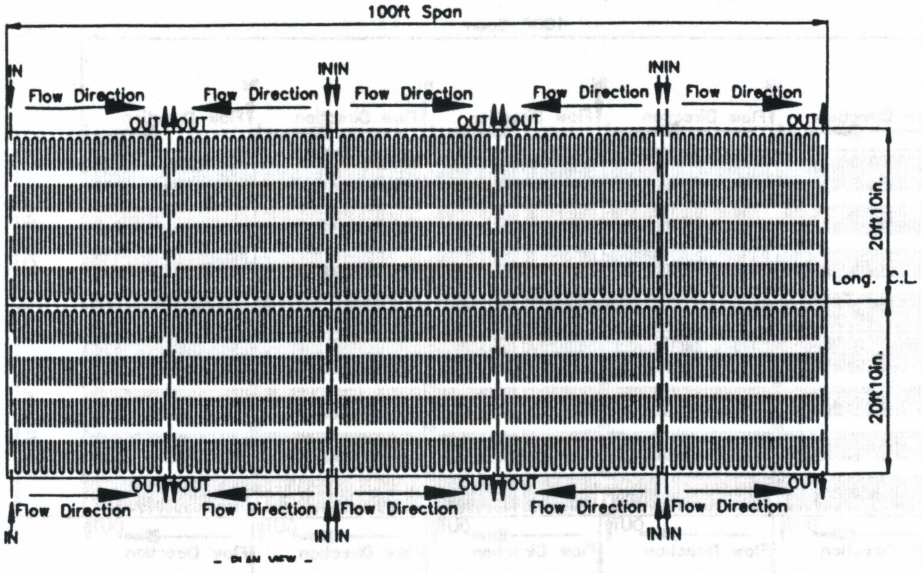

Figure 19. Fluid Flow Pattern A-3.

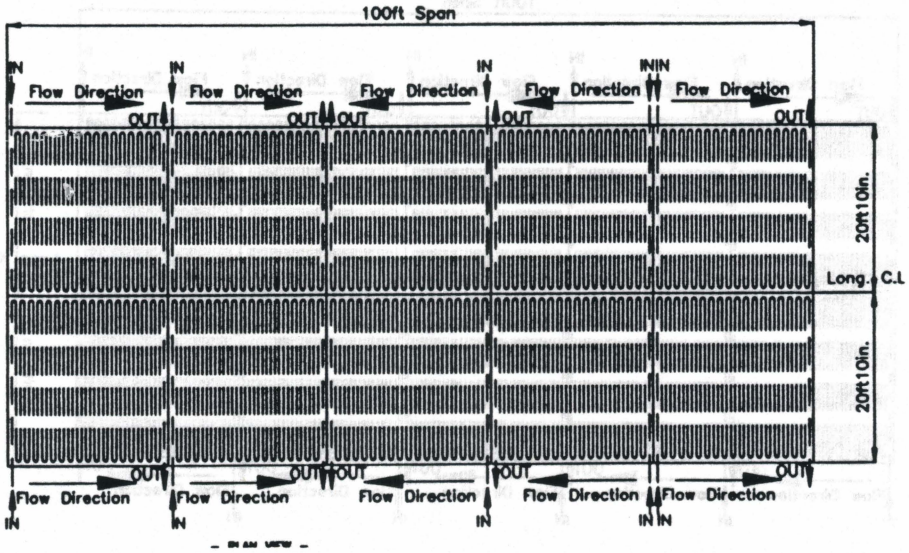

Figure 20. Fluid Flow Pattern A-4.

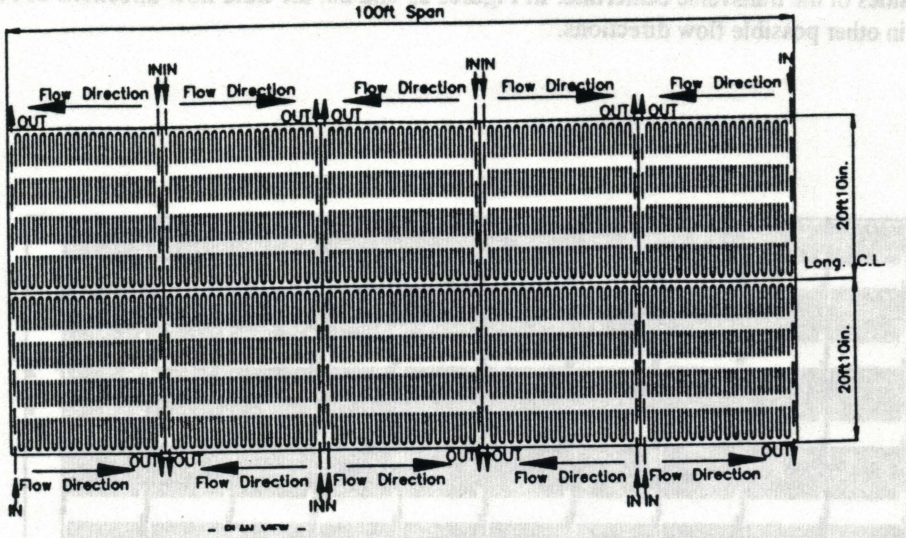

Figure 21. Fluid Flow Pattern A-5.

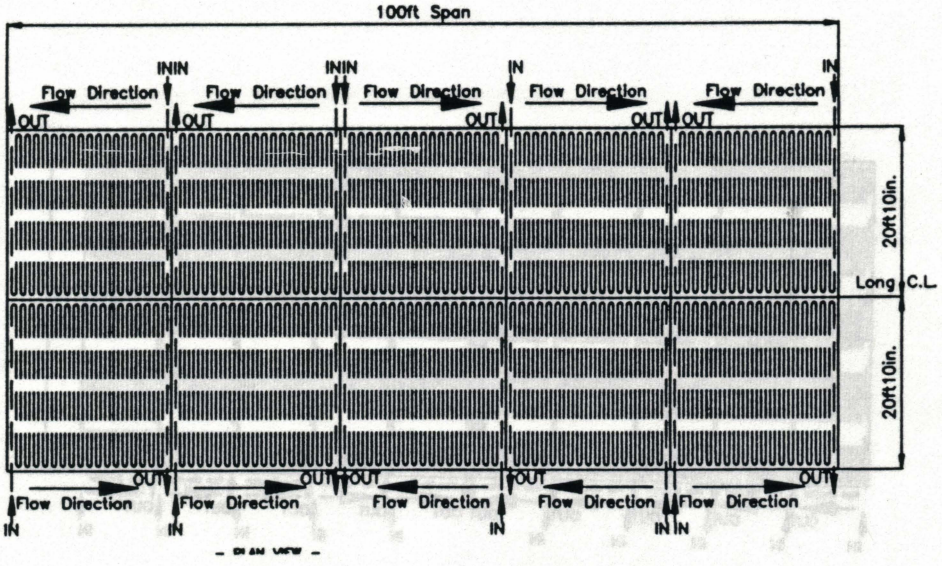

Figure 22. Fluid Flow Pattern A-6.

There are four possible fluid flow patterns based on the base set of Loop B, numbered from Patterns B-1 to B-4, as shown in Figures 23 through 26. In Figure 23, Pattern B-1 shows that each Loop B with the same flow direction is operated from the left to the right. Pattern B-2, as illustrated in Figure 24, shows the opposite flow direction at both sides of the transverse centerline. In Figures 25 and 26, the fluid flow directions of Patterns B-3 and B-4 are operated in other possible flow directions.

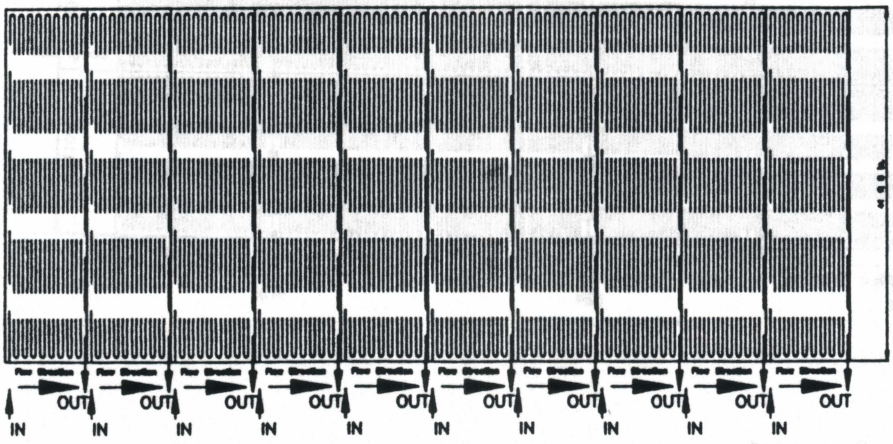

Figure 23. Fluid Flow Pattern B-1.

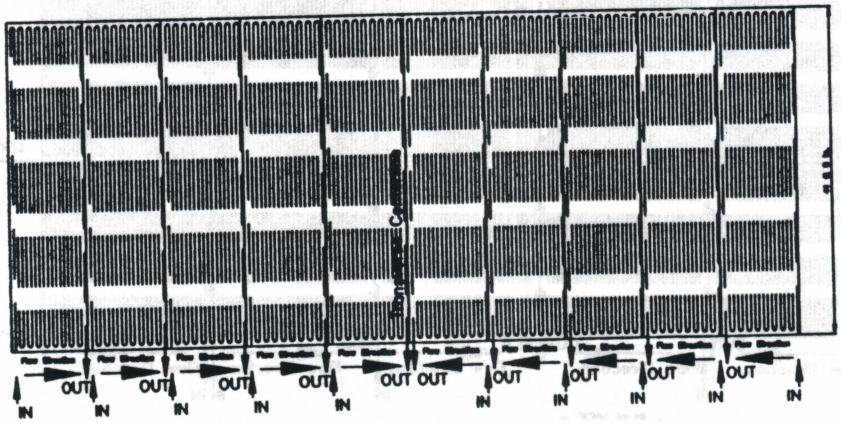

Figure 24. Fluid Flow Pattern B-2.

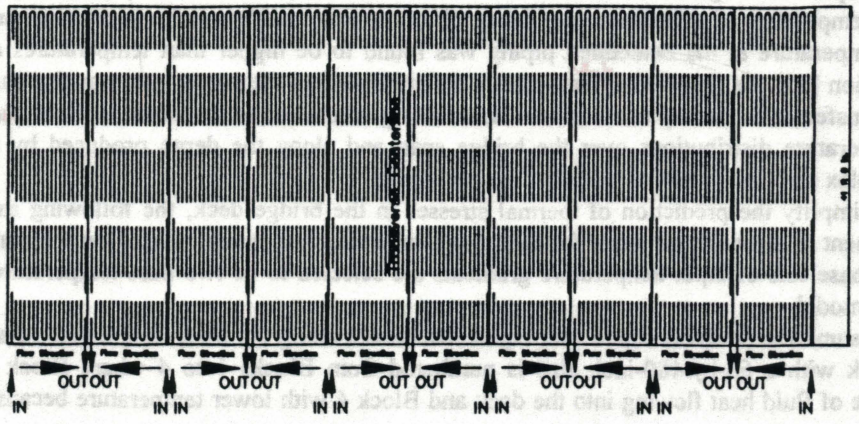

Figure 25. Fluid Flow Pattern B-3.

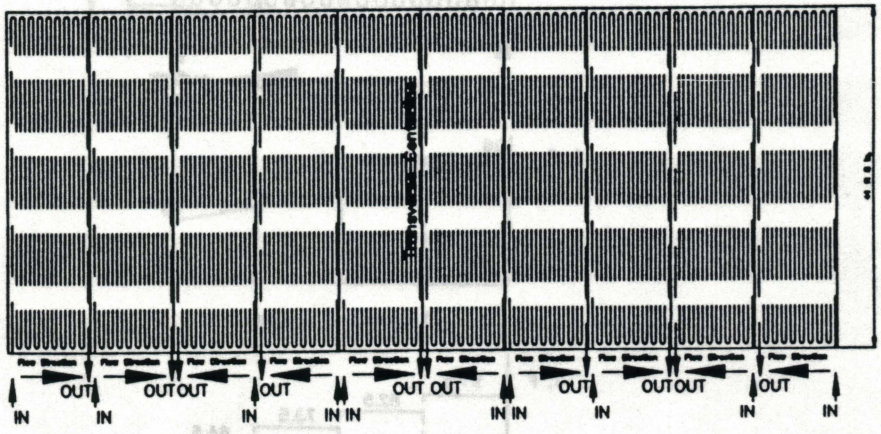

Figure 26. Fluid Flow Pattern B-4.

Temperature Loads

Ten possible fluid flow patterns of Patterns A and B series for the deck heating system embedded piping were discussed in the last section. Temperature distribution over the test deck section was not uniform since fluid heat was gradually dissipated through the test section and was lost with the increase of the piping length.

In addition, temperature distribution along the depth of the test section was found as two nonlinear curves. In the two curves, temperature at the embedded piping was found to be higher than temperatures at the top and bottom of the test section [27]. As time being, temperature difference along the two curves was decreased since fluid heat was gradually transferred to the top and bottom. This finding is referred to the other researchers' investigation [27]. Therefore, temperature distributions over the bridge span and along the depth produced by the fluid flow patterns become complex since temperature gradients are not linear.

In order to simplify the prediction of thermal stresses in the bridge deck, the following assumptions are made in the development of temperature loads for the bridge superstructure model. Based on the embedded piping Loops A and B, two base sets of input temperature gradients are selected to be two base temperature loads for the bridge superstructure model.

Loop A is assumed to be divided into four equal size blocks along the transverse direction as illustrated in Figure 27. Each block with a 60-by-480-inch size is numbered from Blocks 1 to 4 where Block 1 with higher temperature is because of fluid heat flowing into the deck and Block 4 with lower temperature because of fluid heat leaving the deck.

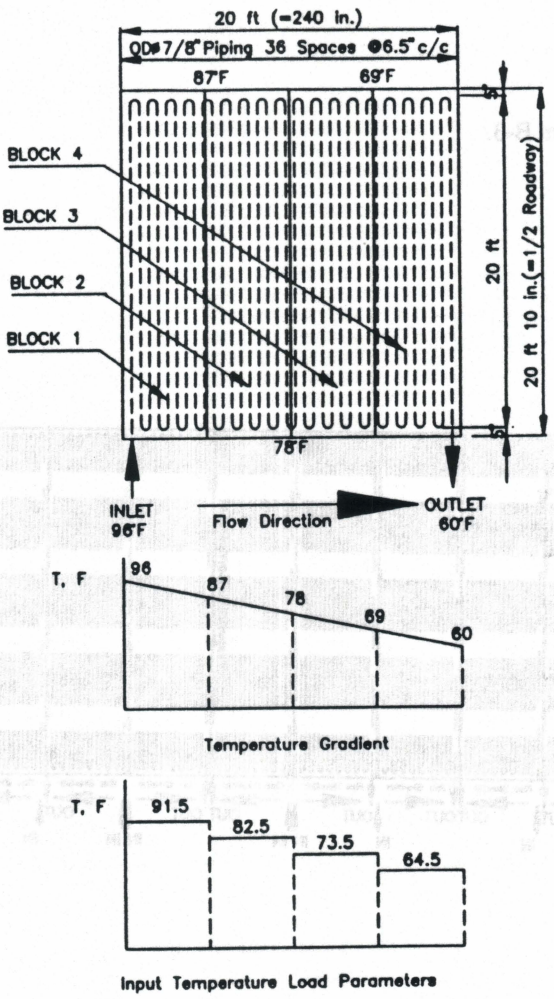

Figure 27. Four Blocks, Temperature Gradient, and Input Temperature Load Parameter of Loop A.

Temperature gradient along the longitudinal axis for each block is assumed to be the temperature entering and leaving each block. The average of the entering and leaving temperature of each block is used to represent block temperature. The average temperature of each block is assumed to be constant. Therefore, a base set of input temperature load parameter of Loop A is composed by four different block temperatures as shown in Figure 27. This assumption is applied to the fluid flow patterns from Patterns A-1 to A-6, as illustrated in Figures 28.

In addition, this assumption is also applicable to develop the second base set of input temperature load parameter of Loop B as shown in Figure 29. The input temperature load parameter of Loop B is also extended to the flow patterns B-series as shown in Figure 30.

However, assuming temperature load parameter applied to the girders of the bridge superstructure is equal to the water freezing temperature of 32 °F. This condition causes higher temperature differences between the deck and girders. Therefore, more thermal stresses would be induced by the higher temperature differences.

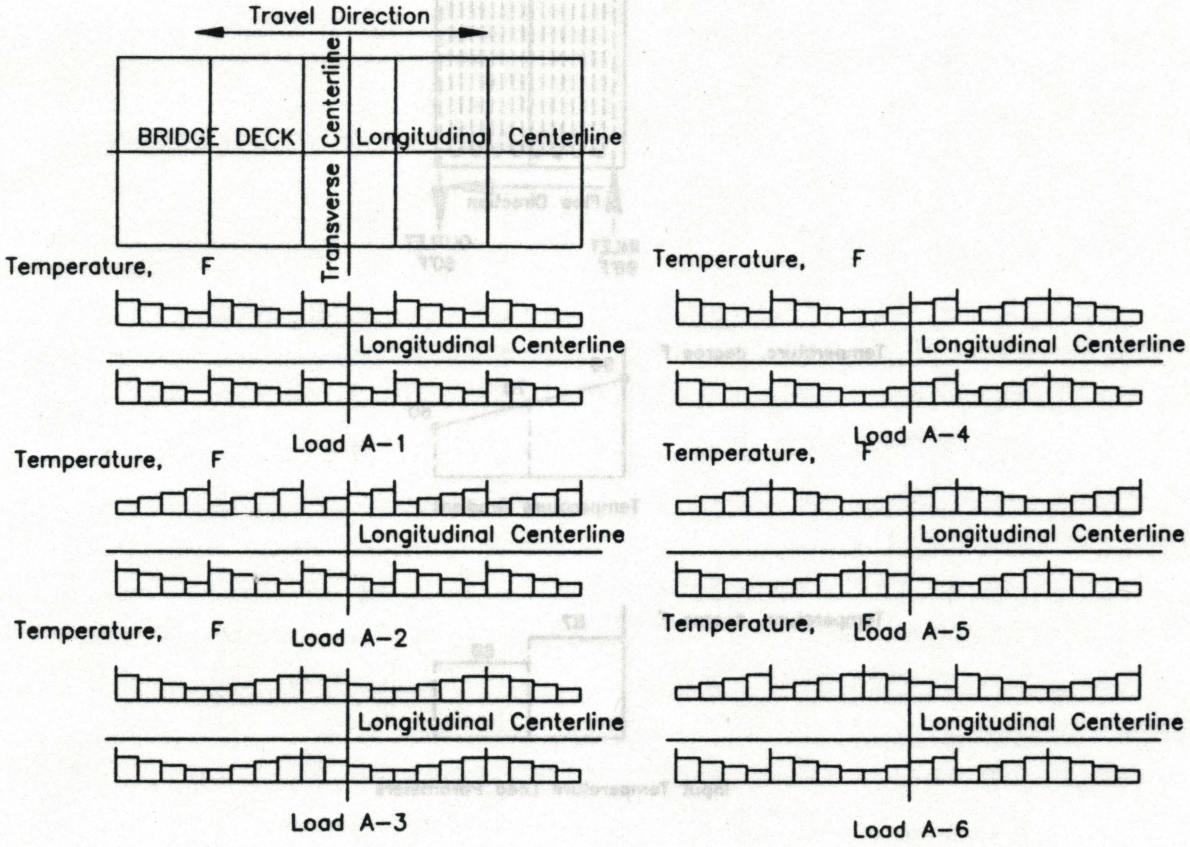

Figure 28. Input Temperature Load Parameters for Flow Patterns A-Series.

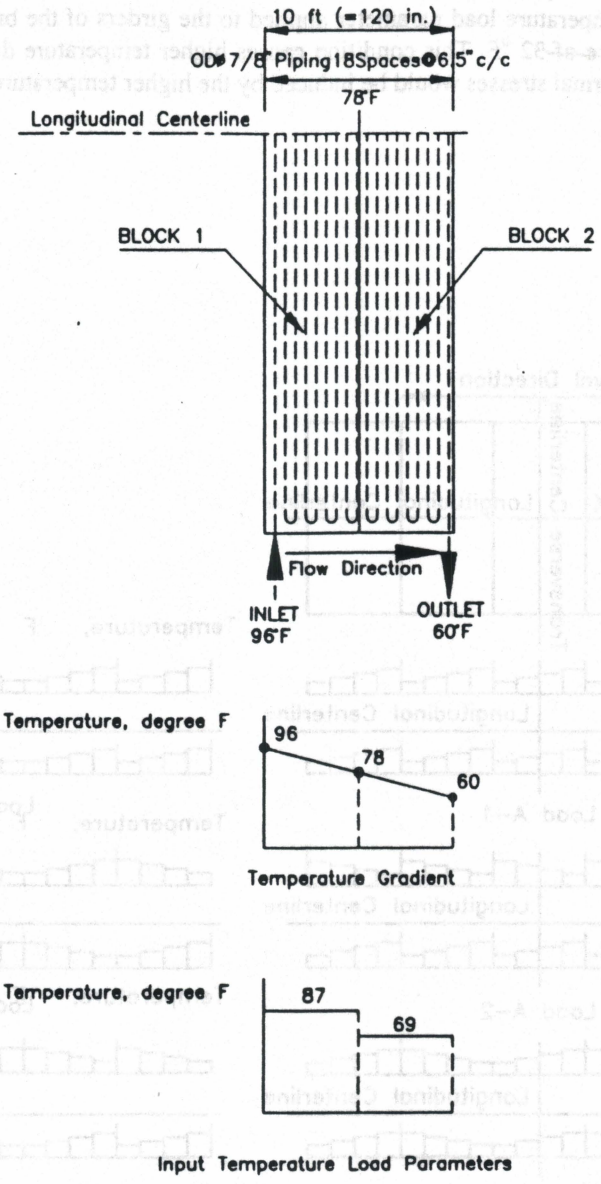

Figure 29. Two Blocks, Temperature Gradient, and Input Temperature Load Parameter of Loop B.

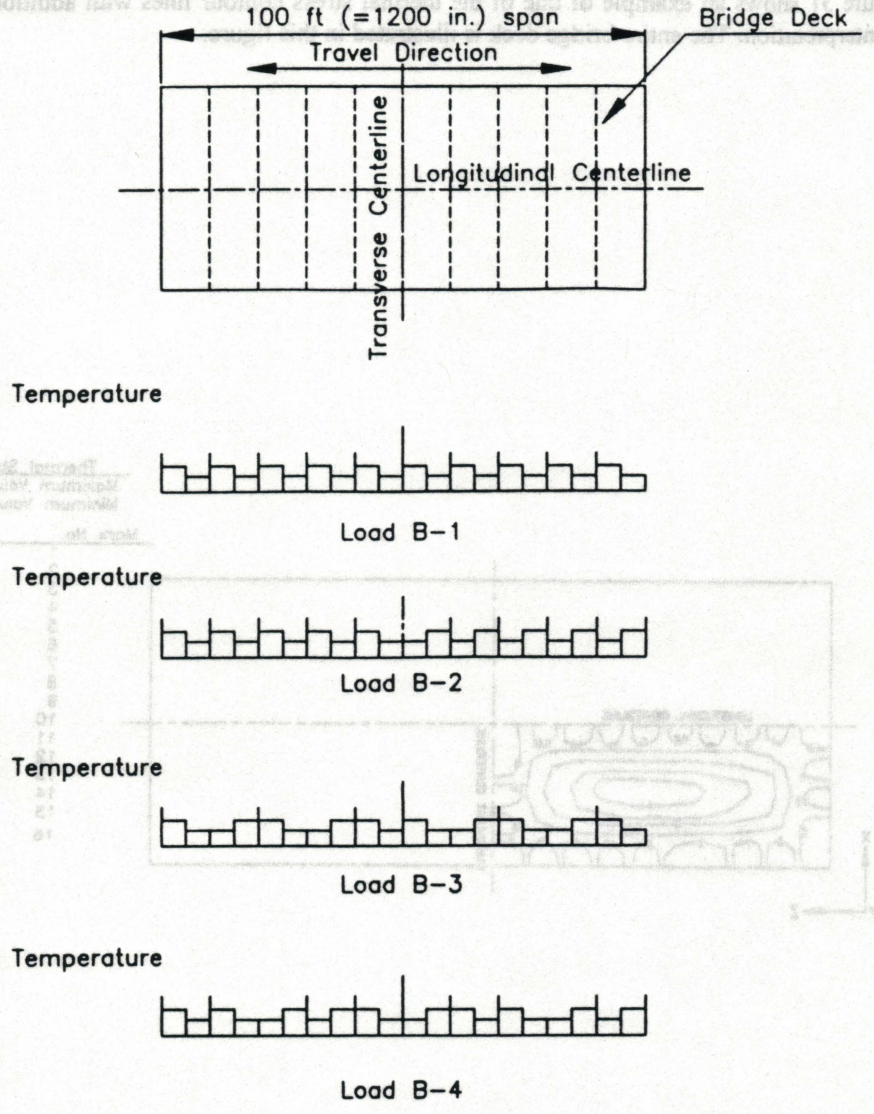

Figure 30. Input Temperature Load Parameters for Flow Patterns B-Series.

Predicted Thermal Stresses

The distribution of thermal stresses in the bridge deck subjected to the input temperature load parameters, as discussed in the previous section, is implemented by STAAD-III. In addition, the three support features as mentioned in the last chapter are used for modeling the bridge superstructure.

(1) Explanation of Thermal Stress Plots

Because of the large amount of numerical data generated by STAAD-III to describe the thermal stress distribution over the bridge deck, post processed graphics are needed to display thermal stresses in the bridge deck. Two-dimensional contour lines on the X-Z plane are plotted to display thermal stress distributions in the bridge deck after maximum thermal stresses with a specified temperature load and support feature were obtained. These plots

condense the large program output in a concise form so that understanding of thermal stresses in the bridge deck will be enhanced.

Figure 31 shows an example of one of the thermal stress contour lines with additional markings added to assist in its interpretation. The entire bridge deck is illustrated in this figure.

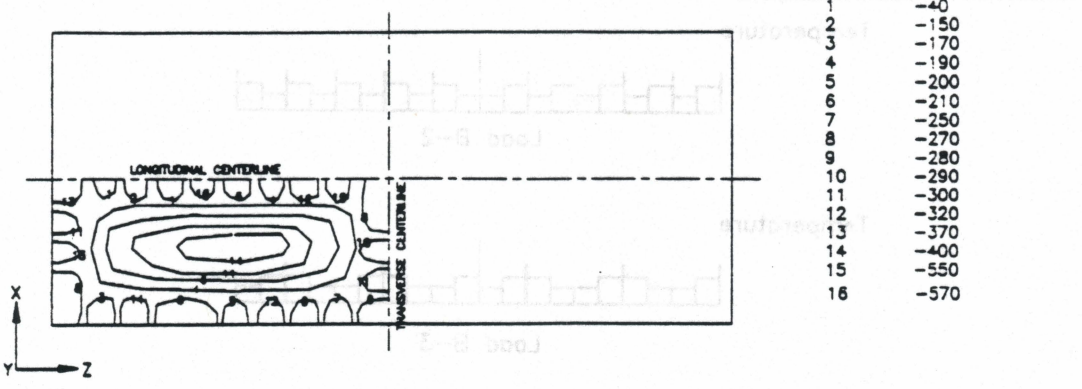

Thermal Stress Values
Maximum Values: −570 psi
Minimum Values: −40 psi

Mark No.	Thermal Stress, psi
1	−40
2	−150
3	−170
4	−190
5	−200
6	−210
7	−250
8	−270
9	−280
10	−290
11	−300
12	−320
13	−370
14	−400
15	−550
16	−570

Figure 31. Sample Thermal Stress Contour Lines

The symmetrical centerlines of the bridge model along the longitudinal and transverse directions are also displayed. In this Figure, the thermal stress contour lines are drawn on only one quarter of the bridge deck when the thermal stresses were found to be symmetrical about the centerlines. If other three quarters of the deck are to be drawn, thermal stress contour lines would be mirrored as the same image of the contour lines with respect to the longitudinal and transverse centerlines. Therefore, on the thermal stress contour lines generated by the post processing procedures, only this one quarter of the bridge deck is plotted to take maximum advantage of the display area.

(2) Thermal Stresses in Bridge Deck

Ten possible sets of the input temperature load parameters with the three support features were chosen to predict thermal stresses in the deck of the bridge superstructure model. After the computation implemented by STAAD-III, the prediction of thermal stresses in the bridge deck is tabulated in Table I. The predicted thermal stresses are obtained by the principal stresses on the top surface of the shell elements in STAAD-III output data files.

Table I. Predicted Values of Thermal Stresses in Bridge Deck.

Input Temperature Load Parameters	THERMAL STRESS RANGES Support Features PINNED-ROLLER	FIXED-ROLLER	FIXED-FIXED
A-1	-40~-569	-133~-566	-172~-569
A-2	-63~-686	-77~-708	-140~-727
A-3	-100~-515	-80~-545	-87~-566
A-4	-85~-608	-148~-605	-133~-607
A-5	-89~-673	-78~-700	-87~-720
A-6	-65~-693	-93~-715	-93~-734
B-1	-142~-437	-143~-449	-147~-450
B-2	-170~-440	-195~-451	-225~-453
B-3	-176~-398	-181~-440	-204~-447
B-4	-159~-434	-161~-442	-187~-448

Table I shows the thermal stress ranges in the deck of the bridge superstructure model subjected to the ten input temperature load parameters and three support features. The negative sign represents compressive thermal stress.

A maximum compressive stress of 734 psi was predicted when the input temperature load Pattern A-6 and support feature FIXED-FIXED were applied to the bridge model. As indicated in Table I, the input temperature load Pattern A-6 and the support feature FIXED-FIXED introduced higher thermal stresses than other temperature load patterns and support features.

According to the ACI code [2], a modulus of rupture of concrete f_r for normal weight concrete is taken to be

$$f_r = 7.5\sqrt{f_c'}$$

The modulus of rupture of concrete f_r is determined to be 475 psi for concrete having a compressive strength of 4000 psi as mentioned in the last chapter. In Table I, thermal stresses due to all B-series temperature load parameters are found within the value of $f_r = 475$ psi. A cracking problem, in the bridge deck under these conditions, will be controlled.

However, thermal stresses in the bridge deck subjected to all A-series temperature load parameters are greater than the value of $f_r = 475$ psi. Even the lowest thermal stress is found to be 515 psi under the temperature load Pattern A-3 and support feature PINNED-ROLLER. A crack will form in the bridge deck under the A-series temperature load parameters.

The thermal stresses, as shown in Table I, indicate the lower thermal stress directly associated with input temperature load parameters having identical heat flow directions from the left to the right. For example, the input temperature load parameters A-1 and B-1 show that temperature gradients follow the same flow direction from the left to the right.

In addition, more temperature values applied in the temperature gradient of each loop will also induce more thermal stresses. For example, the temperature gradient of the load A-1 comprises four temperature values so that the maximum compressive thermal stress of 570 psi is about thirty percent higher than that of 440 psi due to the load B-1. The load B-1 only comprises two temperature values in each temperature gradient.

Temperature gradients in the counterflow direction will incur higher stresses, i.e. the input temperature load parameters A-4, A-5, and A-6. The magnitudes of the thermal stresses due to the loads A-4, A-5, and A-6 are significantly different from those values due to the same flow direction. The lower thermal stresses are also found when the bridge superstructure is supported by the support feature PINNED-ROLLER.

From Table I, the magnitude of those tensile thermal stresses are relatively small compared to the maximum compressive thermal stress. The tensile thermal stresses are not harmful to the bridge deck and negligible. Therefore, A cracking problem in the bridge deck is dominated by the higher compressive thermal stresses.

As previously discussed, the crack will occur in the bridge deck due to the maximum compressive stress of 734 psi. Figure 32 shows the thermal stress distribution in the bridge deck when the bridge superstructure model is subjected to the temperature load A-6 and support feature FIXED-FIXED. Therefore, the potential location of the crack in the bridge deck can be examined by using Figure 32.

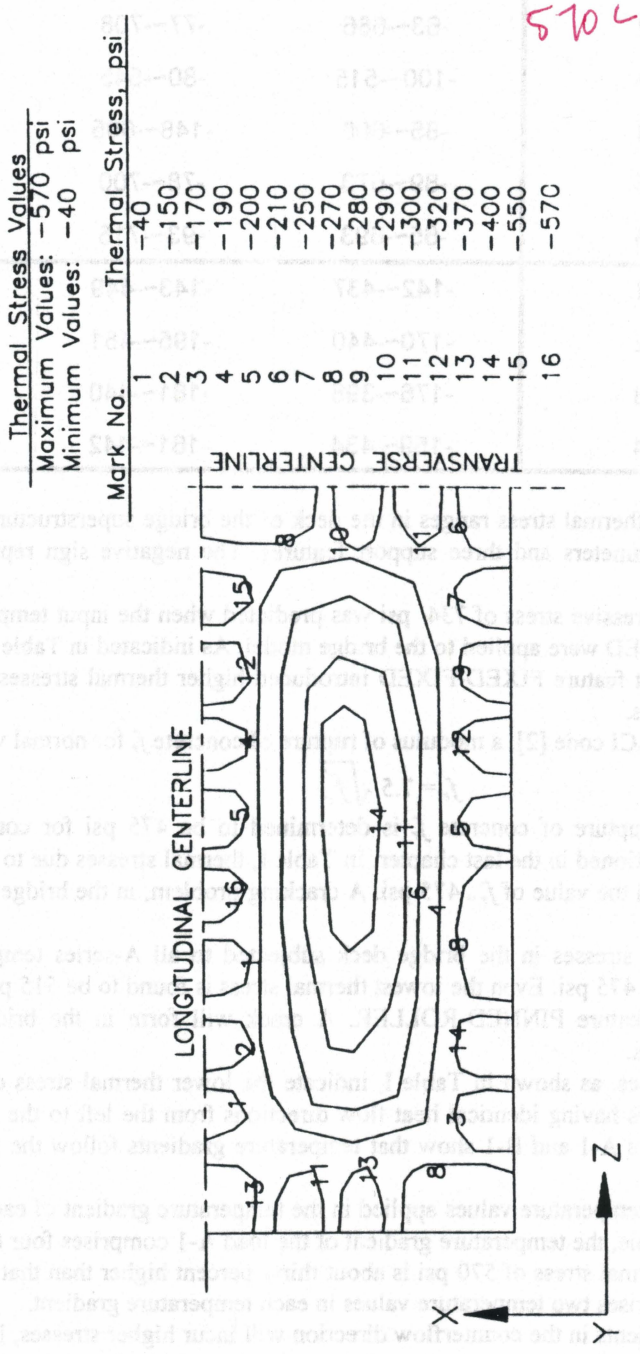

Figure 32. Thermal Stress Distribution in Bridge Deck.

CHAPTER VI

CONCLUSIONS

Summary

The purpose of this study is to predict thermal stresses in bridge decks due to the active geothermal deck heating system. The prototype of the active geothermal deck heating system was tested by the test section. The temperature responses of the test section with the deck heating system were measured by thermocouples.

The 3-D bridge superstructure model was presented by using the computer program STAAD-III to predict thermal stresses in bridge decks. Several input temperature load parameters and support features were applied to the bridge superstructure model. Therefore, the thermal stresses in bridge deck due to the deck heating system were predicted and the potential crack locations in the deck were presented.

Conclusions

In accordance with the objectives for this study were stated in Chapter I, thermal stresses within bridge decks due to possible fluid patterns of the active geothermal deck heating system were predicted by the 3-D bridge superstructure finite element model. On the basis of the finite element analysis, the following conclusions are obtained:

(1). More restraints at bridge supports, more thermal stresses will occur in the bridge deck.

(2). Higher thermal stresses are induced when the fluid flow patterns of the active geothermal deck heating system are not installed in the same direction. Therefore, the most feasible fluid flow patterns are based on geothermal heated fluid flowing through the piping with the identical flow path for the deck heating system.

(3). Higher thermal stresses are introduced when temperature differences along the bridge span are increased.

(4). The maximum compressive thermal stress in the bridge deck was assessed to be around 550 psi when the most feasible fluid flow patterns of the active geothermal deck heating system were assumed to be installed in the bridge deck. The compressive thermal stress of 500 psi was only subjected to several sets of the temperature gradient along the longitudinal direction of the bridge deck without the consideration of other service loads. In addition, the value 500 psi occurred in the few locations along the longitudinal centerline and at the ends of the bridge deck.

Recommendations for Further Research

Based on the observations made during the course of this research, the following recommendations are made:

(1). The input temperature load parameters should be modified to examine thermal stresses in bridge decks subjected to temperature gradients along the depth of the bridge decks.

(2). The developed 3-D bridge superstructure model for the concrete girder bridge should also be modified to predict thermal stresses in different size and configuration of bridge superstructures.

REFERENCES

1. AASHTO, American Associate of State Highway and Transportation Officials. "Standard Specifications for Highway Bridges, AASHTO PCI Standard Beam,." Washington, D.C., 1993.

2. ACI, American Concrete Institute. "Building Code Requirements for Structural Concrete (ACI 318-95) and Commentary (ACI 318R-95)." Farmington Hills, MI, 1995.

3. "Anti-Icing, A Bold New Strategy. " The Preceding Article Is Excerpted from Focus, (December 1994 - January 1995), Published by The U. S. Department of Transportation, Federal Highway Administration, Public Works, pp. 50, July, 1995.

4. Babaei, K., and Hawkins, N. M. "Evaluation of Bridge Deck Protective Strategies." National Cooperative Highway Research Program. Report No. 297, Transportation Board, 1987.

5. Batla, F. A., Reisnour, P. R., and Pathak, D. V. "Deformations and Stresses in Flanged Concrete Structures due to Temperature Differentials." ACI, SP-86-17, pp. 395, 1986.

6. Blackburn, R. R., Glennon, J. C., Glautz, W. D., and St. Johns, A. D. "Economic Evaluation of Ice and Frost on Bridge Decks" National Cooperative Highway Research Program. Report No. 182, Transportation Research Board, 1978.

7. "Deicing Agents: A Primer." Dow Chemical Company. Public Works, July, 1991.

8. Dyment, R. "Snow and Ice Control on The New York State Thruway." Public Works, pp. 37, July, 1995.

9. Fleege, E.d. "Minnesota DOT Tests Deicing Alternatives." Public Works, July, 1990.

10. Ghali, A. and Elliott, E. "Serviceability of Circular Prestressed Concrete Tanks." ACI Structural Journal, No. 89-534, 1989.

11. Hess, L. Y. "Insulation Guide for Buildings and Industrial Processes." Noyes Data, 1988.

12. Husley, J. L. and Emanuel, J.H. "Environmentally Induced Bridge Stresses." Advances in Civil Engineering Through Engineering Mechanics, 1987.

13. Imbsen, R. A., Vandershaf, D. E., Schamber, R. A., and Nutt, R. V. "Thermal Effects in Concrete Bridge Superstructures Report No. 276." Transportation Research Board, National Research Council, 1987.

14. Lee, R. C., Nydahl, J. E., and Pell, K. M. "Design and Implementation of A Water Powered Heat Pipe System for Bridge Heating." Report No. FHWA-WY-86-002, Dec., 1986.

15. Long, D.C. and Baldwin J.S. "Snow and Ice Removal from Pavement Using Stored Earth Energy." Report No. FHWA-TS-80-227, 1980.

16. Mirambell, E. and Aquado, A. "Temperature and Stress Distribution in Concrete Box Girder Bridges." Journal of Structural Engineering, Vol. 116, No. 9, American Society of Civil Engineering, 1990.

17. Moorty, S. and Roeder, C. W. "Temperature-Dependent Bridge Movements." Journal of Structural Engineering, Vol. 118, No. 4, American Society of Civil Engineering, 1991.

18. Nydahl, J.E., Lee, R. C., Sackos, J. and Pell, K. M. "Evaluation of An Earth Heated Bridge Deck." Report No. FHWA-WY-84-001, April, 1984.

19. "Oklahoma State Highway, Plan of Proposed Highway: Interstate Highway No. I-240 at Air Depot Bridge A, Oklahoma County." Department of Transportation, State of Oklahoma, 1992.

20. "Oklahoma Mesonet, The." Pamphlet Published by The Oklahoma Mesonetwork, Norman, OK., 1993.

21. Priebe, L.V. "Deicing Salt Compatibility With Vegetation." Public Works, 121(4), April, 1990.

22. Priestley, M. J. N. "Model Study of A Prestressed Concrete Box-Girder Bridge Under Thermal Loading." Proceedings of The Ninth Congress of The IABSE, Amsterdam, Denmark, May 1972.

23. "STAAD-III/ISDS User's Manual and Example Manual, Revision 15.0." Research Engineers, Inc., CA., 1992.

24. Tanaka, O. et al. "Snow Melting Using Heat Pipes." The IV International Heat Pipe Conference, London, England, pp. 11, 1981.

25. "Thruway Picks Galvanizing." Engineering News Records, 232(10), March 7, 1994.

26. Trost, S. E., Heng, F. J., and Cussler, E. L. "Chemistry of Deicing Roads: Breaking The Bond Between Ice and Road." Journal of Transportation Engineering, ASCE, 114(2), Jan., pp. 15-26, 1987.

27. Wadivkar, O. S. "Undecided Titled" Unpublished Thesis of Master of Science, School of Mechanical and Aerospace Engineering, Oklahoma State University, September, 1996.

APPENDIXES

APPENDIX A

SCHEMATIC DIAGRAM OF TEST SECTION

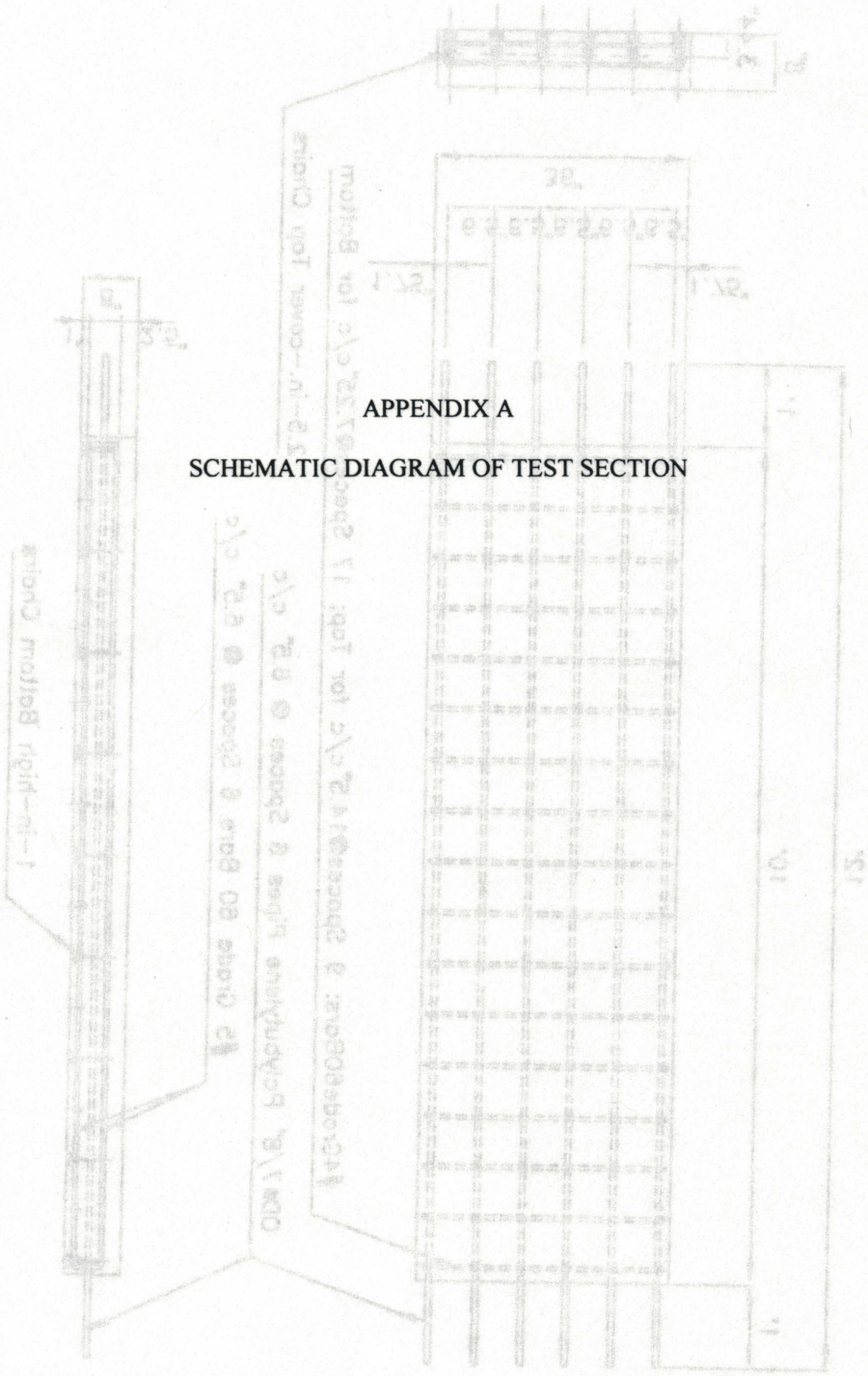

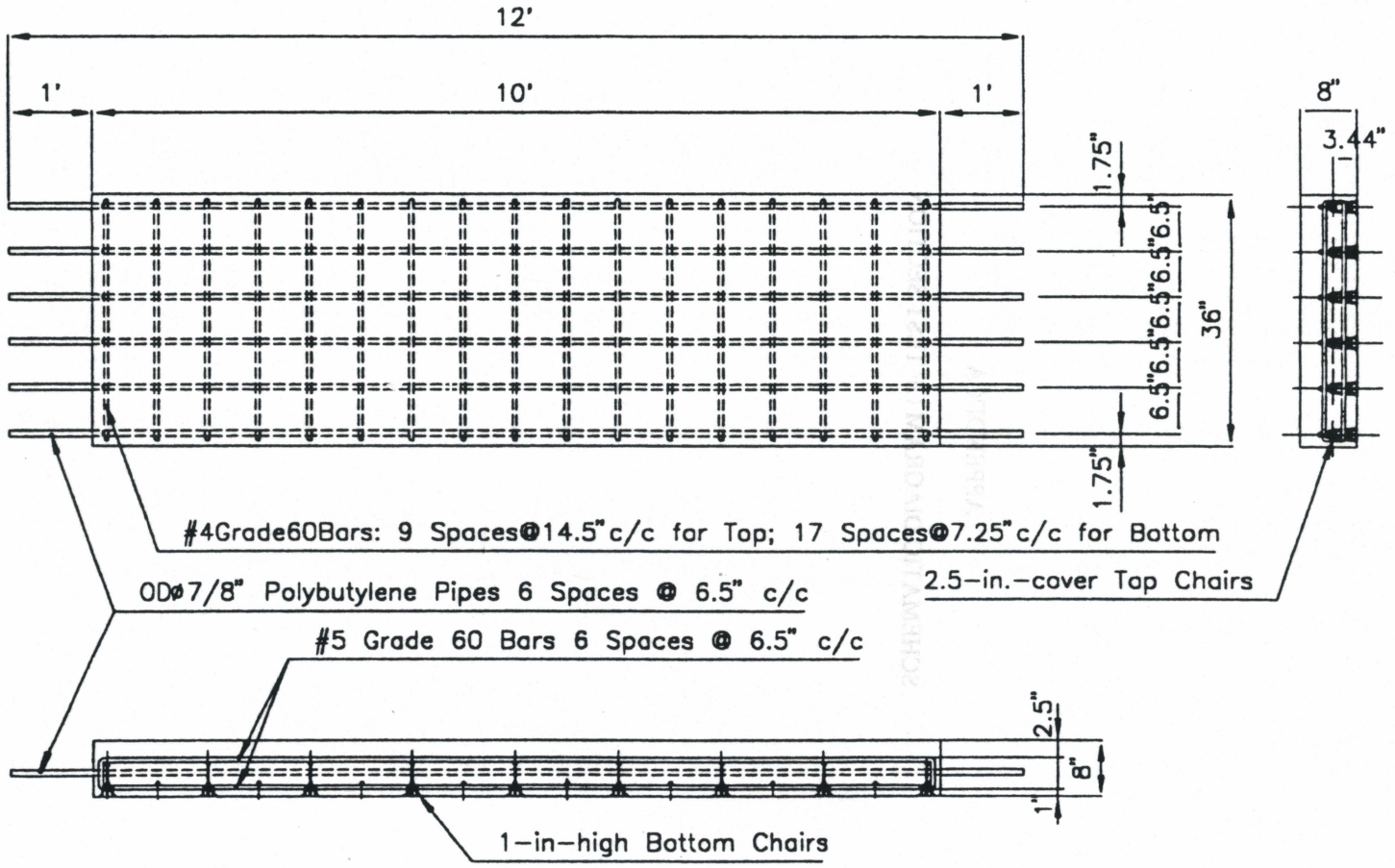
12'
1'
10'
1'
8"
3.44"
1.75"
6.5"
6.5"
6.5"
6.5"
6.5"
6.5"
36"
1.75"
#4Grade60Bars: 9 Spaces@14.5"c/c for Top; 17 Spaces@7.25"c/c for Bottom
OD∅7/8" Polybutylene Pipes 6 Spaces @ 6.5" c/c
2.5-in.-cover Top Chairs
#5 Grade 60 Bars 6 Spaces @ 6.5" c/c
2.5"
8"
1"
1-in-high Bottom Chairs

APPENDIX B

SCHEMATIC DIAGRAM OF SUPPORT STEEL FRAME

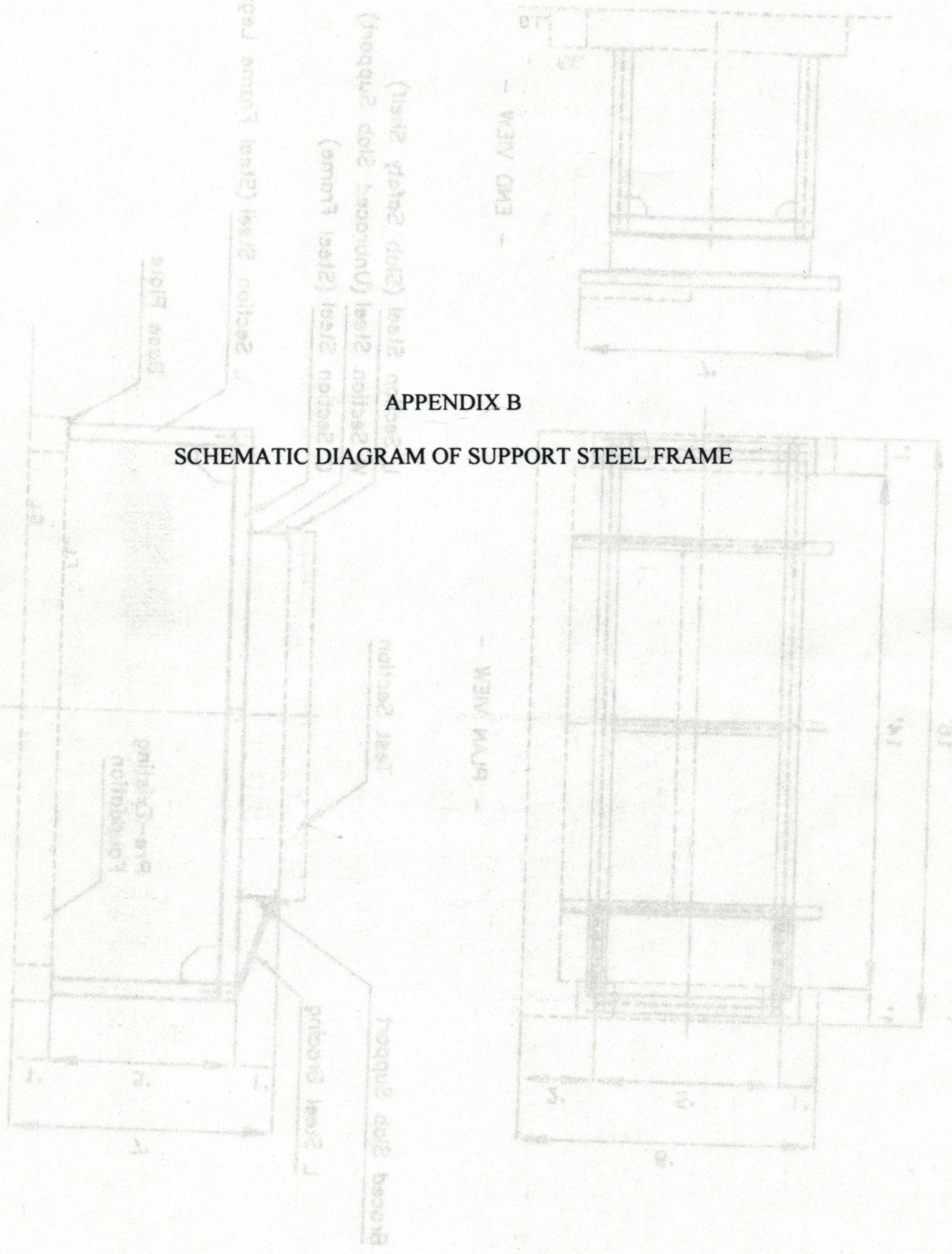

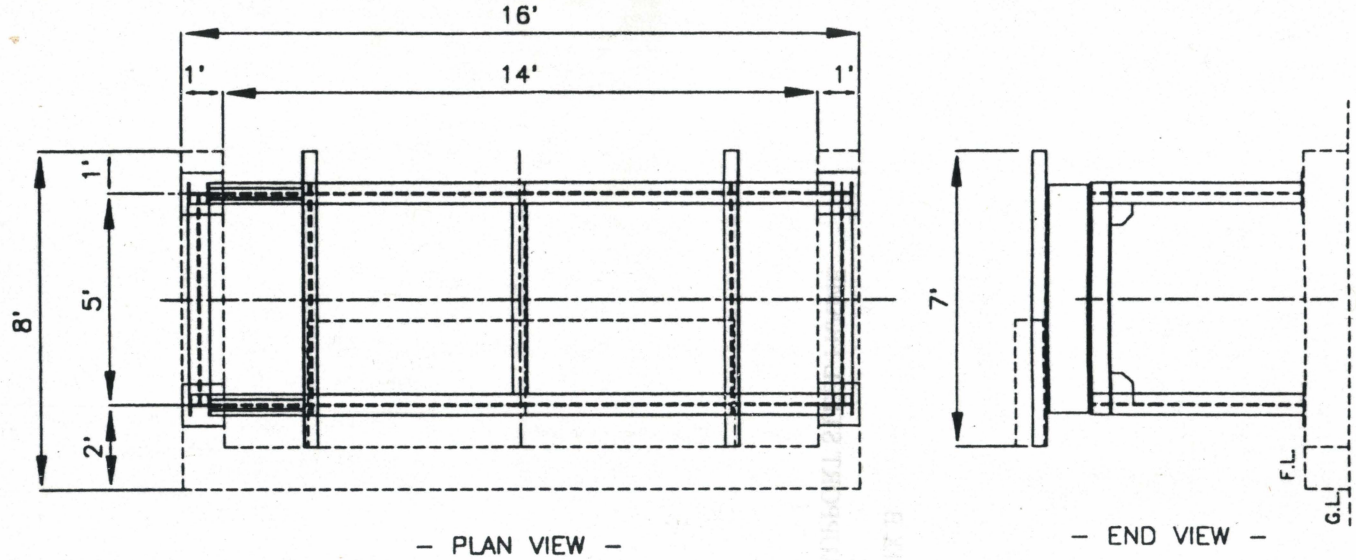

– PLAN VIEW –

– END VIEW –

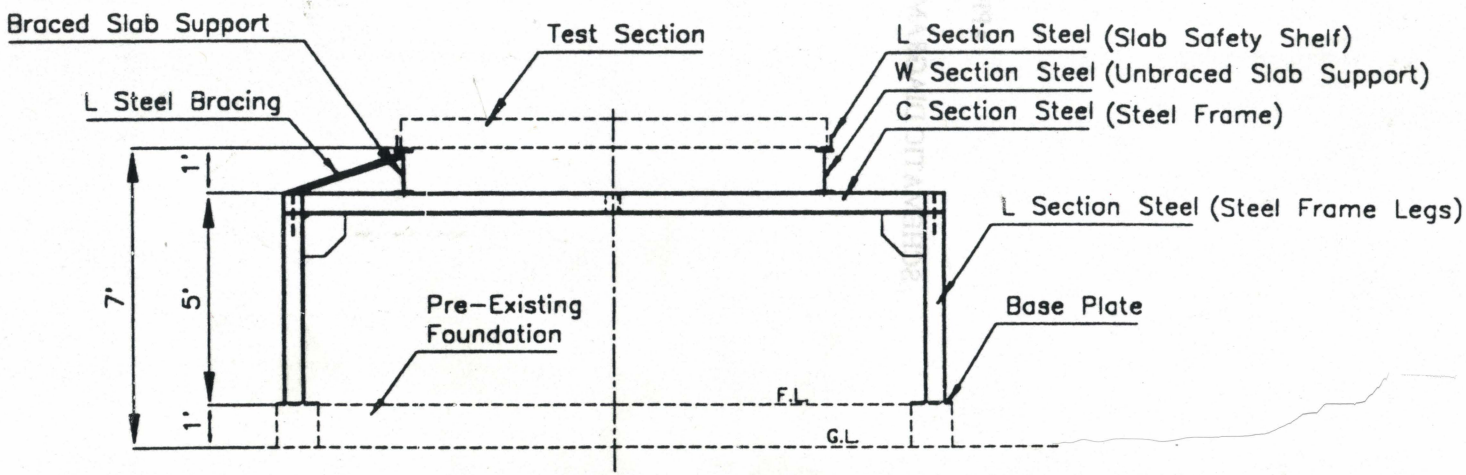

– ELEVATION VIEW –